MONITORING SETTING CHARACTERISTICS OF SILICA FUME CONCRETE USING NON-DESTRUCTIVE TECHNIQUES

A Dissertation submitted

in partial fulfilment of the requirements for
the degree of

Master of Engineering

in

Structural Engineering

by

Nikita Bhalla

Registration No.: 801422022

Under the Supervision of

Dr. Shruti Sharma
(Associate Professor)

Dr. Rafat Siddique
(Senior Professor)

CIVIL ENGINEERING DEPARTMENT

THAPAR UNIVERSITY, PATIALA

June, 2016

CERTIFICATE

I hereby declare that the thesis entitled "**MONITORING SETTING CHARACTERISTICS OF SILICA FUME CONCRETE USING NON-DESTRUCTIVE TECHNIQUES**" is an authentic record of my work carried out as requirements for the award of the degree of **Master of Engineering** in **Structural Engineering** at **Thapar University, Patiala** under the supervision of **Dr. Shruti Sharma**, Associate Professor and **Dr. Rafat Siddique**, Senior Professor, Civil Engineering, Department, Thapar University, Patiala . No part of the matter embodied in this report has been submitted to any other university or institute for the award of any degree.

Nikita Bhalla

Date: 5/07/2016

Nikita Bhalla

It is certified that the above statement made by the student is correct to the best of my/our knowledge and belief.

Dr. Shruti Sharma
Associate Professor
Civil Engineering Department
Thapar University, Patiala – 147004

Dr. Rafat Siddique
Senior Professor
Civil Engineering Department
Thapar University, Patiala - 147004

Countersigned by

Dr. Naveen Kwatra
Head, Civil Engineering Department
Thapar University, Patiala – 147004

Dr. S.S. Bhatia
Dean of Academic Affairs
Thapar University, Patiala - 147004

I

ACKNOWLEDGEMENT

First and foremost, I wish to express my deep sense of gratitude towards my supervisor **Dr. Shruti Sharma**, Associate Professor, Thapar University, Patiala, for her valuable guidance and encouragement in this work. I shall remain grateful to her for providing valuable and remarkable support throughout my thesis work. I am also very thankful to my **Dr. Rafat Siddique**, Senior Professor, Department of Civil Engineering for his precious suggestions and sharing his in depth knowledge regarding the subject.

I am thankful to Dr. Naveen Kwatra and Dr. PremPal Bansal, for providing excellent academic environment and laboratory facilities for experimentation.

I express my sincere gratitude to all the staff of Dynamics Lab and Concrete Structures Lab. Without their active support and enthusiasm, it would not have been possible to carry out the experimental work. I am extremely thankful to Sh. Balwinder Singh for his support and much needed help.

The cheerful support of my friends Jyoti Mandhani, Diksha Jindal, Amitoz Samra, Manan Hashim, Amrita Dayal, Devinder Kaur, Ashutosh Sharma and Nikhil Gupta are sincerely appreciated for helping me in testing of specimens in the laboratory.

I am indeed indebted to my parents, Mr. Amresh Bhalla and Mrs. Samita Bhalla for their encouraging words and constant support . In the end I am thankful to the Almighty for bringing this day in my life.

ABSTRACT

At early ages of concrete structures, strength monitoring is important to determine the optimum time for loading the structure. Concrete setting and hardening process are also very critical stages during construction of structures since it gives an early indication of the strength of concrete at later stages without waiting for longer durations of 3, 7 and 28 days. This purpose can be achieved by using non-destructive test methods for early age concrete properties. With increase in the use of SCMs in concrete, due to increase in number of high rise buildings there is great demand for high strength concrete, high performance concrete and ultra – high strength concrete because of better durability towards the environmental conditions it becomes a necessity to validate these methods for the detection of changes in setting and hardening patterns. In this research concrete containing different replacements of cement by silica fume have been studied at early ages using NDT of Ultrasonic Pulse Velocity (UPV), Ultrasonic Guided Wave (UGW) and Acoustic Emission (AE) Techniques and then validated using compressive strength and SEM/EDS analysis. Both the techniques are different in their nature of application, i.e., Ultrasonic Guided Wave is active in nature and Acoustic Emission Technique is passive in nature. Ultrasonic Guided Wave depends on the transmitted signal whereas the Acoustic Emission Techniques depends on the stress changes occurring inside the system.

The comparison in the setting process of control concrete and concrete containing silica fume is made in the thesis by the use of various NDT techniques. M20 grade of concrete was prepared with w/c ratio of 0.45 and varying replacement levels of silica fume with cement by 3%, 6%, 10% and 12% are made, two NDT techniques of UGW and AE are used to monitor setting of different concrete. Both NDT techniques not only pick up initial setting and hardening of concrete but also that of modified concrete effectively. Clear jump in AE parameters and fall in UGW signals indicate faster setting of SF modified concrete which is further well validated by destructive testing and SEM/EDS analysis.

CONTENTS

LIST OF FIGURES

LIST OF TABLES

CHAPTER 1

INTRODUCTION

1.1 GENERAL

Setting and hardening of fresh concrete are the most crucial phases during the construction work as the properties of concrete structure during its service life depend on it . During setting process, concrete mixture transforms from fluid state (whose properties are important for placing into formwork) into solid (whose properties are important for the proper behaviour of material in the service). Control of hardening phenomena can be used for determination of right time for removal of formwork or applying load on the structure. Thus the knowledge of fresh and young concrete is important from both, technical as well as economical aspects.

Conventional testing methods for fresh concrete and mortar properties determination are slump cone test, flow table test, penetration needle test, Vicat apparatus test, hydration temperature measurement and pull-out test. Main drawback of these methods is missing of continuous measurement data. Rhelological testing methods which use different types of viscosimeters are not successful because they induce shear forces in fresh concrete which destroy microstructure in the early ages of hydration process. Between the various NDT methods, ultrasound testing methods seems to be successful for accurate determination of fresh properties.

1.2 SETTING AND HARDENING OF CONCRETE

The transition from fluid to plastic state is defined as ***Setting Time***. When the concrete sets it stiffens but is weak. This transition from fluid to solid state can less than an hour or could be up to 24 hours. The time when cement paste attains sufficient rigidity that it is no longer in fluid state is called its initial set. When rigidity increases to a point that paste becomes solid of low strength is termed as its final setting time. After final set it attains increase in strength which refers to the ***Hardening Stage***. The gain in strength i.e. hardening is due to formation of C-S-H gels. Hardening can occur in few hours or take up to 2 -3 weeks and concrete attains sufficient capacity to support construction loads.

Hydration is defined as the process of chemical reactions between cement and water.

Table 1.1 Major compounds in cement

Compound Symbol	Compound Name
C_3S	Tricalcium silicate
C_2S	Dicalcium silicate
C_3A	Tricalcium aluminate
C_4AF	Tetracalcium aluminoferrite
$C\underline{S}H_2$	Gypsum

Chemical reactions during hydration

When water is added to cement, the following series of reactions occur:

(a) Ettringite and heat are produced when in the presence of water C_3S reacts with water. Long crystals which are stable with gypsum in solution and do not contribute to strength are called ettringite.

Tricalcium aluminate + gypsum + water = ettringite + heat

$$C_3A + 3C\underline{S}H_2 + 26H = C_6AS_3H_{32}, \Delta H = 207\ cal/g \quad (1.1)$$

(b) Calcium silicate hydrates, lime and heat are produced due to hydration of C_3S (alite), this calcium silicate hydrates formed are short fiber structures which contribute to strength.

Tricalcium silicate + water = calcium silicate hydrate + lime + heat

$$2C_3S + 6H = C_3\underline{S}_2H_3 + 3CH, \quad \Delta H = 120\ cal/g \quad (1.2)$$

(c) Ettringite becomes unstable when gypsum is used up and it reacts with C_3A to form monosulfate aluminate hydrate crystals, these crystals are stable in sulfate deficient solution.

Tricalcium aluminate + ettringite + water = monosulfate aluminate hydrate

$$2C_3A + 3\ C_6A\underline{S}_3H_{32} + 22H = 3C_4ASH_{18}, \quad (1.3)$$

(d) Calcium silicate hydrates and heat also occurs due to hydration of belite (C_2S), the reaction is slow as it is less soluble and generates less heat as compared to the with hydration of C_3S and results in long – term strength.

Dicalcium silicates + water = calcium silicate hydrate + lime

$$C_2S + 4\ H = C_3\underline{S}_2H_3 + CH, \Delta H = 62\ cal/g \quad (1.4)$$

The hydration process is divided into four stages as shown in the **Figure 1.1**. Stage 1 is of short duration as cement and water react to form amorphous layer of hydration product around cement particles and is rapid in nature. Stage 2 is the induction period which prevents quick setting of cement. Many hypothesis were proposed for the presence

of this induction period out of which the one that was found most suitable is as follows: Hydration products which are formed in stage 1 form a thin layer on particles thus preventing C_3S from dissolving. The induction period ends with nuclei formation of C-S-H gel on outer surface of this protective layer; these C-S-H gel nuclei grow and increase rate of hydration by changing morphology of thin layer by making it more permeable. In Stage 3 hydration of C_3S takes place which is very rapid and during this stage cement has paste undergone initial and final set. The products of hydration namely C-S-H gel and CH occupy space in capillary pores thus enhancing strength and reducing total pore volume. Since cement particles are now surrounded by hydration products as this layer become thick, the diffusion of ions becomes slower and Stage 4 starts which is known as Diffusion Limited Period.

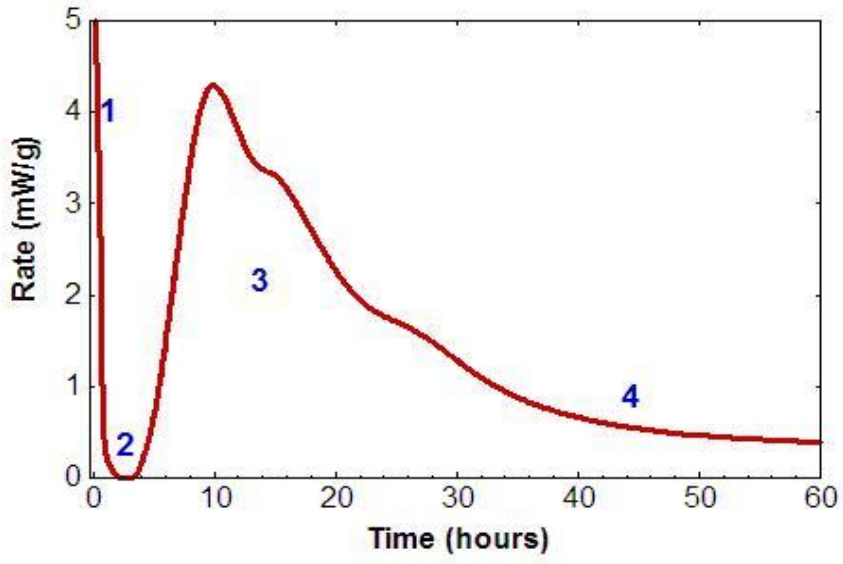

Figure 1.1: Schematic of the rate of hydration or heat evolution as a function of time (http://iti.northwestern.edu)

C-S-H gel

This binds cement particles together into cohesive paste. These gels develop tiny gel pores and grow outward from cement particles; the solid phase volume increases and thus volume of capillary pores decreases and hence permeability of cement paste decreases. Two morphologies of C-S-H gel exist as shown in **Figure 1.2**. One being less dense (occurs in water filled space) and other is more dense (occurs in spaces covered by cement particles). In Stage 3 this less dense morphology occurs while denser one occurs in Stage 4 of hydration process. These are also termed as low density and high density C-

S-H gel; because these gels grow outward low density C-S-H is of more importance than high density.

Calcium Hydroxide (CH)

Calcium Hydroxide is also known as portlandite. It occurs in various sizes and shapes. Hexagonal plate shaped crystals are formed in capillary pores. From durability perspective calcium hydroxide forms a weak link in concrete as it is soluble hydration product and it leaches out on exposure to fresh water and enhances the permeability of concrete thus making it vulnerable to chemical attack.

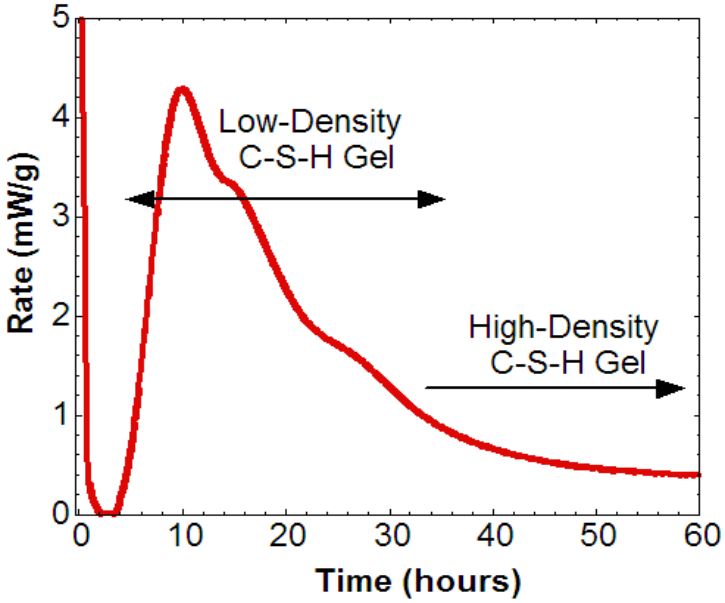

Figure 1.2: **Rate of hydration vs. time, showing when the low-density and high-density morphologies form. (http://iti.northwestern.edu)**

Abnormal Setting Behaviour :

When after mixing or placement the mix stiffens rapidly, this phenomenon is termed as ***false setting***. Formation of gypsum or excessive ettringite formation lead to false set due to accelerated hydration of C_3A. Remixing helps attain the original fluidity.

Formation of monosulaluminate or other calcium aluminate hydrates cause ***flash setting***. Once flash set occurs the hydration process will continue and remixing cannot help instead gypsum is added to control hydration of C_3A to prevent the flash set .

Factors affecting strength:

1. Water Cement ratio
2. Temperature
3. Cement content

4. Type of Cement
5. Fineness of Cement
6. Relative Humidity
7. Admixtures
8. Type and amount of Aggregate

Importance of setting time

1. Whether or not to use any plasticizer
2. To find out effectiveness of set controlling admixture
3. Regulating maximum time of mixing transit, placing and compacting
4. Whether or not to provide protection against adverse weather condition
5. Type of protection to adopt
6. Gives an idea regarding time of removal of formwork
7. Finding out maximum permissible time lapse between placements of successive layer of concrete.

1.3 MOTIVATION AND PHYSICAL BACKGROUND

Modern Concrete Technology faces several challenges:

i. Due to increase in number of high rise buildings there is great demand for high strength concrete, high performance concrete and ultra – high strength concrete because of better durability towards the environmental conditions. Silica Fume is the chief ingredient of all such concretes.
ii. Rising demand for the use of retarders and accelerators to achieve desired workabilities, self levelling concrete .
iii. Due to less availability of workmanship on site .
iv. Need to achieve durability of concrete in aggressive environments .
v. The use of supplementary cementitious material and admixtures in concrete affects the fresh and hardened state of concrete .
vi. The additions meant to achieve desired properties may be contaminated or might not be as per the standard specifications, thereby leading to negative results.

vii. Lack of supervision which might not fulfill the purpose for which SCMs were added .

viii. Certain combinations of SCMs and admixtures being used.

1.4 NDT TO INVESTIGATE SETTING

1.4 .1 Penetration tests

Several penetration tests are used in field , some widely used methods are discussed as follows :

i. **Vicat Needle**: In Vicat needle test loaded needle penetrates the sample and penetration depth is measured. Test is continued till paste becomes hard and needle is no longer able to penetrate. The 33-35 mm depth of penetration indicates start of setting process while when needle is no longer able to penetrate is defined as end of setting process, but these values are not convenient for the use in concrete due to presence of large aggregates.

ii. **Penetrometers**: Sample is supported in the instrument and a needle is driven at a given speed , the force required for the same is measured . The applied load (in Newtons) is divided by a calibration constant and pressure is obtained in MPa . Initial Setting time is determined when of stress reaches 3.5 MPa while value of 27.6 MPa represents the final setting time. Penetrometer operates at speed of 1 μm/s. Since size of needle is large as compared to those in Vicat Test mortars can be studied with this method.

iii. **Proctometer** : In comparison to the penetrometers , in protometers force is applied at much higher velocities . This method consists of a needle mounted on a spring which is manually pushed into the sample and the digital display gives the value of force applied . It have shown that the evolution of stress with the penetration depth is constant after a certain penetration depth (15 mm in the case of a needle of diameter 9 mm) which meant the rod above the tip does not play any role and that the measurement is linked to the penetration of the tip itself.

iv. **Hilti needle gun:** By shooting a nail into the test material the penetration depth is measured. As the nail attains kinetic energy when fired from the nail gun it stops when it’s energy is dissipated through the deformation of test material.

1.4.2 Ultrasonic pulse velocity (UPV)

Ultrasonic pulse velocity method is used to evaluate the quality of concrete, it can be used for detecting internal cracks, defects, deterioration due to chemical environment, freeze and thaw as well as for estimation of strength of concrete. As the technique uses mechanical waves it causes no damage to the concrete being tested and the same location can be tested again and again thus concrete being monitored over a period for any internal changes.

1.4.2.1 Pulse velocity test instrument

The instrument consists of transmitter and receiver for introducing a wave pulse in concrete and for sensing the arrived pulse respectively . The time taken by the pulse to travel certain path length through concrete is measured .

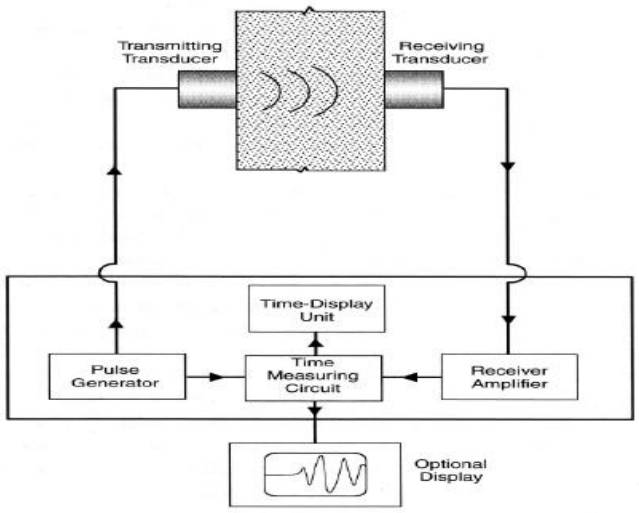

Figure 1.3: Schematic diagram of pulse velocity test circuit (Al-Nu'man et al., 2016)

The equipment for pulse velocity testing consists of two transducers], one transmitter and other receiver . They have frequency range from 25 to 100 kHz. For small size specimens which have short path lengths or for high strength concrete high frequency transducers (above 100 kHz) are used whereas in case of large specimens which have longer paths or in concrete containing large aggregates low frequency transducers (below 25 kHz) are used . The transducers generate compressional waves with wave energy concentrated along axis normal to transducer wave. **Figure 1.3** shows the equipment of pulse velocity testing , it has a rechargeable battery and charging unit. It can measure pulse times up to 6500 µs with resolution of 0.1 µs.

Figure 1.4 : Pulse velocity instrument (http://dir.indiamart.com)

Velocity of Compressional Waves depend on the elastic properties and density of the medium through which they travel . The pulse velocity method is based on this property of compressional waves. L be the distance between transmitter transducer and receiver transducer in pulse velocity setup, t be the transit time displayed by pulse velocity instrument which is the time taken by compressional wave to travel through concrete .Then the compressional wave velocity, V is given by:

$$V = \frac{L}{t}$$

Due to the presence of aggregate – mortar boundaries scattering of compressional waves being transmitted through concrete occurs thus the received pulse is of complex nature which contains multiple compressional and shear waves. Compressional waves being fastest arrive first at the receiver.

The transducers are kept in full contact with test object or otherwise air pockets exist between transducer and test object and only a small amount of wave energy will transmitted through air which will induce an error in transmit time. In order to assure proper contact and eliminate the air pockets couplants such as grease, ultrasonic gel and kaolin glycerol paste etc are used. The layer of couplant is applied on the transducer which should be kept as thin as possible. For travel length of 300 mm and pulse velocity of concrete in the range of 3700-4200 m/s the travel time comes out to be approximately 70-85 μs. Once the transducers are placed on specimen with proper contact pressure, repeated readings are taken until minimum transit time is obtained.

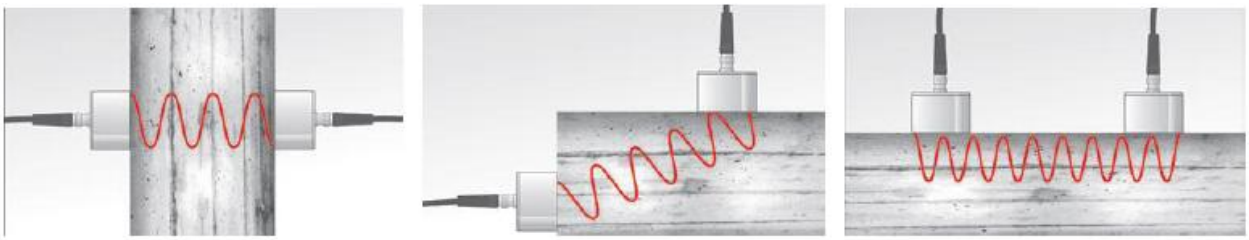

Figure 1.5: Ultrasonic pulse velocity testing transmission methods (Randhawa, 2011)

Figure 1.5 represents three configurations for placing the transducers are possible (1) direct transmission, (2) semi- direct transmission, (3) indirect or surface transmission. Amongst these Direct Method is most desirable and gives satisfactory results. The indirect and surface transmission methods are not preferred as the amplitude of received signal is much lower than in case of direct methods .

1.4.2.2 Advantages

a. Test procedure is simple and standardized by ASTM.
b. Easily implemented in the laboratory as well as in field as it can be performed on laboratory sized test specimens and concrete structures
c. Ensures quality control of concrete in field by investigating uniformity of concrete
d. Equipment is easily available and portable

1.4.2.3 Limitations

Compressive Strength of concrete depends upon number of variables which is why use of UPV for estimation of strength of concrete is not recommended unless any correlation testing has been conducted.

1.5 REVIEW OF PENETRATION TESTS AND ULTRASONIC PULSE VELOCITY METHOD

Reinhardt and Groose (2004) studied setting and hardening continuously of mortar and concrete. Mortar was prepared in ratio 1:0.5:3 (cement : water : fine sand).With rapid hardening Portland cement the wave velocity began from 600ms and gradually increased to 3500m/s in 2 hours, and small variation was observed with use of 0.5,0.55 and 0.6 w/c ratios whereas in case of Rapid Hardening Cement, with increase in w/c ratio from 0.5,0.55 to 0.6 the velocity obtained was 4200m/s, 4000 m/s and 3400 m/s respectively. began from 600m/s

hence velocity was affected with w/c ratio for Rapid Hardening cement. Effect of admixtures i.e. retarders, accelerators and an entraining agent was also studied and prominent changes could be seen only in case of retarders. First maximum point in curvature on velocity versus age plot is beginning of setting and velocity of 1500 m/s marks end of setting.

Kamada et al. (2005) studied setting /hardening properties for which experiments were divided in two phases. In first phase, physical properties were evaluated using viscometer and in second phase chemical propertied were studied using SEM and XRD to investigate hydration product was carried out. In first phase high early strength cement with liquid base oxycarboxylate retarder, 0.2% and 0.4% of cement weight was used; w/c ratio was kept 0.45. In second phase cement pastes were made with w/c ratio of 0.3 and retarder and super plasticizer of 1% and 1.5% by weight of cement. It was observed that in first phase initially velocity was that of in air(340 m/s) and inflexion occurred when velocity reached that of in water (1500m/s), this was stage one in which with the increase in hydration products velocity increased. Stage two is marked by region between two inflexion points and from second inflexion point to the end of measurement was stage three. With addition of retarder dosages the stage durations delayed. Hence with velocity of wave, velocity gradient and time of inflexion point setting states of cement paste can be determined. In the second phase, the velocities attained were larger than that in just phase; at start they were in range of 1100-1600m/s and increased to 1800m/s. It was because w/c ratio was large in first phase. Further final velocity of 4000m/s was recorded with short duration stage 2.

Trtnik et al. (2008) discussed the application of transmitting the ultrasonic wave in order to estimate the initial setting time of cement paste .They studied the influence of water/cement ratio, type of cement, curing temperature, cement fineness, and clinker compositions on the relationship between ultrasonic pulse velocity and the initial setting time . For this twelve cement pastes were used, in the initial stage no Vp was observed and wave propagated through water like viscous suspension while at the start of stage 2 velocity of 300 m/s was obtained between 20 and 60 minutes and within 2nd stage wave velocity increased close to that in case of water and at the end of the stage 2 first inflexion point appeared. In the stage 3 Vp increased to 3000 m/s and second inflection point appeared, further small increase of Vp at end of stage 3 and plateau is reached which is defined as stage 4. Higher w/c ratio show lower ultrasonic pulse velocity, with high temperatures evolution of Vp was rapid in the beginning, higher fineness resulted in higher evolution of Vp due to rapid hydration and lower amount of C3A resulted in slower evolution of Vp.

Sleiman et al. (2010) discussed the study on the Vicat Test and its use to determine intrinsic rheological parameter, then examined the possibility of using alternative tests to the Vicat needle method to monitor setting time of cement pastes, and tried to relate the penetration length to the cement paste yield stress. The plate test device philosophy used by Tchamba et al. and presented by Amziane et al. was adapted to the Vicat needle geometry which remains static and immersed in the studied cement paste during the entire test time. Initially a slow steady increase of the yield stress with time was observed followed by dramatic increase of the yield stress, indicating the change of the cement paste from fluid to solid state. The test results obtained by deformation measurements for normalized consistency cement paste depicted that the deformation increased quickly, contrariwise the yield stress was almost constant. The end of this stage corresponded to the beginning of the setting period. After that the deformation increased slowly. Yield stress increased quickly indicating the transition of the cement paste from fluid to solid state, end of this stage corresponded to the end of the normalized setting period. It clearly appeared that the cement paste's rapid deformation allows measuring the cement paste yield stress. As a result, the static vicat needle was found to be sufficient to monitor the yield stress evolution and was able to monitor the evolution of a cement-based paste during thixotropic reversible period and during setting period.

Lootens et al. (2011) inferred that Penetration tests are widely used to follow cementitious materials during setting. The case of penetrometer was examined in detail with various needles. All results combined well to demonstrate that the measured force scales with the yield stress of the tested material. Cement pastes were prepared with water to cement ratio w/c of 0.3. Penetrometer and the needle was driven into the sample until the tip was fully submerged , sample holder was rised at 1 μm/min, while the force on the needle was recorded. The penetration force was equal to the load of the needle (300 g) and the yield stress could be deduced from the penetration depth . As the needle was stopping, the flow may again be considered as slow and the contribution of the plastic viscosity neglected. Since the critical shear strain in cementitious materials was more or less constant, this force scaled directly with shear modulus and thus with results from ultrasonic techniques.

Zhu et al. (2011) investigated the effects of air voids on ultrasonic wave propagation and related its parameters to setting times of cement. The variation of air void content 0.1 to 5.3 % by cement paste volume with 0.4 and 0.5 w/c ratios and using both compressional (P) and shear (S) waves were monitored. Test results of vicat show air entrained specimens have delayed setting and the increase in setting time is not linear. In UPV case of P wave with

0.2% AEA specimen at 2 hours the arrival of P wave is much later than non- AEA moreover signal had low amplitude and was noisy .With increase in AEA the P wave velocity decreased from 1500 m/s to 200 m/s . The AEA specimens with w/c of 0.5 as compared to those with w/c ratio of 0.4 show more decrease of Vp at later stages . In case of S waves very little effect in specimens of w/c ratio of 0.4 and with w/c of 0.5 variation with ir content could be seen . The effect on P wave velocity is more at early stages and also more than the effect of S wave velocity.

Gams and Trtnik (2013) presented TG parameter in order to determine the transition of cementitious materials from liquid to solid state. The characteristic points in the evolution of TG parameter and penetration resistance were correlated for different samples. Two types of cements (differ in fineness) and two types of aggregates(differ in shape) were used. Specimens of $50 \times 50 \times 50$ mm^3 and $80 \times 80 \times 80$ mm^3 were prepared and influence of maximum aggregate size , amount of aggregate , type of aggregate , w/c ratio and cement type were analyzed. When no penetration resistance was offered by material it depicted stage 1 and 2 on TG-t curves, when material offers resistance to penetration TG parameter shows rapid increase. Further on solidification no changes in TG parameter could be observed . Higher w/c ratio, lower cement fineness and increase in maximum diameter of aggregate resulted in prolongation of the beginning and ending of setting periods resulting in longer t_{CP2} and t_{CP4} times.

Trtnik and turk (2013) studied the influence of superplasticizers on the formation of structure of cement pastes at early ages using an ultrasonic wave transmission method . For this study they used type I ordinary Portland, two sulfonate naphthalene formaldehyde and two comb shaped polycarboxylate ether SPs. It was observed that the evolution of Vp-t curves were delayed and this delay increased with increasing dosage of admixture and the delay is more in case of PCE type of SPs . The lengths of second stage increased in case of each SP while the third stage length was increased by both PCEs whereas sulfonate naphthalene-formaldehyde types of SP decreased the length

Liu et al. (2014) extensively investigated the effect of air voids by P wave velocity parameter in the fresh state and need to access both sides of a structural member . For this eight mixtures were investigated in which the effects of w/c ratio , size of coarse aggregate on setting time and wave velocities were studied. It was observed that as the w/c increased

the setting times increased significantly with coarse aggregate being river gravel and the coarse aggregates had much higher velocities than cement paste and mortar .

Trtnik and Gams (2015) addressed a new US approach for observing initial compressive strength development of different cement based materials with different compositions. Nine different mixtures were used which studied the effect of: (1) water/cement (w/c) ratio, (2) cement type , (3) aggregate shape , and (4) maximum aggregate size on the development of early age compressive strength and US characteristics was analyzed. Tests were conducted on cubic specimens with the dimensions of 70 x 70 x 70 mm. It showed the strong influence of formation of ettringite on P-wave velocity which had small influence on stiffening and compressive strength., the Vp velocity increased substantially at time tfci .

Carette and Staquet (2016) studied the influence of eco –binders by ultrasonic P and S wave transmission on setting time in mortar and concrete. Limestone, Blast furnace slag and gypsum were used; five composition concrete were made; Reference Mix (C1 contains only Portland cement), C2 (Blast furnace slag) and C3(Limestone filler). C4 combined LF and BFS. With high w/b ratio from C1 (w/b=0.4) to C5 (0.57=w/b). P and S waves velocities decreased due to increase in particle spacing. Due to replacement of 30% LMF both initial and final setting time are accelerated. Due to 70% BFS replacement setting and hardening are delayed. But when 30% of BFS was replaced by LMF the setting process shifted to an earlier age and duration of setting also decreased.

Daake and Stephan (2016) monitored setting of cement containing super plasticizer by ultrasonic measurements. w/c ratio was kept 0.35 and SP with 0.25%, 0.8% and 1.4% dosages by cement weight; another polycarboxylate based P-wave velocity and wave acceleration(V_p) were studied. V_p increases with increase aggregate size whereas $V_p´$ was independent of aggregate size and attained peak in 3-6 hours after hydration started. Both V_p and $V_p´$ Decrease with increase in aggregate content. With increase in SP the development of V_p was delayed due to its retarding effect, and the maxima was also delayed in case of V_p.

Lootens and Bentz (2016) investigated relation of porosity and hydration with setting and early age strength development. Two types of cement CEM I 42.5 and CEM II 42.5 and chemical admixtures namely chemical accelerator $CaCl_2$, retarder (P) and seeding admixtures for nucleation sites for C-S-H gels were used with w/c of 0.35 . To study the evolution of shear wave attenuation with time shear sensors of 1 MHz frequency were used. Graph between heat release, strength, velocity of wave and time depicted the linear portion of

strength curve was corresponding to increase in velocity which was attributed to clustering of particles , then the rapid strength gain marked beginning of setting then in the last zone heat and strength curves overlapped with slow rate of strength development. When the heat release is normalized per unit volume of water which is initially present in the mixture linear relationship between this heat release and strength exists, according to conventional methods this existed from one day and beyond but Contiuous measurements using ultrasonic indicates that this relation is valid from 8h onwards.

1.6 OBJECTIVE OF THESIS

Wave propagation characteristics of amplitude and velocity are affected by setting of concrete during early age and are used to monitor the entire setting and hardening process of concrete. Till date NDT techniques of Ultrasonic Pulse Velocity (UPV), Penetration Tests and Rebound Hammer etc. have been used to relate the setting and hardening of concrete at early ages. NDT latest tools of Ultrasonic Guided Waves (UGW) and Acoustic Emission Technique (AET) have been investigated in this study to monitor the setting of concrete modified with Silica Fume (SF) as a replacement of cement in varying proportions. With increase in the use of SCMs in concrete, it becomes a necessity to validate these emerging NDT of UGW and AET methods for the detection of changes in setting and hardening patterns. A comparison has been drawn between the various NDT tools of UPV, UGW and AE techniques and then validated using compressive strength and SEM/EDS analysis .

1.7 LAYOUT OF THESIS

Chapter 1, the process of setting and hardening of concrete with the importance to study the same and the previous research on it using various methods has been discussed. The objectives of thesis has been assigned.

Chapter 2, the Supplementary Cementitious Material used in this study that is Silica Fume has been discussed . The production, advantages, applications, physical and chemical properties and work done till date in terms of setting, compressive strength and SEM/EDS analysis has been detailed.

Chapter 3, highlights the theory of Ultrasonics and Acoustic Emission. The modes of wave propagation, its classification, applications, advantages, limitations and previous research are explained.

Chapter 4, the experimental setup, specimens used and methodology of conducting various tests included in this study have been explained in detail .

Chapter 5, results and discussions of guided wave, acoustic emission, upv, compressive strength and sem/eds have been presented and discussed.

Chapter 6, conclusions from various techniques are drawn out.

In the end, references cited in the work have been listed.

CHAPTER 2

SILICA FUME AS SUPPLEMENTARY CEMENTITIOUS MATERIAL

2.1 GENERAL

Supplementary cementitious materials (SCM) are commonly used in concrete these days as they improve the microstructure and durability of concrete. They may be in the form of natural pozzolan or industrial by-products. Silica Fume is one such SCM which has been found to be most effective as it not only enhances the strength of concrete (Alaa et al., 2009; Bhanja and Segupta, 2005 and Enfedaque et al., 2010) but also through pore size refinement , matrix densification and reaction with free lime improves the durability of concrete (Song et al., 2010) to great extent. All the properties are found to be modified when an optimum amount of silica fume is used. Portland Cement is nowadays primary material used in construction and previous research work shows that silica fume has enhanced both mechanical and durability properties of Portland Cement Concrete (Nochaiya et al ., 2010; Shih et al., 2006 ;Gleize et al., 2003;Wongkeo and Chaipanich, 2010 and Siddique 2011) . High rise buildings demand the use of High performance concrete and Ultra High Strength Concrete in construction work as they lead to reduction in the size of structural elements and Silica Fume is the key ingredient of HPC and UHSC.

Silica fume is defined as "a very fine non crystalline silica produced in electric arc furnaces as a byproduct of production of elemental silicon or alloys containing silicon'' by the American concrete institute (ACI). It can exhibit pozzolanic as well as cementitious properties. It is a grey colored powder, similar to Portland cement. Silica fume is known by other names like micro silica, condensed silica fume, volatilzed silica or silica dust. Silica fume (SF) is produced as a byproduct in the silicon and ferrosilicon industry during the smelting process. When high purity quartz is reduced to silicon at temperatures in excess of 2000 ^{0}C , SiO_2 vapours are produced which are further subjected to low temperature zone to oxidize and condense to tiny particles consisting of non- crystalline silica. Silica Fume consists of spherical particles with mean diameter of about 0.15 microns and is a very fine powder with high specific surface area (15000-25000 m^2/ kg). Size of silica particle is 100

times smaller than average size of cement grain thus 10 percent by mass of cement will give 50,000 – 100,000 silica particles per cement grain.

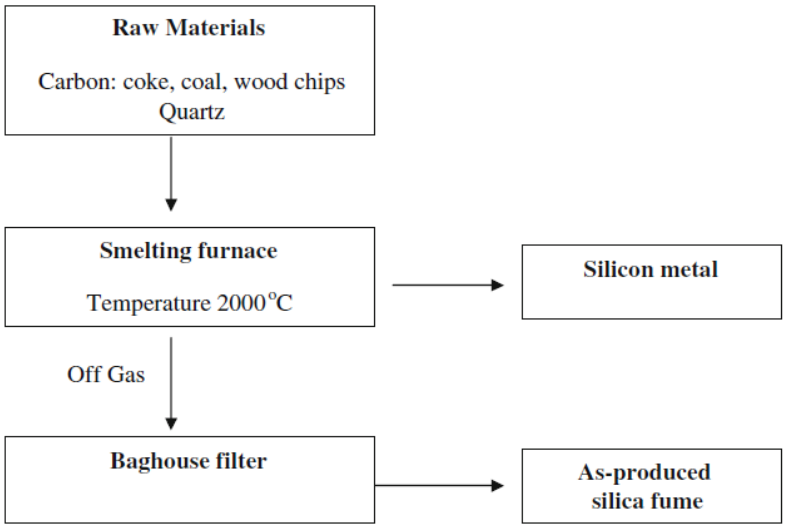

Figure 2.1: Schematic diagram of silica fume production (Siddique, 2011)

2.2 PHYSICAL PROPERTIES

Silica fume particles are extremely small spherical particles. Generally more than 95% of the particles are finer than 1 µm. Its colour is white or grey. Its typical physical properties are given in **Table 2.1**.

Table 2.1: Physical Properties of Silica Fume (ACI, 2000)

Property	**Typical Values**
Particle Size (µm)	< 1
Bulk Density (kg / m^3)- (a) as produced	130-430
(b) Slurry	1320-1440
(c) Densified	480-720
Specific Gravity (g / cm^3)	2.22
Surface Area (BET)	13000-30000
45 µm residue (%)	0.1-50

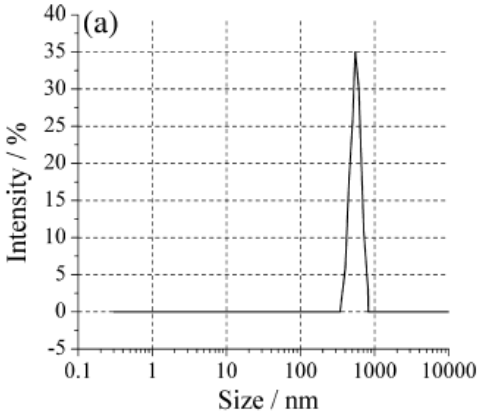

Fig 2.2: Particle size distribution of silica fume (Zhang et al ., 2016)

2.3 CHEMICAL COMPOSITION

Silica fume primarily consists of pure silica in non-crystalline form. It has a very high content of amorphous silicon dioxide generally more than 90 % and small amounts of iron, magnesium, and alkali oxides are also found. Oxides analyses of silica fume by some authors are given in **Table 2.2**.

Table 2.2: **Chemical Composition (%) of Silica Fume Samples**

Oxides	**Yazici (2008)**	**Nili and Ehsani (2015)**	**Sanjuan (2015)**
SiO_2	92.26	85-95	94.49
Al_2O_3	0.89	0.5-1.7	0.252
Fe_2O_3	1.97	0.4-2	0.084
CaO	0.49	-	0.452
MgO	0.96	0.1-0.9	0.278
K_2O	1.31	0.15-1.02	0.448
Na_2O	0.42	0.15-0.2	0.186
SO_3	0.33	-	0.130
LOI	-	1.5-2.5	2.89

2.4 REACTION MECHANISM

Mechanism of silica fume in concrete is studied under three roles:

(a) **Pore-size Refinement and Matrix Densification**: Reduction in the volume of large pores is caused due to silica fume in portland cement at all ages as because of its fineness it acts as filler material and occupies the spaces between cement grains.

(b) **Reaction with Free-Lime (From Hydration of Cement)**: Presence of CH crystals can cause cracks as they are a source of weakness. Due to presence of siliceous and aluminious material in silica fume reacts and decreases the amount of these crystals and forms binding calcium silicate hydrates (C-S-H gels).

(c) **Cement Paste–Aggregate Interfacial Refinement**: Silica fume reduces the thickness of transition zone between cement particles and aggregate Further the orientation of CH crystals in transition zone is reduced. This improvement in transition zone improves the mechanical as well as durability properties

2.5 ADVANTAGES

I. Fresh Properties

(a) Reduced Bleeding

(b) Increased cohesion

II. Hardened Properties

(a) High early compressive strength

(b) High tensile, flexural strength, and modulus of elasticity

(c) Increased toughness (Seze, 2012; Bhanja and Sengupta, 2005)

(d) Higher bond strength (Sezer, 2012; Bhanja and Sengupta, 2005)

III. Durability Properties

(a) Enhanced durability i.e. sulphate resistance (Wee et al ., 2000 and Sezer, 2012)

(b) Very low permeability to chloride and water intrusion (Eshmaiel and Sadeghi, 2009)

(c) Increased abrasion resistance on decks, floors, overlays and marine structures (Nader and Hamidou, 2007)

(d) High electrical resistivity and low permeability

(e) Superior resistance to chemical attack from chlorides, acids, nitrates and sulfates and life-cycle cost efficiencies (Eshmaiel and Sadeghi, 2009)

(f) Good fire resistance (Morsy et al., 2008)

2.6 APPLICATIONS

i. **High Performance Concrete (HPC) :**

(a) Marine structures, bridge deck overlays, highways bridges and parking decks which are exposed to salts, seawater, freeze thaw cycles and traffic and may deteriorate under such exposure conditions and steel used will corrode are protected by the use of silica fume due to higher strength (Alaa et al., 2009;Bhanja and Segupta, 2005;Enfedaque et al., 2010) and reduced permeability (Song et al., 2010) , hence reducing the maintenance cost.

(b) Prestressed and precast long span girders in bridges.

(c) High rise buildings due to reduction in size of structural elements and hence increasing the usable space

ii. **Oil Well Grouting** — silica fume produces blocking effect which prevents gas migration, it provides improved flow, decreased permeability, used for leak repairs, closings of depleted zones and in gout as hydraulic seal .

iii. **Silica-fume Shotcrete** — Greater bonding strength ensures superior shotcrete for use in mine tunnel lining, rock stabilization, marine columns and piles and deteriorating bridge. Use of silica fume delivers greater economy, time savings and more efficient use of sprayed concrete and thicker applications with each pass of the shotcrete nozzle.

iv. **Repair Products**—silica fume is used in a variety of cementitious repair products due to its ability to increase surface adhesion. It is ideal in underwater grouts as it is cohesive, decreases permeability and due to increased resistance to aggressive chemicals.

2.7 REVIEW OF CONCRETE CONTAINING SILICA FUME

Sidhu (2001) studied early age behavior of concrete containing silica fume. Cement conforming to IS 8112-1989 was used. M30 and M50 grades of concrete were prepared; until 7 days not much affect of silica fume was observed on compressive strength. Whereas influence of silica fume was observed between 7 and 21 days. Maximum increase in strength, modules of elasticity was observed with concrete containing 15% silica fume.

Ding and Li (2002) studied properties of concrete containing metakaolin and silica fume.The concrete specimens consisted of w/b ratio of 0.35, 0,5,10 and 15% replacement by metakaolin or silica fume and 40% sand/aggregate ratio. Ratio of 1: 1.55: 2.33 (Binder :

Fine aggregate : Coarse Aggregate) in which binder included cement and silica fume or MK. Results show that with increasing percentage replacement of cement by silica fume the compressed strength increased.

Kamada et al. (2005) studied setting /hardening properties for which experiments were divided in two phases. In first phase, physical properties were evaluated using viscometer and in second phase chemical propertied were studied using SEM and XRD to investigate hydration product was carried out. In first phase high early strength cement with liquid base oxycarboxylate retarder, 0.2% and 0.4% of cement weight was used; w/c ratio was kept 0.45. In second phase cement pastes were made with w/c ratio of 0.3 and retarder and super plasticizer of 1% and 1.5% by weight of cement. In stage I only cement particles were observed and acicular crystals increased in stage two and hydration products were rarely found in SEM images. X-ray diffraction was further carried out. Peaks occurred in stage two and during stage 3, not much change in diffraction pattern could be observed. These peaks and acicular crystals which appeared were found to be ettringite crystals. The ettringte crystals resulted in denser cement paste texture and increase in wave velocity of cement paste.

Qing et al. (2007) discussed influence of nano-SiO_2 on properties of cement paste and with that cement paste containing silica fume. Ordinary Portland cement and cement containing nano SiO_2 or silica fume: water: super plasticizer ratio of 1:0.22:0.025 was used. 2, 3, and 5% cement was replaced with silica fume. The depth of penetration increased and paste became thin with increasing levels of silica fume; thus silica fume had retarding effect and this effect decreased as the silica fume content increased. With increase in silica fume content; compressive strength decreased at 1 and 3 days but at 28 and 68 days the strength of silica fume samples was higher than that of control concrete. SEM results showed that in case of control specimen CH crystals had hexagonal like shapes and maximum size of crystal observed was 10µm whereas in case of silica fume size of 7µm of CH crystal was observed thus concluded that it was efficient in reducing the size of CH crystals at interface of paste aggregate.

Xuan et al. (2009) investigated influence of silica fume on interfacial bond . For this silica fume additions 0, 6, 9 and 12 % by mass of cement and different cement dosages 400 and 450 kg/ m^3 were used. Micro hardness test and pull out tests were studied to evaluate interfacial bond properties as SF content increased pull forces became higher hence indicating

interfacial bond strength was stronger but with increase from 9 to 12 % SF the increase was not significant which shows that an optimal SF dosage exists . In near surface zone of concrete weak micro hardness layer exists thickness of which decreases with addition of silica fume. The wall effect and micro bleeding water accumulation under aggregates influence the ITZ of concrete in near surface layer.

Kar et al (2012) estimated C-S-H and calcium hydroxide in pastes containing silica fume and slag. Portland cement (ASTMC 150); Ground granulated blast furnace slag (ASTMC 989) and silica fume (ASTMC 1240) were used w/b of 0.3, 0.4 and 0.5 and 35%; 45% cement replacement by slag whereas 35 % and 10 % silica fume cement slag replacement were studied at 1,7,28 and 90days. Ca/Si ratio for pure Portland Cement, that containing slag and silica fume and the one with slag only obtained from no linear optimization and that from SEM/EDS microanalysis were alike.

Duan et al. (2013) studied the effects on interfacial transition zone, pore structure and compressive strength of of concrete containing metakaolin, silica fume and slag. For this tests like SEM, mercury intrusion porosimetry (MIP), micro hardness testing were carried out at 28 days and 180 days . the tests revealed that 10 % mineral admixture as replacement material makes matrix denser as needle like ettringite is reduced and further production of C-S-H and calcium aluminosilicate hydrates . With matrix admixture addition ITZ becomes denser and the sequence is metakaolin > silica fume > slag which is attributed to microaggregate filling and pozzolanic effect

Birick and Sarier (2014) compared cement mortars containing nano silica , silica fume and fly ash by various techniques which include Fourier infrared Spectrometer (FTIR) , thermogravimeter – differential thermogravimeter (TG-DTG) and scanning electron microscop (SEM). OPC was used and mineral admixtures were used as 5 % and 10 % by weight and tests were conducted after 7 and 28 days. At 7 days of curing NS5 had greater compressive strength as compared to OPC while SF5 and FA5 had slightly more and less respectively with respect to OPC.Whereas at 28 days both NS5 and SF5 showed improvement in strength as compared to OPC, NS5 showing much percentage increase while that of FA5 was still less than that of OPC . Whereas with increase in percentage replacement of mineral admixtures from 5 to 10 percentage strength increased in all 3 (NS, SF and FA) both at 7 and 28 days of curing with order of percentage increase being NS > SF > FA , same pattern follows for flexural strength. At 7 days heterogeneous distribution of C-S-H, CH

grains and needle like ettringite crystals could be seen on fractured surface of OPC samples .Whereas at 7 days samples of SF 10 and FA 10 show condense packing of cement hydration products , further between C-S-H crystals, CH and ettringite crystals were visible with FA and SF particles dispersed throughout the paste. In case of NS10 clusters of NS particles were dispersed in hydrated products of cement. In comparison to SF10, FA10 and OPC, CH grains are less visible in case of NS10 At 28 days OPC, SF10 and FA 10 apart from C-S-H, small and large CH crystals were prominent in OPC than in case of FA10 and SF 10 and that of NS10 varied as large crystals of CH were not observed and denser and compact hydration products appeared .

Sanjuan et al. (2015) studied the effect of fineness of silica fume on strength characteristic of Portland cement. Coarse silica fume having residue of 32.11 % SF 1 (A) on 45 micrometer sieve was grounded to have residue 4.13 % SF 1 (B) and SF 1 (C) of 0.98 % further Portland cement was replaced by 25 % . It was concluded that SF 1 (C) and SF 1 (B) with 25 % replacement gives higher strength whereas SF 1 (A) does not give good results at such high replacement levels . Further SF 1 (C) and SF 1 (B) have same strength after 28 days of curing and both are suitable for production of high performance mortar / concrete. High fineness silica fume is much better from permeability point as well as due to chemical effect on microstructure of cement / mortar.

Muller et al. (2015) studied microstructure of cement paste containing silica fume using HNMR relaxometry. White Portland Cement was used with pastes containing 10% silica fume by mass of cement with addition of silica fume at early age nucleation of C-S-H gel and chemical reaction of cement with water enhanced. The ratio of Ca/ (Si + Al) of C-S-H decreases due to pozzolanic reaction which is due to addition of silicon, hence less calcium ions in inter layer. Further Ca/Si ratio decreased significantly. It was observed that ¼ of Calcium was used to form C-S-H when reacted with silica fume and rest of calcium ions came from C-S-H previously formed in early stages with reaction with alite.

Nili and Ehsani (2015) investigated effect of cement paste and transition zone on strength development of concrete containing nanosilica and silica fume. The heterogeneous deficiencies of concrete could be overcome by use of pozzolanic materials for this purpose NS and SF are used, NS at 0 % , 1.5 % , 3% , 5 % and 7. 5 % and SF at 0 %, 5 % and 7.5 % by weight of cement. Compressive strength tests were carried out at early and later stages and to know the reasons for results obtained SEM , XRD and EDS results were obtained , 15

samples were prepared , compressive strength test conducted at 3, 7 , 28 and 91 days . The results show that NS addition enhanced strength at 3 and 7 days by much higher amount than in case of SF addition in pastes .This strength followed from 0 to 5 % NS replacement , but with 7.5 % ns strength of cement paste decreased which was due to agglomeration of nano particles due to vander wall forces and high specific area . Same trends appeared in case of concrete specimens.

Rossen et al. (2015) studied compositions of C-S-H in pastes with addition of silica fume. Portland cement and silica fume were used , tube samples of 35mm diameter and 70 mm height were made and kept for 24 hours at 10,20 and 38^0C and they were then removed and kept at same respective temperature in larger moulds of 38 mm diameter and 62 mm height. It was observed that with addition of silica fume CH content depleted and hence Ca/Si ratio which was earlier 1.4-1.5 dropped to 1.0 in the absence of CH. It indicated that when CH is present C-S-H which is formed is Calcium rich. But at later stages SiO_2 reacts with CH and its content reduces which further leads to C-S-H gel which is rich in Si and Ca/Si reduces. Thus due to reaction of CH with silica fume leads to consumption of calcium and hence loss of calcium from C-S-H. Thus changes in pore solution occur as calcium concentration decreases and pH also decreases with increase in levels of silicon concentration .

Zhang et al. (2016) investigated effect of 5 % and 10 % densified silica fume in paste , mortar and concrete by various tests such as non- evaporable water content , compressive strength and interfacial transition zone in concrete . The water to binder ratio is 0.29 and 0.24 were used. It was observed that compressive strength of paste, mortar and concrete at later stages increased and in concrete it was most significant, difference became smaller in concrete at later stages. At same water content and at same replacement level raw silica fume has higher compressive strength than densified silica. Addition of silica fume improves the orientation degree and Ca $(OH)_2$ content at interface of aggregate and matrix reduced which lead to improvement of interfacial bond and this ITZ is main factor which causes differences in effect of silica fume on paste , mortar and concrete . Moreover it was found that agglomeration occurs in pastes which does not participate in hydration whereas in concrete so much problem occurs .Silica Fume increased non-evaporable water content at later stages of pastes due to pozzolanic activity.

2.8 CLOSING REMARKS

Silica Fume is the most common SCMs used these days due to its very many advantages amongst which increase in strength and improvement in durability are the most important .Because of which it has many applications and is a chief ingredient of High Strength Concrete and High Performance Concrete . As it is a common SCM in concrete nowadays it becomes necessary to investigate its early age properties of curing using non-destructive tools to facilitate ND evaluation. The focus of research is that the Non – Destructive Techniques of UGW and AE pick up the initial setting and hardening of silica fume modified concrete effectively.

CHAPTER 3

WAVE PROPAGATION AS A NON–DESTRUCTIVE TESTING TOOL

3.1 GENERAL

The role of structure engineer is to enforce a codal provision of design and in addition to the demand of structure serving well. During its design life its safety factors are taken during analysis and designing. A structure which is capable of taking load needs regular checks to make sure that no substantial damages occur; as if any unavoidable deterioration occurs it can lead to weakening of structure and can emerge as a major problem. There exists a need for continuous monitoring of structures and evaluating them for repair and rehabilitation be made if necessary. This concept of monitoring structures condition is called Structural Health Monitoring (SHM). Health may be defined as the ability to perform and main the integrity throughout life of structure; Monitoring refers to diagnosis and damage is a structure, material or functional failure. The structures have been monitored for any damage during earlier times as well. But in recent years lot of research studies have been carried out to increase the accuracy and reliability of these inspection techniques. Traditional structural inspection consisted of visual inspections followed by advanced non-destructive techniques such as eddy currents, ultrasound etc. Traditional methods were labor intensive and costly and required accessibility of the structure to be examined. This led to the need of techniques through which structural data would be collected automatically and further analyzed to identify the damage in the structure.

The main objective of SHM is to detect damage and take decisions based on present day health of the structure. Certain steps are carried out to diagnose the state of the structure and take decisions regarding its maintenance and performance

1. Damage detection
2. Damage localization
3. Damage detection and type

4. Damage prognosis- Refers to decision making based on structures remaining life and expected future chances

Technique for SHM;

1. Local techniques

2. Global techniques

1. **Local Techniques**: These are based in visual inspection or certain not developed early to mid 1960's. These are as follows:

a) Impact Eco Method

b) Eddy current Method

c) Magnetic Particle Testing

d) Visual and Optical Testing

e) Ultrasonic Testing

f) Acoustic Emission Testing

2. **Global Techniques**: In this technique dynamic characteristics of structure are used to identify the damage and reduce the need of manual inspection. These techniques are beneficial as there is no need of direct access to structural member and no previous knowledge of structural damage is needed; thus reduction in time and cost to access the structural damage.

Global Techniques include:

i) Dynamically Measured Flexibility

ii) Mode Shape Changes

iii) Frequency Changes

iv) Inverse Problem Strain Mode Shape Changes.

Elastic propagation method involving Ultrasonic Guided Wave which is active in nature and Acoustic Emission which is passive in nature are discussed in detail.

3.2 USE OF ULTRASONICS

3.2.1 Basic principle

Sound audible to humans is in the frequency range of 20 to 20,000 Hz (cycles per second). Ultrasound simply refers to the sound above the frequency range of human hearing. Any disturbance occurring in an elastic medium propagates in medium as a mechanical sound wave by the vibrations of molecules or atoms which are called elastic waves. Ultrasound waves or ultrasonic waves are elastic waves with frequency greater than 20,000 Hz and exist in solids, liquids, and gases.

High frequency sound energy is used in Ultrasonic Testing. Inspection by Ultrasonic to detect flaws, evaluate the flaws, measure dimensions and determine characteristics of material can be carried out. **Figure 3.1** shows pulse / echo configuration to illustrate the working of UT. The inspection system constitutes of pulser/receiver, transducer, and display devices. High voltage electrical signals are generated by pulser/receiver which is an electronic device and high frequency ultrasonic energy is generated by the transducer. The sound energy propagates through the materials in the form of waves. In case of presence of discontinuity in the path of wave, part of it will be reflected back and will get transformed by the transducer into an electrical signal which will displayed on the screen. The travel time of the signal is related to the distance it travels. The received signal can be used to get information about the location of flaw, its size and orientation.

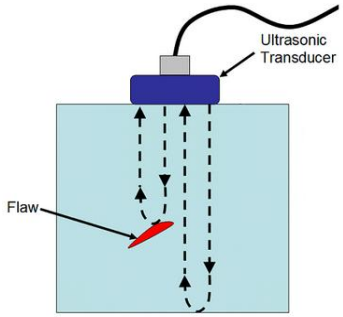

Fig 3.1: General ultrasonic inspection principle (pulse echo method).
(http://www.ni.com)

3.2.2 Methods of ultrasonic testing

1. Pulse echo method

2. Pulse transmission method

3. Two Transducer Method

1. **Pulse echo method: Figure 3.2** shows the piezoelectric transducer is placed in such a way that its longitudinal axis is perpendicular to the surface of the test material. The transducer transmits and receives ultrasonic waves. The waves are transmitted and received at the same transducer. The transmitted waves are reflected back either by the opposite face of the material or due to presence of discontinuities, voids, or inclusions in the material. The reflected wave is then converted into an electrical signal . This signal is then processed and displayed on monitor screen. Information such as thickness of the material, depth of the flaws etc is obtained from this received signal .

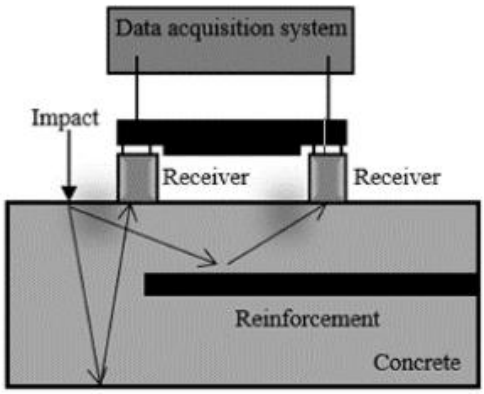

Figure 3.2: Principle of pulse echo method of ultrasonic testing (Zaki et al ., 2015)

2. **Pulse-Transmission Method:** Two transducers are used such as one acts as transmitter and other as receiver. The transmitter and receiver are placed on two opposite faces of the material to be tested.

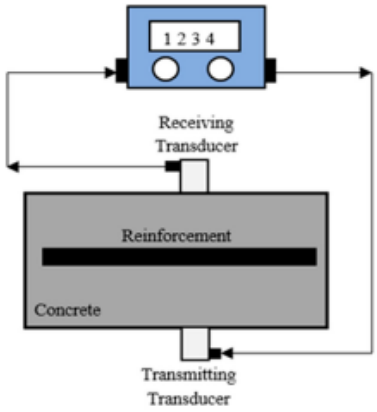

Figure 3.3: Principle of through transmission method of ultrasonic testing (Zaki et al ., 2015)

3. **Two Transducer Method:** Two transducers are used on the same side of specimen. The transmitter (T) transmits the pulse wave which gets reflected and is received by receiver (R). The system is also known as twin or T-R probes. They can be used to measure wall thickness or to detect damage in a plate as shown in the **figure 3.4.**

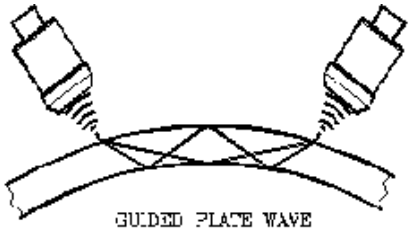

Figure 3.4: Transducers attached at an angle to the plate (http://www.ndt.net)

3.2.3 Modes of wave propagation:

The ultrasonic waves propagate in a number of ways in a medium. On the basis of the mode of particle displacement, these waves can be classified as given.

a) Longitudinal or Compressional waves (L-waves)
b) Transverse or Shear waves (S-waves)
c) Surface or Rayleigh waves
d) Lamb or Plate waves
e) Creeping or Head waves

Out of these longitudinal and transverse wave propagations are most important and are extensively used in ultrasonic NDT applications for Civil structures.

a) **Longitudinal or Compressional waves**:

They are also known as pressure or compressional waves. In these waves particles oscillate in direction of wave motion. Since energy travels through the atomic structure by a series of comparison and expansion movements theses waves can be generated in liquids as well as solids.

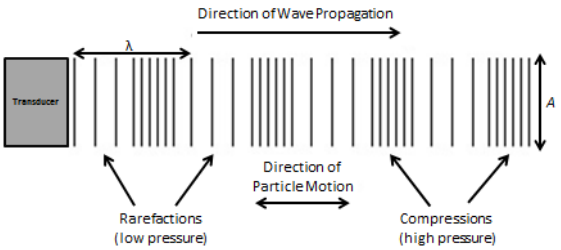

Figure 3.5: Propagation of longitudinal waves (http://viet-anag-jenius.blogspot.in)

b) **Transverse or Shear waves:**

In the transverse or shear wave the particles oscillate at a right angle or transverse to the direction of propagation. Shear waves propagate effectively in acoustically solid material and not in liquids or gasses. They are relatively weak as compared to longitudinal waves.

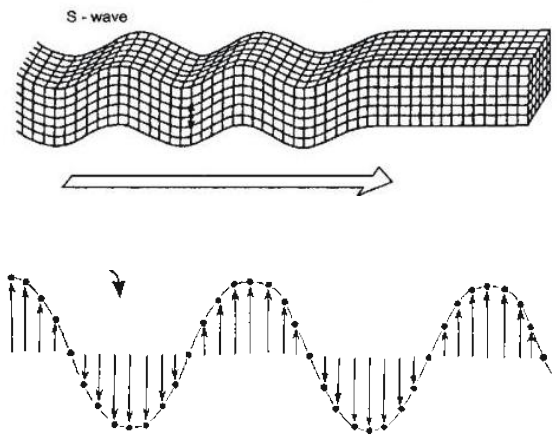

Figure 3.6: Propagation of transverse or shear waves (https://magareyphysics.wikispaces.com)

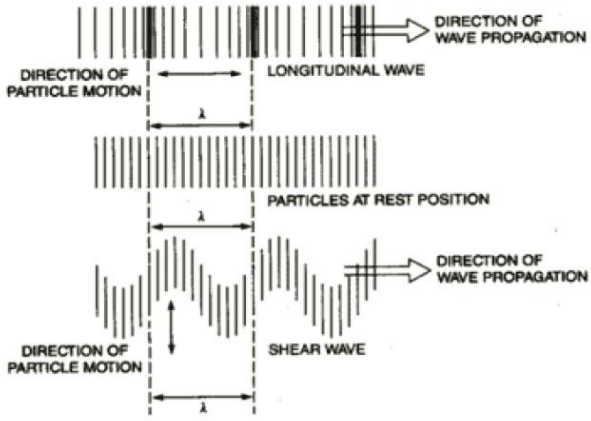

Figure 3.7: Particle movement showing the propagation of longitudinal and shear waves (www.ndt-ed.org)

c) **Surface (or Rayleigh) waves:**

Surface (or Rayleigh) waves travel the surface of a relatively thick solid material penetrating to a depth of one wavelength. The particle movement has an elliptical orbit as shown in the **Figure 3.8**. Rayleigh waves are useful because they are very sensitive to surface defects and are therefore used to inspect areas that other waves might have difficulty reaching.

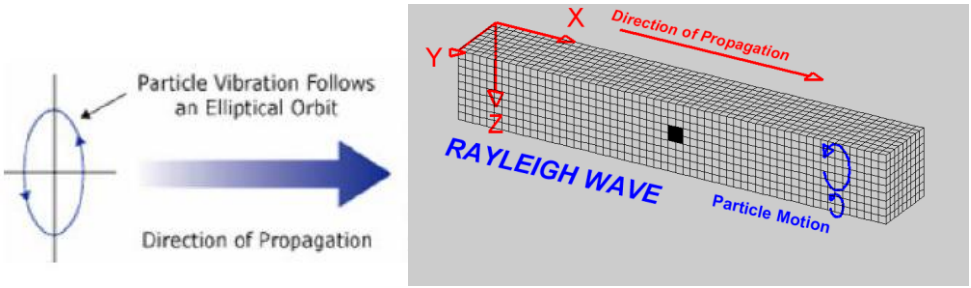

Figure 3.8: Propagation of surface or rayleigh waves (http://www.geo.mtu.edu)

3.2.4 Classification of ultrasonic waves

Depending upon NDT applications Ultrasonic waves are classified into two types , which are as follows :

i. Body waves or bulk waves.
ii. Surface waves or guided waves.

Table 3.1: Comparison of Body and Surface Waves

Body Waves	Surface Waves
✓ Attenuation is more as they propagate through the bulk material	✓ Surface waves are guided by the surface and geometry of the body and are termed as guided waves
✓ Inspection of large structures using longitudinal and shear waves is slow since in order to test the entire structure scanning is required .	✓ They have the potential to inspect large structures as once excited at a location on the structure , they will propagate covering many meters (Cawley, 2002)
✓ Classified as Longitudinal and shear waves .	✓ Classified as Rayleigh , Lamb , bar , cylindrical and bar guided waves as they propagate through bonded medium parallel to the plane of its boundary .

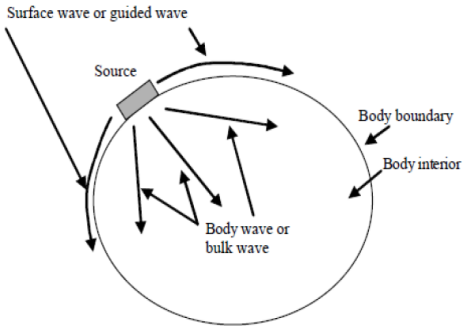

Figure 3.9: **Body waves and surface waves generated by ultrasonic source (Kundu, 2007)**

Classification of Guided Waves

Figure 3.10 represents various guided waves :

1. **Bar Waves** : Waves propagating through a rod or bar are termed as Bar waves .
2. **Cylindrical Waves** : Elastic waves are termed as cylindrical guided waves as they propagate through hollow cylinder or pipe . These are also termed as Lamb Waves as for cylinders two free surfaces inner and outer parallel to each other exist**.**
3. **Rayleigh Waves :** Guided Waves propagating along the surface of half space of a homogeneous structure are called Rayleigh Waves
4. **Lamb Waves :** Waves propagating through plates are called Lamb waves , plate type structures have two parallel stress free boundaries
5. **Rayleigh –** Lamb Waves :Waves propagating in multi-layered solid half space such that they are parallel to its free surface are called Rayleigh – Lamb Waves .

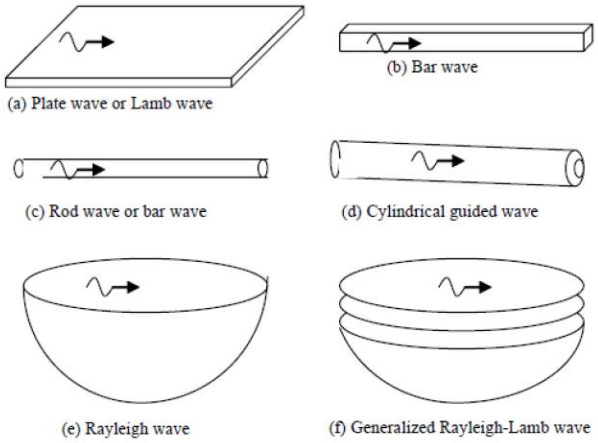

Figure 3.10: Different types of guided waves in various geometries (Kundu , 2007)

3.3 ULTRASONIC GUIDED WAVES

3.3.1 Need

Ultrasonic wave propagation offers an exciting way of monitoring the solidification of concrete . Velocity of ultrasonic pulses through a material increases as it solidifies. Thus, time taken by it to traverse through the depth of concrete is proportional to the degree of solidification. Ultrasonic waves attenuate very rapidly in fresh concrete. This limits the applicability of the technique in large structures. Concrete is almost always reinforced with steel bars. Ultrasonic waves propagate more easily through steel than concrete. The bars can be used as guides to carry the wave deep into the concrete. Thus, the attenuation of bulk waves through concrete can be alleviated and large structures can be monitored. As concrete sets, its bond with steel gets stronger. Studying the bond development between the rebar and concrete its setting process can be assessed . Guided waves were chosen because they have the capability of testing over long distances with a sensitivity often greater than conventional non-destructive testing techniques, have the ability to test multi layered structures, and are relatively inexpensive due to simplicity and sensor cost. By studying the modal displacement and energy distribution functions specific modes are identified that are sensitive to surface changes .

Two types of independent wave propagations namely compressional and shear exist in an infinite isotropic solid medium . These are non-dispersive and travel with constant velocities but when dimensions are closed and geometry constraints are imposed these become dispersive . Such dispersive waves are called *guided waves* (Reis et al., 2005) . Ultrasonic waves propagate as bulk waves and decay in amplitude due to spread of the wave front in infinite perfectly elastic material . But in finite perfectly elastic material because of structure boundaries the sound waves are reflected from boundaries and the energy remains within the medium as a guided wave, which propagates with constant amplitude .

The chief advantage of guided waves is that it can inspect long distances with eminent sensitivity from a single probe position. With guided waves hidden structures, structures under water, insulations can be inspected. Ultrasonic Guided Waves are used to inspect plates, multi-layer structures, rods, piping, rods, tubing and curved or flat layers on a half space (Rose, 2004)

3.3.2 Features :

- Since the waves travel along medium which is guided by its geometric boundaries, the geometry has a strong influence on the behavior of the wave (Redwood et al., 1960 and Achenbach, 1975).
- The velocity of guide waves vary with the wave frequency and geometry of the medium . Moreover at a given frequency different modes of guided waves can propagate (Sang-Young Kim et al., 2001).
- The interactions at the interface of two different materials result in Guided Waves. These interactions lead to reflection, refraction and mode conversion between longitudinal and shear waves.
- Guided Waves are dependent on wavelength and frequency and they exist at a particular combination of frequency, wave number and attenuation.

Dispersion of waves occur due to complex effect of boundaries and due to this dispersion different modes are generated which have frequency dependent properties. The dispersion curves represent the velocity –frequency relation of guided waves (Pavalakovic et al., 2000) . These dispersion curves represent the possibilities in which the wave can propagate in the structure. The dispersion curve depicts a frequency bandwidth associated with the abscissa value and a phase velocity bandwidth associated with the ordinate value on the phase velocity dispersion curve . This meant that we excite a large zone and multiple modes propagate in the structure at same time. (Rose, 2004)

In case of RC structures finite layers exist around the material which is concrete around steel bar and energy is passed between the layers. In such systems properties of guided waves depend on elastic and damping properties of all the layers . At the boundaries between the layers stress and displacement boundary conditions need to be satisfied. In RC system steel bar in concrete is modelled as a solid cylinder which is embedded in an infinite concrete medium (so that attenuation through leakage in concrete can occur) , both the materials are considered to be isotropic , homogenous and elastic . For the solution of wave propagation equation a global matrix method is employed using optimization techniques (Ervin et al. , 2009) which was then developed into standard software Disperse (Pavalakovic et al., 2000)

The solution for a layered structure includes phase velocity, frequency and attenuation. Material absorption and energy leakage into surrounding concrete lead to attenuation. Due to

complex boundary effects waves propagate in longitudinal, flexural and torsional modes and have frequency dependent properties. The various modes are represented as L (m,n) ; F(m,n) and T(m,n) respectively where m and n denote the circumferential displacements and sequential order of mode respectively .

3.3.3 Advantages :

1. High sensitivity, enabling the detection of small flaws.
2. High penetrating power, enabling the detection of flaws that are deep inside the structure.
3. Testing is possible through the accessibility of only one surface.
4. Capability of testing over long distances.
5. Some capability of estimating the size, orientation, shape and nature of defects.
6. Greater accuracy than other NDT techniques.
7. Easily portable.
8. Non-hazardous to the surrounding materials.
9. Frequency and mode tuning can be done to evaluate different types of deterioration or damage in structures .

3.4 REVIEW OF ULTRASONIC GUIDED WAVES TECHNIQUE

Na et al (2002) investigated the feasibility of detecting and quantifying delaminating at the steel concrete interface using ultrasonic guided waves. The experiments were performed on three sets of specimens. Specimen sets 1 and 2 comprised of four cylindrical structures each with different amounts of separation (0, 25, 50, 75% of concrete steel interface). Specimen set 3 comprised of three concrete beam structures-specimen with different amounts of separation without stirrups, specimen with different amount of separation with stirrups and, specimen with same amount of separation at different positions with stirrups. Ultrasonic testing was conducted in through transmission mode. Four Transmitter/ Receiver arrangements (TRA1, TRA2, TRA3, TRA4) were designed to generate. For specimen sets 1 and 2, it was observed that TRA1 is most efficient in predicting or quantifying the degree of separation. The sensitivity was affected by the selection of transducer frequency in TRA3. In case of TRA4, the detection sensitivity was affected by the distance between concrete surface and separation region further the amplitude of V(f) curves of specimens without stirrups were stronger than the specimens with stirrups. The experimental investigation showed that the efficiency of annular shaped holders used for exciting flexural cylindrical guided waves

modes was comparatively more than other holders. It was observed that though signals generated by relatively larger angles of incidence were more sensitive to discontinuities, however the propagating signal strength for a large incident angle was not always higher than the signals generated by smaller incident angles. It was concluded that guided wave technique can be applied to quantify the degree of separation or delamination using pulse through transmission mode and pulse-echo method are required to predict the exact location of separation.

Na et al (2003) investigated the feasibility of using ultrasonic guided wave testing technique for detecting delamination at GFRP rod-concrete interface. The experimental investigations involved ultrasonic testing in through transmission mode for both glass fibre reinforced polymer and steel bars embedded in concrete to study the effect of high attenuation shown by GFRP. Two transmitter-receiver arrangements with transducer's centre frequency of 50 kHz, 150kHz and 1 MHz,were applied to propagate guided waves through the specimens, and ultrasonic tests were carried out. Frequency v/s signal amplitude curves i.e., V(f) curves were obtained after ultrasonic testing. It was observed that the testing sensitivity was not affected by the high attenuation of GFRP bar and therefore, guided wave technique can be applied equally well for detecting delamination at GFRP/Concrete and Steel/Concrete interface. The dispersive behavior shown by the guided waves was also studied. The specimens were modeled as GFRP bars of finite diameter embedded in an infinite concrete medium, for wave mode identification. Ultrasonic testing was done to obtain the material properties, and these were used to plot energy velocity curves and attenuation dispersion curves. The experimental observations from the curves conclude that ultrasonic guided wave technique can be used for GFRP-concrete interface testing.

Kundu et al. (2003) investigated the feasibility of using Lamb waves for detecting interface degradation and steel bars separation in concrete beams. The Lamb wave can propagate a long distance along the reinforcing steel bars embedded in concrete as a guided wave and is sensitive to the interface bonding between the steel bar and the concrete. The traditional ultrasonic methods for inspecting defects in concrete use reflection, transmission, and scattering of longitudinal waves by internal defects. These methods are good for detecting large voids in concrete, but they are not very efficient for detecting delamination at the interface between concrete and steel bars. A special coupler between the steel bar and ultrasonic transducers had been used to launch non-axisymmetric guided waves in the steel

bar. This investigation showed that the Lamb wave inspection technique is an efficient and effective tool for health monitoring of reinforced concrete structures.

Reis et al. (2005) studied the development of a wireless embedded sensor system to monitor and assess corrosion damage in reinforced concrete, reinforced mortar specimens were manufactured with seeded defects to simulate corrosion damage. Taking advantage of waveguide effects of the reinforcing bars, these specimens were then tested using an ultrasonic approach. Using the same ultrasonic approach, specimens without seeded defects were also monitored during accelerated corrosion tests. Both the ultrasonic sending and the receiving transducers were mounted on the steel rebar. Advantage was taken of the lower frequency (<250 kHz) fundamental flexural propagation mode because of its relatively large displacements at the interface between the reinforcing steel and the surrounding mortar. Waveform energy (indicative of attenuation) was presented and discussed in terms of corrosion damage. Current results indicated that the loss of bond strength between the reinforcing steel and the surrounding concrete can be detected and evaluated.

Reis et al. (2008) studied damage due to accelerated corrosion using low and high frequency ranges in longitudinal modes of guided waves. High frequency ranges from 2-8 MHz and low frequency covers values below 200KHz. For low frequency testing L(0,1) mode was used; and due to its high attenuation initially it was not detected but once corrosion began and mortar cracking occurred due to corrosion accumulation. For high frequency L(0,9) mode was used; due to negligible radial and axial displacement it is relatively insensitive to interface conditions.

Ervin et al.(2009) studied an embedded network based on ultrasonics to detect reinforcement deterioration. Localized and accelerated corrosion in reinforced mortar specimens was monitored using ultrasonic guided waves. Longitudinal waves were used in through transmission configuration. Due to localized corrosion incident waves were scattered, attenuated and modal conversions occurred.

Sharma and Mukherjee (2010) discussed the use of longitudinal guided ultrasonic waves to monitor notch and debond defects in steel bars in concrete simulating pitting and delamination phenomenon caused by corrosion. The low and high frequency ultrasonic pulse echo and pulse transmission technique was used for early detection of damages in steel in RC beams. The exact location and magnitude of damage was indicated by efficient combination of the two ultrasonic monitoring techniques. Ultrasonic guided wave monitoring utilizing

specific core and surface seeking modes was applied to identify corrosion mechanism in a bar embedded in concrete. In general, huge pitting and non-uniform area loss highlighted by severe signal attenuation marks chloride corrosion, which was well unraveled by core seeking mode. It began with delamination shown by signal rise with surface seeking mode. It was concluded that judicious selection of ultrasonic modes, the complete corrosion mechanism in RC structures can be successfully identified.

Sharma and Mukherjee (2011) investigated the type of corrosion mechanism in chloride and oxide environments in RC beams. Ultrasonic guided waves with specific core and surface seeking modes were used for monitoring rebar corrosion in beams. It was observed that in case of chloride corrosion in beams, when core-seeking mode was propagated, the signal was highly attenuated, thus indicating pitting and non-uniform area loss. When surface seeking mode was propagated, there was an initial rise in signal strength and then a fall, thus indicating delamination followed by local loss of material. In case of Oxide corrosion in beams, it was observed that when core-seeking mode was propagated, there was a slow fall in signal strength, indicating the absence of pitting. When the surface seeking mode was propagated, there was an initial drop in the signal due to pressure built up by the formation of corrosion products, indicating a slow corrosion rate and localized corrosion and eventually, a gradual rise in signal strength was observed, indicating slow bond deterioration. The ultrasonic voltage trends of the received signal in both chloride and oxide corrosion specimens using surface-seeking and core-seeking mode were obtained. The mechanism and rate of rebar corrosion was successfully monitored in chloride and oxide environments through appropriate selection of modes. Simultaneous destructive tests were also carried out on RC beams, and it was found, that non-destructive Ultrasonic technique correlate well with the destructive technique.

Lai et al. (2013) studied the dispersion of guided wave in early aged concrete due to presence of honeycombs. For this work pair of sensors were used which were placed 100mm apart on same side of formwork at the soffit. Results show that frequency spectra was dispersed due to water which filled up honeycombs. 100 mm cubes were cast for 7 and 28 days. For compressive strength and ultrasonic testing specimens of 600 mm x 290 mm x 100 mm were made. The amount of super plasticizer was varied. The surface wave was incoherent in samples having honey combs; but not so after 28 days which is attributed to the presence of water in first few hours. Strong signals occurred in specimen which had better workability

due to back echo from concrete top as wave could penetrate the thick (100 mm) fresh concrete specimen.

Kundu (2014) discussed ultrasonic and electromagnetic waves for NDE and SHM. Guide waves are commonly used for NDE as they propagate long distances and access difficult regions. But ultrasonic waves attenuate fast in porous and in few non-porous materials which is why electromagnetic waves were used. Experimental studies were carried on composite plate and composite concrete interface. Fibers in the plate in the top, bottom and middle layers run in 0^o direction whereas second and fourth layer in 90^o direction. The results depict that ultrasonic guided waves detect internal defects while electromagnetic radiations detect in highly porous materials mechanical and heat induced damage. Results show flexibility of DPSM in modeling elastic and electromagnetic wave scattering.

Sharma and Mukherjee (2014) carried out ultrasonic guided wave technique for monitoring the setting behavior of freshly poured concrete of different workabilities. The two mixes were control concrete(CC) and self compacting concrete (SCC) for which slab specimens of dimensions 100 mm x 300 mm x 300 mm were used such that one 25 mm diameter bar was embedded at the centre of the specimen of 500 mm length with 100 mm projecting on both the sides . For the two mixes of varying workabilities the results using L(0,l) mode depicted fall in the signal strength with time due to better bond development between the bar and concrete . After the initial setting as the concrete hardens leakage from steel bar to concrete enhanced which lead to a fall in R value . Further on completion of hardening i.e. final setting the slope of curve reduced to zero . The fall was sharp in case of CC as compared to SCC , in case of SCC there was gradual reduction in R value till 26 hours and then it gathered speed .

Sharma and Mukherjee (2015) conducted an ultrasonic monitoring technique for freshly poured concrete with composition as 1:1.5:2.9 (cement, sand and aggregates) with 0.45 as the water-cement ratio . Specimen dimension of 150mm x 150mm x 300 mm with 25 diameter mild steel bar at the centre of it having 600mm length , 150 mm projected on both sides . It was observed that with 1 MHz frequency no drastic change was noticed whereas with 0.1 MHz as the concrete hardened , bond developed between bar and concrete and signal leaked and attenuated with fall in peak to peak voltage amplitude . Thus with increasing age of concrete the signal drops continuously . Hence L(0,1) mode with 0.1 MHz is called Surface Seeking Mode as it detects the interfacial changes . The R value fell from 1

to 0.9 in first 1½–2 h indicating the voltage amplitudes remain steady , further value dropped from 0.9 to 0.1 indicating phase change of concrete from fluid to solid in 2 to 18 hours , after that it fell from 0.1 to 0 marking the solidification of concrete .

3.5 Acoustic Emission Technique

3.5.1 Background (Aggelis, 2011)

The word " acoustic " is derived from Greek word *akoustikos* . Acoustic emission is an NDE testing technique which utilizes high –frequency and has been applied to civil engineering structures. As per the ASTM 1316 (ASTM 2010) the AE phenomenon consists of transient elastic waves that are generated by rapid release of energy from localized sources within a material . Other terms such as stress wave emission, micro seismic emission and micro seismic activity describe the same phenomenon. For the structural monitoring of a bridge in 1939 this concept was first applied. J. Kaiser originated this method in 1950's.

AE has been used to monitor cracks in highway bridge structures (Ghorbanpoor, 1987) , further AE was used to study fatigue cracks in steel (Mathieson, 1987) and concluded that secondary AE sources from crack closure , friction and crushing of corrosion products determines from presence and location of cracks (Clark, 1992) . AE has been extensively used for the study of crack conditions in steel bridges (Ghorbanpoor and Rentmeester, 1993 ; Gong et al., 1992 and Hopwood 1988) . It was used for detection and assessment of damage as well as location of damage. The structural integrity of reinforced concrete structure was assessed using AE. It has been designed to hear sounds due to microcracking and plastic deformation (Fowler and Berkowitzi, 1995). AE was used determine the location of cracks (Watson et al., 2001). Stress waves generated due to structural discontinuities were detected (Ativitavas, 2002). AE was used in prestressed concrete bridges to evaluate and detect failures in high strength tendons and it was found 82-86 % reliable (Yuyama et al., 2007) . RC deck girder bridges subjected to diagonal tension cracking were tested using AE procedures (Lovejoy, 2006). Prestressed Concrete Structures were evaluated using AE technique and new method based on signal strength moment was proposed (Xu, 2008) , corrosion and cracks in early stage were detected in prestressed concrete beams (Elfergani et al., 2013) . AE was used to characterize modes of cracks to have an early assessment of material condition. It was concluded that initial cracks come from tensile load on surface of concrete and diagonal shear cracks cause ultimate failure of member . (Ohno and Ohtsu,

2010). Cracking Pattern in long Structures like bridges in order to locate sensors on surface to detect each cracking event (Shiotani et al., 2009). Agglelis et al., 2010 b obtained different signatures of AE and concluded that it depends upon the mode of crack. Short time rise and high frequency waveforms were formed due to tensile cracks while lower frequency, longer time rise and longer waveforms generate shear cracks. Similar studies were conducted by Philippidis et al., 1998, Aggelis et al.,2010 c and Shiotani, 2006 .

3.5.2 Applications

1. To monitor and examine the behavior of ceramics, rock, composites, metals and concrete for fatigue, corrosion, yielding, stress concentration and creep.
2. To determine the safety of earth embankments
3. Monitor behavior of fiber – reinforced plastic, asphalts and mortar.
4. Crack detection, in-situ stress, expansion joint evaluation and fracture toughness in concrete structures.

This technology uses frequencies above that of audible sound i.e. in the range of 150-300 KHz and ultrasonic sensors (20 KHz – 1MHz). AE differs from other NDE methods, AE being passive technique as the energy initiated within the component or material under test is relied upon whereas in ultrasonic, radiographic or other NDT methods the information source is derived by external application of energy or compounds, hence making it active in nature.

3.5.3 Principle

Information on origin of discontinuity and development of it in a stressed material is provided by AE . Discontinuities release energy which travel in the form of high frequency stress waves, received by use of sensors (transducers) that convert the energy into a voltage, this voltage is electronically amplified and AE data is processed by timing circuits. The received voltage (signals) are characterized according to their source location , voltage intensity and frequency content .

Elastic waves generated by source are detected and recorded by transducers (sensors) on the surface of material (Grosse and Ohtsu, 2008; Mindess, 2004) . The detected waves are then transformed into electric wave by the transducers , the information of the waveform include location and density of cracks as well as severity of material condition (Kurz et al .2006 , Aggelis et al. 2010a, Carpinteri et al. 2010, Matikas 2008, Zhou et al. 2010)

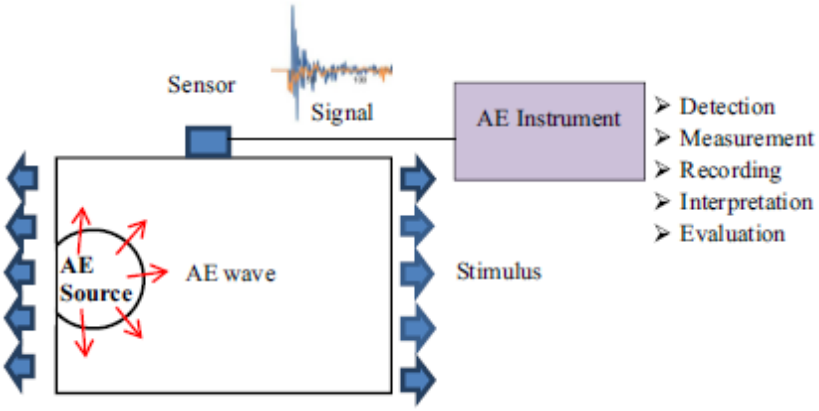

Figure 3.11: Principle of AE technique (Pollock, 1995 and Noorsuhada, 2016)

Aspects of wave propagation process :

1) Attenuation: As wave travels outward from the source the amplitude decreases. It helps detect waves from distinct sources.
2) Wave velocity: It is the speed with which disturbance travels through the structure. It helps detect source location.

   Attenuation: Decrease in amplitude of acoustic wave as it travels through the structure is termed as attenuation. Scale used to measure is decibel (dB), it is logarithmic, condenses wide range of AE signal amplitudes and is referenced to 1 µv. Attenuation is caused due to:

   - Geometric Spreading
   - Scattering at Structural Boundaries
   - Absorption.

   When distance between source and sensor is less geometric spreading takes place and when distance between source and sensor is large energy absorption and scattering lead to attenuation.

   Geometric Spreading: change in static stress field near the source is maximum. It was found that in rods which are small well defined structures geometric beam spreading is minimum and greater distances can be travelled by stress waves. At geometric discontinuities and at structural boundaries reflection occurs, modal conversion occurs due to discontinuities. The material through which waves travel the elastic and kinematic energies of wave are absorbed and converted to heat by it,

absorption is greater at higher frequencies and is more in non metals like paint etc than in case of steel at high frequencies.

Pencil lead pressed against structural member is a good AE source. The break of lead generates localized impulse which is of short duration and similar to that of crack source, moreover its amplitude is also near to that of crack. This is widely used to decide maximum permissible spacing of sensor. Amplitude curve helps determine sensor placement. The lead is broken several times at different distances from sensor and amplitude is recorded then these are averaged, average mplitudes are plotted against distance.

Wave Velocity: The time of arrival of wave from source to sensor is used to locate the source, this arrival time depends upon the wave velocity. Lamb waves are used as wave mode in AE testing of structures, two motion fall under this wave mode, in first motion is symmetrical and in second it is asymmetrical about median plane of the plate . The S_0 mode is called extensional mode as it stretches and compresses in the direction of wave motion, in plane force generates this type of motion whereas a_0 mode is flexural mode and it causes body of plate to bend with 2 surfaces moving in same direction, forces perpendicular to the plane produce this type of motion.

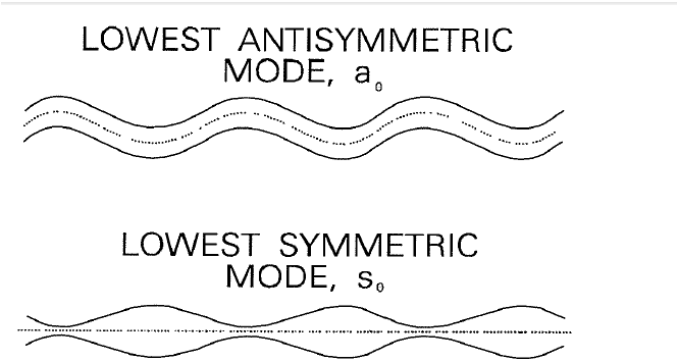

Figure 3.12: Basic Lamb Wave modes (https://www.nde-ed.org)

3.5.4 Parameters

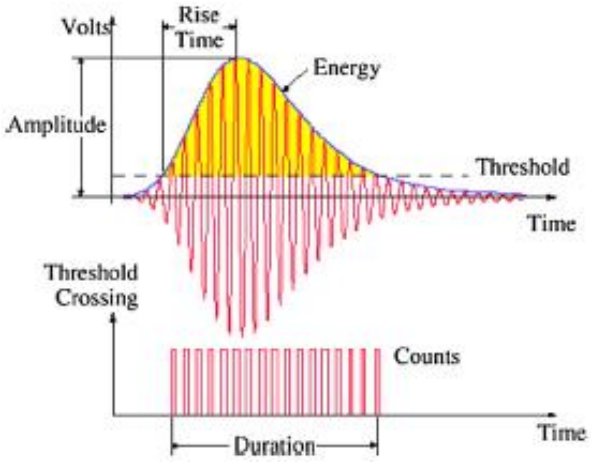

Figure 3.13: Typical AE parameters (Noorsuhada, 2016 , Huang et al., 1998)

Threshold: User defined value of amplitude in decibels (dB) . It is set based on background noise.

AE counts: Number of times an AE burst crosses the threshold.

Amplitude: Maximum voltage of AE signals. Units – Decibels.

AE energy: The area under amplitude – time curve above threshold value.

AE duration: Time between first and last threshold crossing.

Rise – time: Time between first threshold crossing and maximum peak amplitude.

RA value: Rise time / maximum amplitude

Average Frequency = AE counts / duration.

KAISER EFFECT and FELICITY EFFECT

AE has memory known as Kaiser effect, when material is loaded, unloaded and then reloaded, AEs will not produced until previous maximum load is crossed. In the **Figure 3.14** during the load rise AB emissions are generated but when load is lowered in region BC or raised again in region CB there was no emission . As the load is raised in BD emission continues and in DE load is lowered the emission stops . At point F emissions start before maximum load is attained and further with increase in load emissions increased FG. The behavior where no emission occurs until maximum load is increased is called Kaiser Effect and when emission occurs below the maximum load is called felicity effect . Kaiser effect is shown by insignificant flaws and felicity by structurally significant flaws.

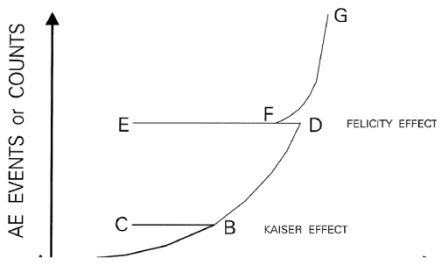

Figure 3.14: Emission on repeated loading (https://www.nde-ed.org)

3.5.5 Advantages

i. It can be used in all stages of testing :
   - Preservice (proof) testing
   - Inservice (requalification) testing
   - On line monitoring of components and systems
   - Leak detection and location
   - In –process weld monitoring
   - Mechanical property testing and characterization

ii. Less intrusive

iii. Global Monitoring

iv. Material anisotropy is good

v. Less geometry sensitive

vi. Real time evaluation

vii. Remote scanning

viii. Performance / price ratio

3.5.6 Limitations

i. Repeatability: It is stress unique and each loading is different.

ii. Noise: The unwanted signal in AE testing is termed as noise, the sources of which include friction and impact . Rain, wind driven dust, flying objects fall under the category of impact sources whereas structural loading such as movement due to loose bolts or connectors give rise to frictional sources.

iii. History: If the loading history of structure is known only then tests can be performed.

Table 3.2: Comparison between AE and other NDT techniques

Acoustic Emission	Most other NDT methods
• Discontinuity growth / movement	• Discontinuity presence
• Stress, Damage related	• Shape related
• Material anisotropy is good	• Material anisotropy is bad
• Less geometry sensitive	• More geometry sensitive
• Each loading is unique	• Inspections are readily repeated
• Less intrusive	• More intrusive
• Global Monitoring	• Local Scanning
• Limitations: attenuation, history dependence and noise	• Limitations: access, geometry and dependence on discontinuity orientation and proximity to surface.

3.6 REVIEW OF ACOUSTIC EMISSION TECHNIQUE FOR MONITORING SETTING

Chotard et al. (2001) studied setting of calcium aluminate cement using acoustic emission technique. Paste was prepared with w/c of 0.33 and moulds of 100 mm x 100 mm x 30 mm were used. The entire acoustic emission was divided into three stages; in first stage during 0-3 hours no acoustic emission activity occurred. It indicates dormant period and hydrates are found to nucleate in this period. In second stage during 3-6 hours strong variation in acoustic emission counts as well as in this condition temperature was observed as in this stage water is consumed, material changes from liquid to solid state and empty capillary pores are left. In terms of frequency, at early hydration stage, paste acts as low pass frequency filter. Whereas when it hardens it becomes elastic and lesser attenuation of higher frequencies occurred.

Chotard et al. (2002) discussed new applications for real time monitoring of material processes by acoustic emission. Molds of 100 x100 x 30 mm were used. It was observed that no acoustic emission activity occurred in initial 30 minutes which was attributed to dissolution of calcium hemihydrates along with nucleation and growth of gypsum. It was found that as average grain size of different mixtures increased the cumulative count between 1 and 4 hour also increased. Another test in which two solutions were taken, Solution 1 contained $Al(NO_3)_3.9H_2O$ and in Solution 2 hydrochloric acid was added in $Al(NO_3)_3.9H_2O$.

The cumulative hit values were found to be higher in Solution 2; it was due to more elongated crystals formed in Solution 2. In terms of acoustic emission signal energy Solution 2 shows more energetic signals than Solution 1. Hence sensitivity of acoustic emission signals to the number of crystals and the way they grow is proved.

Skal S'kyi et al. (2004) used acoustic emission technique to study solidification of concrete. Moulds of 100 x100 x 100 mm in size were used and solidified at temperature of 300 K. After 600-1200 sec acoustic emission started in concrete mixture, initially the signals had amplitude of about 10-30 V which later increased in about one hour. It was found that period of first 6 hours was most active period of acoustic signals which was attributed to the completion of formation of crystal structure. But the intensity decreased in comparison to that in first two hours which was due to crystallized products merging together and thus continued for 25-30 hours. As the concrete strength increased acoustic emission energy enhanced which was attributed to contact of aggregates and formation of shrinkage cracks. Further decrease in activity was observed which was due to pores being filled by products of hydration and structure become compact in addition to cement particles shielded by products of hydration.

Abeele et al. (2009) conducted active and passive monitoring on early hydration in concrete .Specimens constituted of 200 x 150 x 100 mm^3 cubicles and was studied for 72 h of hydration process. The apparatus constituted of 4 openings for 4 transducer holders transmitter and receiver both for compressional (P) and shear (S) waves with 2 thermocouples inserted. AE signals were recorded through sensors attached on 2 protruding bars. Samples with w/c ratio of 0.5 and 0.33, self compacting concrete 0.5 were prepared. The increase in temperature of 0.33 samples began as early as about 2 h and lasted for 12 hours, then after reaching peak it gradually decreased to room temperature. Initially not much rise in AE counts was observed and prior to temperature change the increase of counts accelerated indicating intense hydration activity. The trend of accumulation of AE counts even after fall of temperature continued which was attributed to shrinkage of concrete during hardening process. With increase in w/.c ratio from 0.33 to 0.5 the values of temperature retarded and a reduction in magnitude of peak value of temperature. Whereas in case of SCC and 0.5 w/c ratio peak was more pronounced due to larger amount of hydration products. In case of AE the readings for SCC 0.5 start earlier but is less intense during the mechanical setting as compared to 0.5 normal concrete.

Zura et al. (2009) investigated cavitation due to self dessication during solidification process in cement paste using acoustic emission technique. Type1 Portland cement was used in this investigation with w/c ratio of 0.3, 0.35 and 0.4 and high range water reducer by 0.5% cement weight was also added. Another cement paste containing 20% silica fume, 0.33% water reducing agent and w/c of 0.3 was prepared. The results show that in cement paste with w/c 0.3 no acoustic emissions occurred for initial two hours and in 2-3 hours some minor activity occurred which was followed by quiet period of 3-7 hours. The activities occurring after 7 hours corresponded to setting (solidification) of cement paste. In paste (w/c=0.3) initial set was at 6 hours whereas final set occurred at about 7h and peak of Acoustic emissions hits occurred for sample with 0.3 and 0.35 w/c ratio occurred at 7 to 12 hours. In order to explain these acoustic emission events several hypothesis were given namely dissolution of cement grains; formation of hydrates (10-15) microcracking, friction due to shrinkage with walls of mould and cavitation. Due to chemical shrinkage cavitation of air bubbles occurs which empties the capillary pores. It was observed that with increase in w/c ratio the acoustic emission events decrease around setting; this is because with low w/c ratio the acoustic emission events decrease around setting; this is because with low w/c ratio stiffness of paste changes rapidly and in shorter time period capillary pores being smaller small bubbles are generated, the water on top is sucked inside the paste and it replaces water which was consumed by chemical shrinkage and eliminates cavitation of gas bubbles in paste.

Shah and Kishen (2010) used acoustic emission to study fracture behavior of concrete-concrete interface, closed loop servo controlled machine was used to test samples and beams were subjected to three point loading and monitored using 8 AE sensors. 4 mixes were prepared and notched beams with span to depth ratio of 2.5 and notch with of 2mm are casted and interface between two mixes of concrete at mid span was created in such a way that 5 such types existed namely AI – no interface, AA- interface between A and A, AB – interface between A and C and AD – interface between A and D . The AE events were maximum in AI followed by AA,AB ,AC and AD respectively indicating large process zone for AI and further density of AE events was large. It was found that as compressive strength increases the number of AE events decreases thus AD is brittle as compared to AA. Similar pattern for AE energy existed. AE energy was maximum for AI then followed by AA, AB, AC and AD. The emitted AE energy was initially high and then as specimen fails it became gradual. The

size of process zone and damage zone was analyzed using number of events, it was found that the width reduced as the compressive strength on either side of interface increased.

Aggelis (2011) used acoustic emission parameters to classify cracking mode. For this 25 mixtures with prismatic specimens of dimensions 400 x 100 x100 mm; w/c ratio of 0.5 to 0.6 and 0.7 were prepared. Steel fibers were introduced which were straight and with hooked ends. The content varied from 0%, 0.5%, 1%, 1.5% and 2%. Curing with water saturated with calcium hydroxide was carried out for 28 days. Two acoustic sensors were placed on bottom tensile face. Cracks were classified based on graphs between average frequency and RA values. Pure tension and other modes of concrete were strongly discriminated between various stages of fracture with the help of relationship between RA value and average frequency.

Gabrijel et al. (2011) studied setting and hardening process of cement paste using both active and passive monitoring techniques. Cement paste prepared consisted of w/c ratio of 0.3 by weight, molds (made of polietilen) of dimensions 100 x 200 x 40 mm were used for active testing and distance between sensors was kept 40 mm. While for passive monitoring the dimension was 100 x 100 x 40 mm and were made up of hard rubber. Results of active ultrasonic technique show that ultrasonic pulse velocity increased before initial setting time i.e. after 1 hr 8 minutes from the time of mixing and its speed is 1180 m/s at initial set . Signal energy and number of counts against time also increased and showed same trend as that of UPV.Similar was the trend of duration of signal over threshold level. The results of passive ultrasonic technique reflected that at final setting greatest amplitude of acoustic emission is recorded. It was concluded that active technique represents large number of parameters such as counts, duration and energy of signal to study changes in structure of material.

Haneef et al. (2013) discussed acoustic emission technique in order to study influence of fly ash and curing on cracking behavior of concrete. Specimens of size 150 x 150 x 150 mm^3 were casted of both plain and fly ash concrete , 30 % replacement of cement by flyash was done, w/c ratio of 0.44 and specimens were cured for 7, 14, 28 and 56 days. During compression testing AE signals were generated using resonant frequency of 150 KHz and 40 db pre-amplification with band pass filter (100-300 KHz). Initially compressive strength of plain concrete is more than that of fly ash concrete and the difference decreases with age, at and beyond 56 days it becomes equal to that of plain concrete. AE signals at beginning of

compression test were due to closure of pre-existing cracks and due to formation of micro-cracks through weak boundaries of particles, in second stage due to interconnection of large pores, aggregate to cement interface cracking and multiple crack branching AE counts increase. When the load reaches ultimate load sudden increase in AE counts was observed due to unstable cracking. At 7 and 14 days of curing both plain and fly ash concrete have similar variation of cumulative AE counts in compression testing but at 28 and 56 days initial AE activity in fly ash concrete is less .During initial stage peak amplitude of AE hits decreased with curing for both concrete and fall was more in case of fly ash samples which was due to reduction of micro cracking. It was found with AE technique that only tensile cracks occurred in case of fly ash concrete whereas both tensile and shear cracks existed in case of plain concrete.

Shahidan et al. (2013) investigated reinforced concrete beams by acoustic emission technique and classified damage. Beams had cross-section of 150 x 250 x1900mm and were subjected to 4-point loading. The load was increased from 2.5 KN until failure. Acoustic emission activities were found to be low at mid span and at certain distances from support. Acoustic emission activities were high but the cracks initiated and propagated from mid span. It was found that location of sensors was cause of it, it was suggested to place sensors near the mid span. Using RA value versus frequency for both low and high signal in acoustic emission wave form, high acoustic emission wave form occurred in case of fatigue test and in case of constant load acoustic emission waveforms reduced. Low waveforms were found to be dominant which lie in low RA region in RA versus frequency graph.

3.7 CLOSING REMARKS

In this chapter background of ultrasonic guided wave and acoustic emission as a NDT technique has been discussed . The literature review reveals that very few works have been reported to monitor freshly poured concrete using ultrasonic guided waves and acoustic emission techniques. No work has been reported till date which investigates the early age properties of silica fume concrete using NDT. In the present study an attempt has been made to investigate silica fume concrete using latest NDT of ultrasonic guided waves and acoustic emission techniques.

CHAPTER 4

EXPERIMENTAL INVESTIGATIONS: MONITORING SETTING AND HARDENING OF CONCRETE

4.1 GENERAL

Most crucial phases on which properties of concrete depend during its service life are the setting and hardening stages of fresh concrete. In this chapter Ultrasonic Guided Wave and Acoustic Emission techniques have been discussed to characterize the setting and hardening of concrete without any replacement and concrete containing various percentage replacements of cement by Silica Fume. The development of setting is also related to UPV and destructive tests of compressive strength along with microstructural analysis SEM/EDS.

In this chapter different testing techniques, equipment, specimen and concrete mixes used are highlighted.

4.2 EXPERIMENTAL INVESTIGATIONS

The experimental programme was divided into two phases namely destructive and non destructive. The layout is as shown in the **Figure 4.1.**

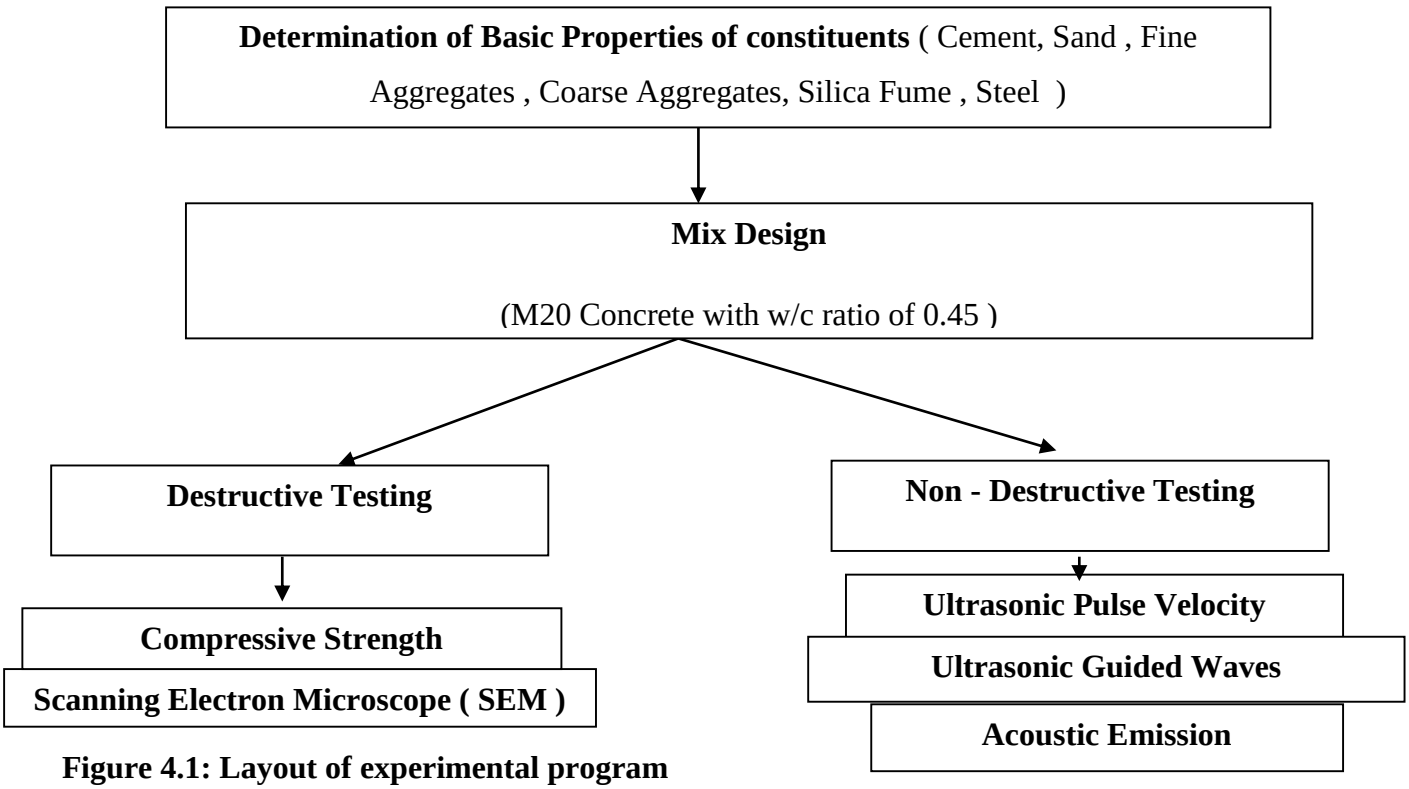

Figure 4.1: Layout of experimental program

4.2.1 Physical Properties of the Materials

4.2.1.1 Cement

Fly ash based Pozzlana Portland Cement (PPC) was used and tested as per IS 1489 – 1991 Part 1, the results are given in **Table 4.1**:

Table 4.1: Physical properties of PPC

Physical Properties	**Test Result**	**IS 1489-1991**
Setting time (in minutes)		
Initial	126	30 min.
Final	307	600 max
Compressive Strength (MPa)		
3 days	17.76	16
7 days	26.11	22
28 days	37.8	33
Specific Gravity	3.08	_
Standard Consistency	35%	_

4.2.1.2 Fine aggregates

Natural Sand locally available with maximum size of 4.75 mm was used as fine aggregate. It's sieve analysis and physical properties in accordance with specifications given in IS 383-1970 were conducted, the results of which are given in **Table 4.2** and **Table 4.3** respectively

Table 4.2: Sieve analysis of fine aggregates

I.S. Sieve Size	Weight retained (in grams)	Percentage weight retained (in grams)	Cumulative percentage of Weight retained	Percentage passing
4.75 mm	52	5.2	5.2	94.8
2.36 mm	132	13.2	18.4	81.6
1.18 mm	135	13.5	31.9	68.1
600 micron	177	17.7	49.6	50.4
300 micron	266.5	26.65	76.25	23.75
150 micron	141.5	14.15	90.4	9.6
Pan	96	9.6	$\sum = 271.75$	

Fineness modulus of fine aggregate = 2.71

Sand conforms to grading Zone III as per IS 383-1970

Table 4.3: Physical properties of fine aggregates

Characteristics	**Observed Values**
Specific Gravity	2.64
Water Absorption (%)	1.1
Bulk Density (compacted) kg/m^3	1856
Fineness Modulus	2.71

4.2.1.3 Coarse Aggregate

Crushed stone aggregate locally available were used .Results of Physical properties and sieve analysis are given in **Table 4.4** and **Table 4.5** .

Table 4.4: Physical properties of coarse aggregates

Property	**Observed Values**
Bulk density (kg/m^3)	1670
Water Absortion (%)	1.1
Fineness Modulus	6.74

Table 4.5: Sieve analysis of coarse aggregates

I.S. Sieve Size	Weight retained (in grams)	Percentage weight retained (in grams)	Cumulative percentage of Weight retained	Percentage passing
80 mm	0	0	0	0
40 mm	0	0	0	0
20 mm	114	3.8	3.8	96.2
10 mm	2086.8	69.56	73.36	26.64
4.75 mm	721.8	24.06	97.42	2.58
Pan	77.4			
	3000			

Fineness Modulus of Coarse Aggregates = 6.74

4.2.1.4 Silica Fume

Silica fume was obtained from KGR AGRO FUSIONS Mullanpur Road, Humbran, Ludhiana, Punjab. The chemical properties of which are given in **Table 4.6.**

(a) Silica Fume Bag

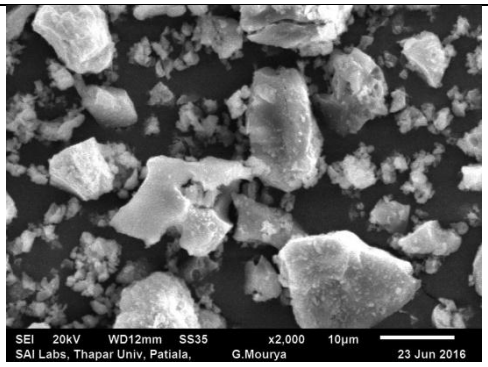

(b) SEM of Silica Fume

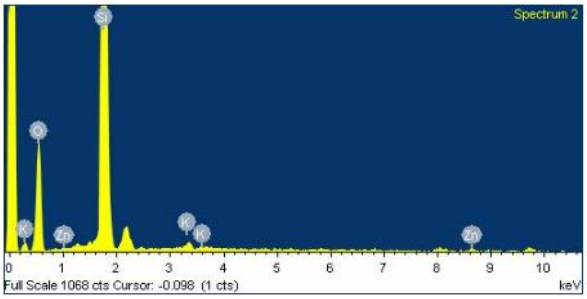

(c)EDS of Silica Fume

Figure 4.2: Silica fume used (KGR AGRO FUSIONS)

Table 4.6: Properties of silica fume

Parameter	Percentage by weight (used in present study)
SiO_2	95
Al_2O_3	0.03
Carbon	<1
CaO	0.05
MgO	0.1
FeO	0.02
TiO_2	0.03
LOI	<2
Moisture	0.1-3
Bulk Density	600 kg/m^3

4.2.1.5 Water

Clean and fresh tap water which was free of organic matter, acidic material, suspended solids and conforming to Indian Standard IS 456-2000 was used .

4.2.1.6 Steel reinforcement

Mild steel bars from Vardhman Steels, H.O. Lower Mall, Patiala were used .

Table 4.7: Specifications of Bars Used:

Technique Used	Diameter of Bar(in mm)	Length of the Bar (in mm)
Ultrasonic Guided Waves	25	300
Acoustic Emission	12	200

4.6.1.7 Mix Design: Mix Design of M20 grade of concrete (IS 10262: 2009)

STEP 1 : Test Data for Materials	
Cement used	PPC as per IS 1489 (Part 1) Fly ash based
Specific Gravity of Cement	3.08
Chemical Admixture	-
Specific Gravity of Admixture	-
Specific Gravity of Aggregate	
Coarse Aggregate	2.6
Fine Aggregate	2.74
Grading of Fine Aggregate	Zone III

STEP 2 : Stipulations for Mix Design	
Grade Designation	M20
Type of Cement	PPC as per IS 1489 (Part 1) Flyash based
Maximum nominal size of Aggregate (in mm)	20
Minimum Cement content (in kg/m^3)	300
Maximum Cement content (in kg/m^3)	450
Maximum water cement ratio	0.45
Desired Slump (in mm)	75
Exposure Condition	Moderate
High Workability required (due to placement by concrete pump,congested reinforcement etc.)	No
Deviation from Quality Control Conditions (Table 1 , IS 10262 -2009)	No
Type of Aggregate	Angular Aggregate
Type of Admixture used	-

STEP 3 : Target Strength for Mix Proportioning	
$f_{ck}'=f_{ck} + 1.65\ s$	
where :	
f_{ck}'=Target average Compressive Strength at 28 days	
f_{ck}=Characteristic Compressive Strength at 28 days (in N/mm^2)	20
s= Standard Deviation	

Standard Deviation (in N/mm^2)	4
Adopted Standard Deviation (in N/mm^2)	4
Target Strength (in N/mm^2)	26.6

STEP 4 : Selection of Water- Cement Ratio	
Maximum water cement as per Table 5 of IS 456	0.5
Adopt water cement ratio	0.45

STEP 5 : Selection of Water Content	
Maximum Water Content (in kg/m^3 of concrete) as per Table 2 of IS10262-2009 for 20mm aggregate size	186
Water content(in kg/m^3 of concrete) after applying Correction for type of aggregate used	-
Water Content (in kg/m^3 of concrete) after applying Correction for Desired Slump	186 + (3/100)x 186 = 191.58
%age reduction in Water Content due to use of water reducing admixture	-
%age reduction in Water Content due to use of Superplasticizer	-
Calculated Water Content (in kg/m^3 of concrete), after applying correction for use of admixture	-
Adopted Water Content , in kg/m^3 of concrete	191.58

STEP 6 : Calculation of Cement Content	
Calculated Cement Content (kg/m^3) = Water Content / Water Cement Ratio	191.58/0.45 = 425.73
Adopted Cement Content (kg/m^3)	425.73

STEP 7 : Proportion of volume of coarse aggregate and fine aggregate content	
Volume of Coarse Aggregate per unit volume of Total Aggregate	0.62
Calculated Volume of Coarse Aggregate per unit volume of Total Aggregate ,after correction for water - cement ratio	0.62 + 0.01=0.63
Desirable % reduction in Coarse Aggregate proportion for concrete requiring higher workability	0
Calculated Volume of Coarse Aggregate per unit volume of Total Aggregate,after adjustment for higher workability requirement	0.63

Adopted Volume of Coarse Aggregate per unit volume of Total Aggregate	0.63
Volume of Fine Aggregate content	0.37

STEP 8 : Mix Calculations per unit volume of concrete	
Volume of concrete (in m^3)	1
Volume of cement (in m^3) (Mass of cement /Specific Gravity of Cement) x 1/1000	425.73/3.08x1000 = 0.124
Volume of Water (in m^3) (Mass of water / Specific Gravity of Water) x 1/1000	191.58 /1000 = 0.191
Dosage of Water Reducing Admixture (%age by mass of cementetious material)	-
Volume of Water Reducing Admixture (in m^3) (Mass of water reducing admixture / Specific Gravity of Water Reducing Admixture) x 1/1000	-
Dosage of Superplasticizer (%age by mass of cementetious material)	-
Volume of Superplasticizer (in m^3) (Mass of Superplasticizer / Specific Gravity of Superplasticizer x 1/1000	-
Volume of all aggregates (f) (in m^3) 1-b-c-d-e	0.685
Mass of coarse aggregate (kg)= f x volume of coarse aggregate x specific gravity of coarse aggregate x 1000	0.685 x 0.63x2.6x 1000 = 1104.2
Mass of fine aggregate (kg)= f x volume of fine aggregate x specific gravity of fine x 1000	0.685 x 0.37 x 2.74 x 1000 = 713.211

STEP 9 : Mix proportions for Adopted Mix	
Cement (kg/m^3)	425.73
Water (kg/m^3)	191.58
Fine Aggregate (kg/m^3)	713.211
Coarse Aggregate (kg/m^3)	1104.2
Water Cement Ratio	0.45

Ratio of **cement: fine aggregate: coarse aggregate 1:1.67: 2.59**

4.2.1.8 Description of concrete mixes

Replacement of cement by 3, 6, 10 and 12 % silica fume

Name	Description
S	**0 % SF**
S1	**3 % SF**
S2	**6 % SF**
S3	**10 % SF**
S4	**12 % SF**

4.3 ULTRASONIC PULSE VELOCITY (UPV) INVESTIGATIONS

4.3.1 Setup and specimen details

The Ultrasonic Pulse Velocity is measured by TICO Ultrasonic Instrument as shown in the **Figure 4.3.**

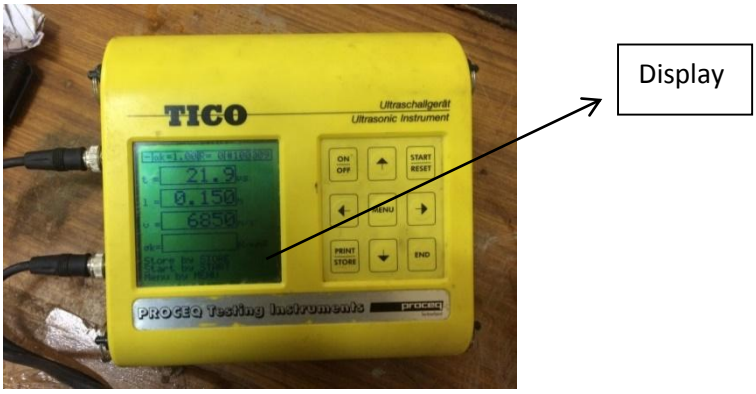

Figure 4.3: TICO ultrasonic instrument

The specimen used was cube of size 150mm x 150mm x 150 mm. 3 sides of specimens were removed after 2 hours of casting, ultrasonic waves were passed and velocity was measured after every 2 hours for a total of 48 hours.

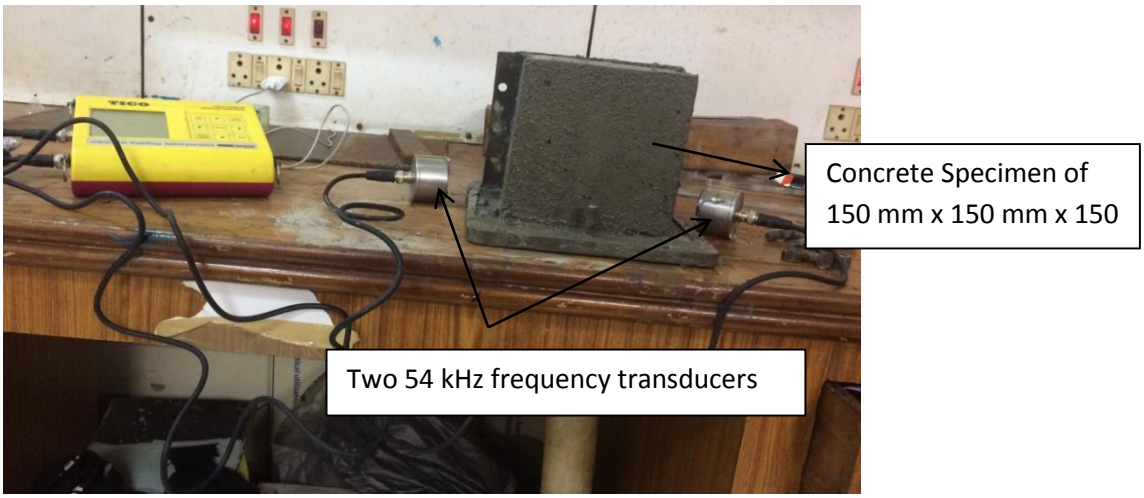

Figure 4.4: Specimen of UPV testing and TICO instrument

4.3.2 Methodology

Two Transducers were placed (one transmitter and other receiver) on two opposite faces of the cube specimen such that waves are directly transmitted. This arrangement is preferred since loss of energy between the transmitters is minimum and velocity to be measured is governed by the path length (150 mm in this case).

The electro-acoustical transducers (transmitter) generate a pulse of longitudinal waves. The transducers are held in contact with concrete surface with help of coupling gel (ultrasonic gel in the present work). Longitudinal waves generated then travel through concrete are then converted into electrical signal by the receiver transducer. The received signal is displayed on the digital display unit. Longitudinal Pulse Velocity is given by:

$$V = \frac{L}{T}$$

Where V is velocity of longitudinal pulse wave, L is the path length and T is time taken by the pulse.

(a) Side View

(b) Top View

Figure 4.5: UPV test sample

4.4 ULTRASONIC GUIDED WAVES INVESTIGATIONS

4.4.1 Setup details and specimen specifications

The ultrasonic testing constitutes of DPR 300, JSR ultrasonics which is pulse receiver device, Karl Deutsch ultrasonic transducers, Aquiris DC 438 Dual Channel, 12-bit, 100 MHz, 200 Ms/s, 4-M data acquisition card and display device. Wooden cube specimens of size 150 x150x 150mm **(Figure 4.6)** with 25 mm hole on two opposite faces and a mild steel bar of 25 mm diameter was inserted through the hole such that it is 75 mm projected from both the sides .Two transducers one acting as transmitter and the other as receiver were kept at two ends of bar with help of coupling gel (ultrasonic gel) and steady pressure was ensured between bar and transducers throughout the experiment. The DPR 300 generates the pulse which the transducers transfer into compressive spike ultrasonic pulse which further propagates through the MS bar in the form of longitudinal wave and was received at the other

end by the receiver. The received signal is sent to digitizer card (Acquiris) through DPR 300 and the ultrasonic signal is recorded. After pouring concrete in the wooden moulds the ultrasonic signatures were taken at 30 minutes interval for first 2 hour interval for 48 hours. Repetition of specimens ensured reliability of the technique.

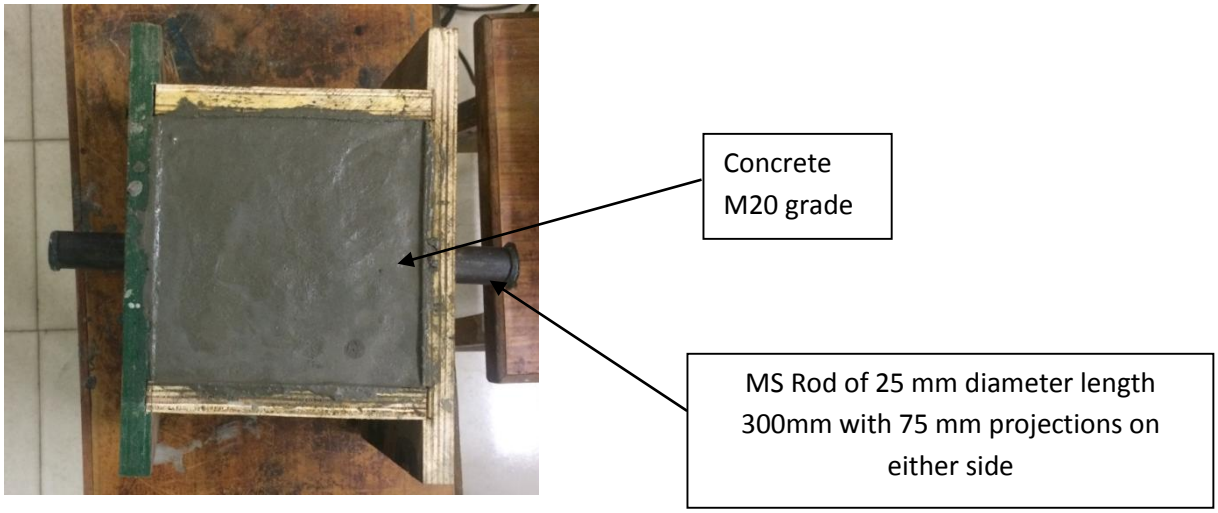

Figure 4.6: Top view of concrete specimen for Ultrasonic Guided Wave

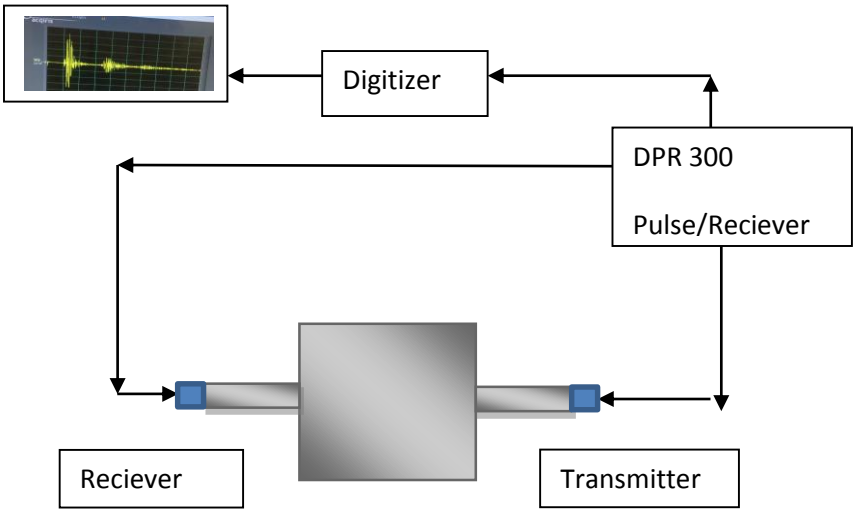

Figure 4.7: Schematic setup for UGW of cube specimen

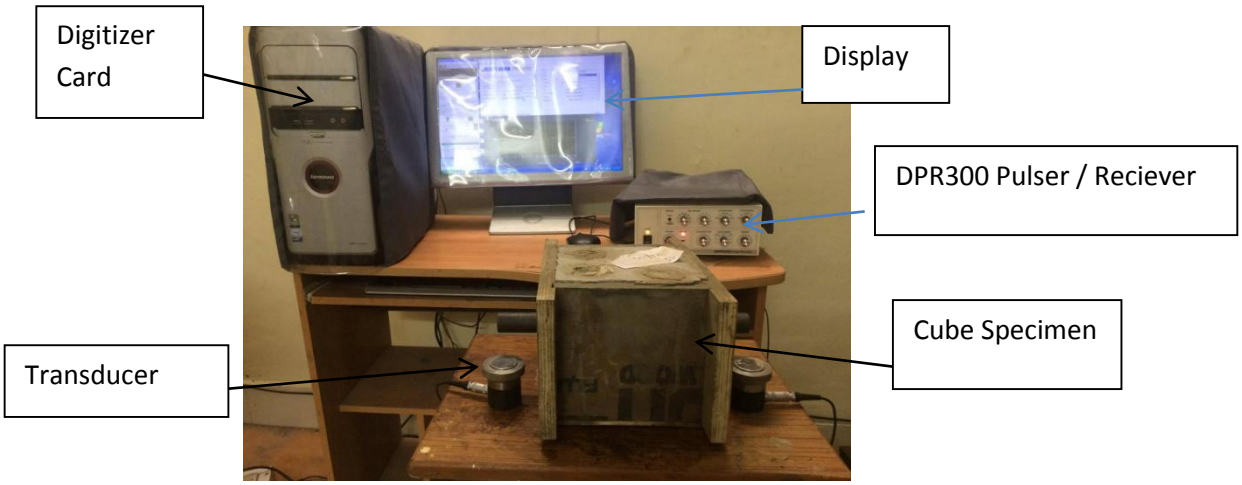

Figure 4.8: Actual UGW set up

Features of the equipment used are as follows :

(a) Transducer: It is a longitudinal wave transducer. It has various applications like it can be used for sound velocity measurements, detection of delamination, inspection of plates , thickness gauging etc . In this study Karl Deutsch transducers of 0.1 MHz and 1 MHz frequency namely S 24 HB 0.1S (THROUGH) , S 24 HB 0.1 E (T/R) , S 24 HB 1 (receiver) and S 24 HB 1 (transmitter) with 24mm diameter as shown in the **Figure 4.9** were used .

Figure 4.9: Ultrasonic transducers used in study (Karl Deutsch)

(b) **JSR Ultrasonics DPR 300 Pulser/ Receiver System :**

Figure 4.5 shows JSR Ultrasonics DPR300, it produces an electrical excitation pulse which is of high voltage (475 Volt) . For the conversion of electrical energy a into ultrasonic pulse transducer is used which is connected to T/R connector with a coaxial cable . Both pulse-echo and through mode operation can be configured using DPR 300. For pulse – echo, the waves are reflected from interfaces or defects within the test.

(a) Front View

(b) Back View

Fig 4.10: JSR Ultrasonic's DPR300 Pulser/Receiver (a) Front View & (b) Back View

Table 4.8: Specifications of JSR pulser/receiver

PULSER	
PULSE TYPE	NEGATIVE SPIKE PULSE
HIGH VOLTAGE SUPPLY	100 - 475 V
INITIAL TRANSITION (FALL TIME)	< 5 ns (10-90%) TYPICAL FOR 475 V PULSERS
PULSE AMPLITUDE	475 V peak
PULSE ENERGY	1.55 μJoules mimimum , 304μJoules maximum
PULSE DURATION	10-70 ns
DAMPING	16 DAMPING VALUES : 331,198,142,110,92,77,67,59,52,47,43,39,37,34,32 AND 30 Ω
MODE	PULSE ECHO OR THROUGH TRANSMISSION
THROUGH MODE ISOLATION	80 dB at 10 MHz
PULSE REPETITION RATE	INTERNAL : 100Hz - 5 KHz ; EXTERNAL : 0-5KHz

RECIEVER	
GAIN	-13 to 66 in 1 dB
PHASE	0 ^{0} (non inverting)
INPUT IMPEDANCE	500 W (through transmission)
BANDWIDTH	0.001-35 MHz OR 0.001-50 MHz
HIGH PASS FILTER	DC 1,2.5,5,7.5 AND 12.5 MHz
LOW PASS FILTER	3,5,7,10,15,22.5 (35 MHz BW) or 5,10,15,22.5,35 (50 MHz BW)
RECIEVER NOISE	49mV pk-pk input
OUTPUT IMPEDANCE	50 W
OUTPUT VOLTAGE	+_ 0.5 V INTO 50Ω

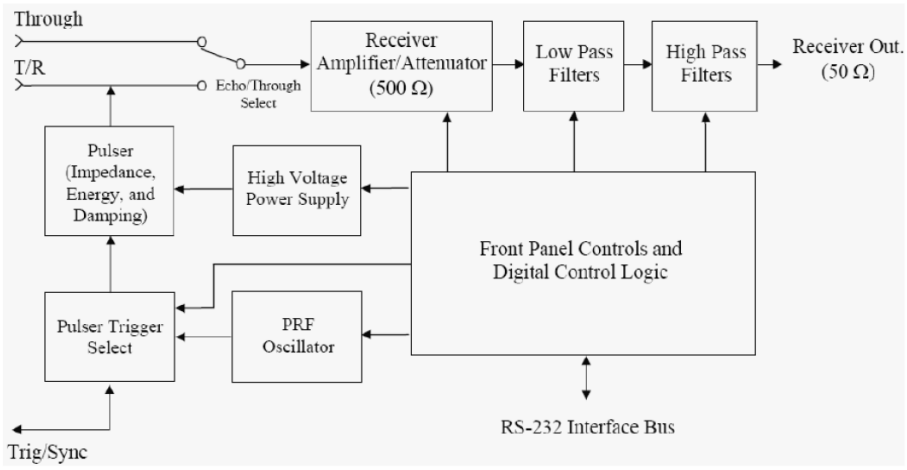

Figure 4.11: Detail circuit diagram of pulser/reciever system

PRF Oscillator and Pulse Trigger Control

Repetitive pulses are generated by internal PRF oscillator. Trigger source is selected for DPR 300 pulser by Pulse Trigger Control which selects between internal oscillator and external source applied to Trig / Sync connector.

Pulser

From above selected source, pulser upon receiving a trigger event generates excitation pulse .

Reciever Amplifier

Signal processed by DPR 300 reciever are controlled by this. It attenuates or amplifies the signal. The gain can be varied from -13dB to 66 dB.

Low Pass and High Pass Filters

Low pass filters reduce the bandwidth of receiver and high pass filters eliminates low frequency energy, they also provide faster receiver recovery from strong signals .

(c) Dual Channel High Resolution Waveform Digitizer

In order to capture the waveform an acquisition memory card model DC 438 Dual channel, 12-bit , 100-MHz , 200 MS/s , 4M point has been used . For storing complex signals for very long periods of time waveforms are transferred into digitizer acquisition memories.

Table 4.9: Specifications of Digitizer Card

MODEL DC 438	
BANDWIDTH (-3 dB)	DC to 100 MHz
FULL SCALE RANGE	250mV ,500 mV, 1 V , 2V , 5V and 10 V
IMPEDANCE	50 W+_ 1 % @ DC
CONNECTOR	BNC , gold plated
CHANNELS	Two
COUPLING	DC
MAXIMUM INPUT VOLTAGE	+_ 10 V DC (2W) OR 10 V RMS at 50W
BANDWIDTH LIMIT FILTER	35 MHz
MINIMUM AMPLITUDE	1 V pk-pk
IMPEDANCE	50

4.4.2 Methodology

4.4.2.1 Method of Testing

For monitoring setting and hardening of fresh concrete pulse transmission method was used . Two transducers one acting as transmitter and other as receiver were used to produce longitudinal guided waves in bar embedded in concrete. Both transducers were attached at either ends of bar and are placed parallel to the axis. In order to monitor the bond between MS rod and surrounding concrete surface seeking mode of central frequency 0.1 MHz and Core Seeking mode of frequency 1 MHz has been used .

4.4.2.2 Selection of Excitation Mode and Frequency

For reinforcing bars which fall under cylindrical system, due to effect of boundaries waves propagate in three modes namely Longitudanal (L), Flexural (F) and Torsional (T). The different placement of transducers produce these different types of modes . The longitudinal waves are produced by attaching transducer at ends of bar on both sides (Na et al., 2002; Pavlakovic, 1999 ; Rose, 1999). While placing them perpendicular to the bar generates flexural waves which exhibit high attenuation. Two transducers when placed at equal distances from bar axis with help of connector torsional waves are generated and this assembly limits the domain that can be studied as it absorbs substantial energy.

Longitudnal waves were chosen for the present investigation. Disperse software is used for selection of excitation frequencies (Pavlakovic and Cawley, 2000). Modes with lowest attenuation and those which are easily distinguished were selected (Pavlakovic, 1998; Pavlakovic and Cawley, 2001). In order to maximize the inspection range, to limit the dispersive effect and to reduce risk of complications due to other modes in received signal, mode at maximum energy velocity should be used.(Beard et al., 2003) **Figure 4.12** shows the dispersion curve for 25 mm bar embedded in concrete. The excitation frequencies are varied to obtain various longitudinal modes, and these frequencies are selected on the basis of phase velocity dispersion curves. In the present work, bar is embedded in concrete which falls under layered waveguide system. In such systems leakage plays a vital role and high frequencies to minimize leakage low attenuating modes are suitable. From the phase velocity , group velocity and attenuation characteristics it can be seen that L (0,1) mode has lowest attenuation when 0.1 MHz transducer was used as plateau region around steel longitudinal bulk velocity line was observed with higher modes. Whereas L(0,7) mode with 1 MHz transducer links plateau region and forms low leakage mode which propagates with longitudinal bulk velocity close to that of steel, further plateau corresponds to maximum energy velocity and minimum attenuation. From **Figure 4.13 and 4.14** it was observed that for L(0,7) mode concentration of energy is in the bar central core portion which has less surface component. Hence called as *Core Seeking Mode* as it is sensitive to loss of material and not to changes in surface profile . Therefore L(0,1) mode at 0.1 MHz which is sensitive to bond between concrete and steel and has significant axial displacement at interface is chosen for monitoring setting and development of bond between steel and concrete. It is called *Surface Seeking Mode*.

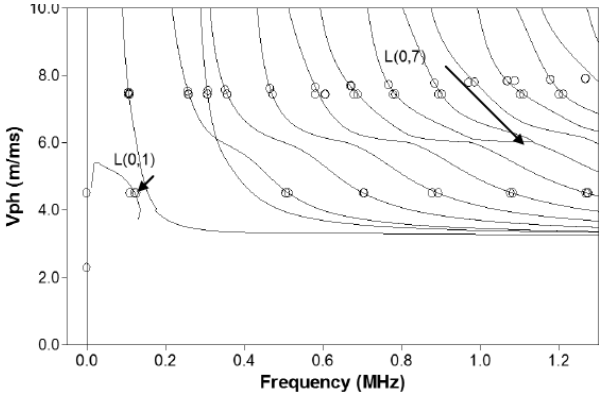

(a) **Phase Velocity vs Frequency**

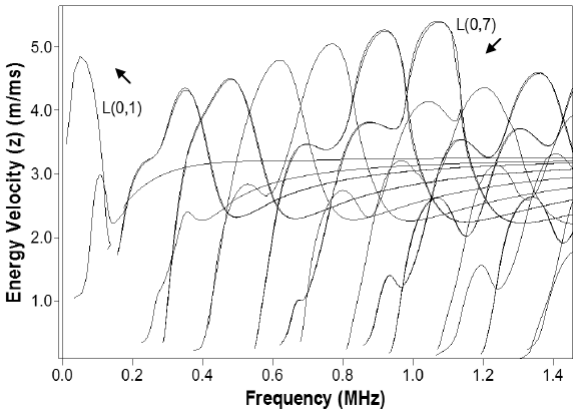

(b) **Energy Velocity vs Frequency**

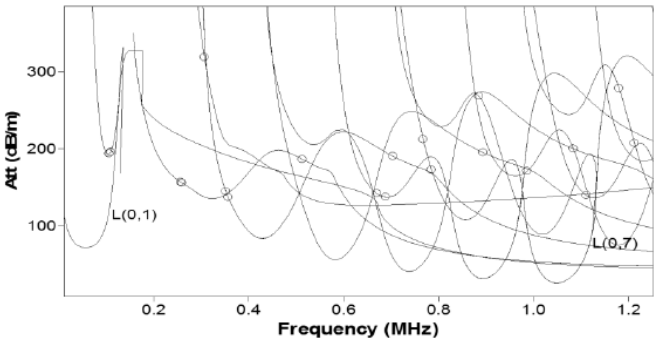

(c) **Attenuation vs Frequency**

Figure 4.12: Dispersion curves for 25 mm diameter bar (Sharma and Mukherjee, 2010)

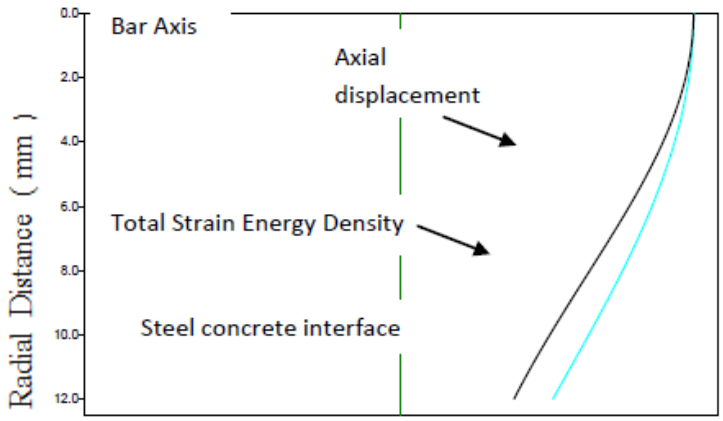

Figure 4.13: Surface seeking mode L(0,1) at 0.1 MHz (Sharma and Mukherjee, 2010)

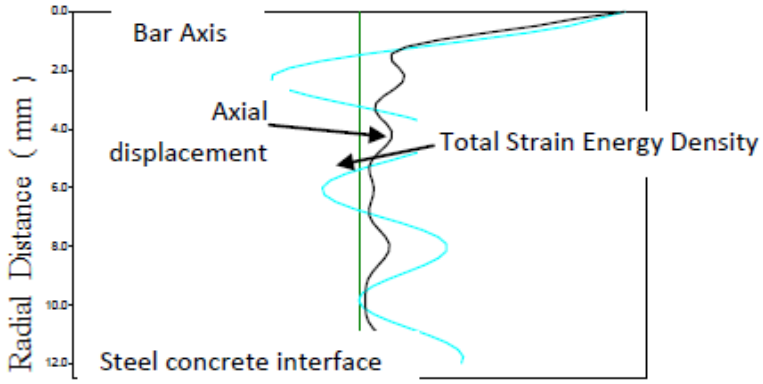

Figure 4.14: Surface seeking mode at L(0,7) at 1 MHz (Sharma and Mukherjee, 2010)

4.5 ACOUSTIC EMISSION INVESTIGATIONS

4.5.1 Setup and specimen details

Cube specimen of size 150mm x 150mm x150 mm with 12 mm mild steel bars immersed at one of the diagonal as shown in the **Figure 4.15** were used. The AE testing for civil investigations uses frequency in the range of 100-300 KHz. Two sensors R15α (resonant at 150 KHz) were mounted on 12 mm diameter mild steel bars . For effective transmission of AE signals to the sensors a layer of couplant like ultrasonic gel, oil, grease is applied between two surfaces and sensors are attached using magnetic holders, tapes, rubber bands or glues. In the present study couplant used was grease and tape was used to hold the sensors

In order to make sure that the sensors were mounted correctly on 12 mm bars and are capable of detecting the reflections pencil break test was carried out. For this AE signals are generated by breaking pencil lead of 0.5mm on different locations on the surface of cube specimen. Two amplifiers, one for each sensor were used with gain at 40 dB and 20-1200

KHz of frequency range . In the data acquisition system, band pass filter of 20-400 KHz was set and threshold value was set to 45 dB.

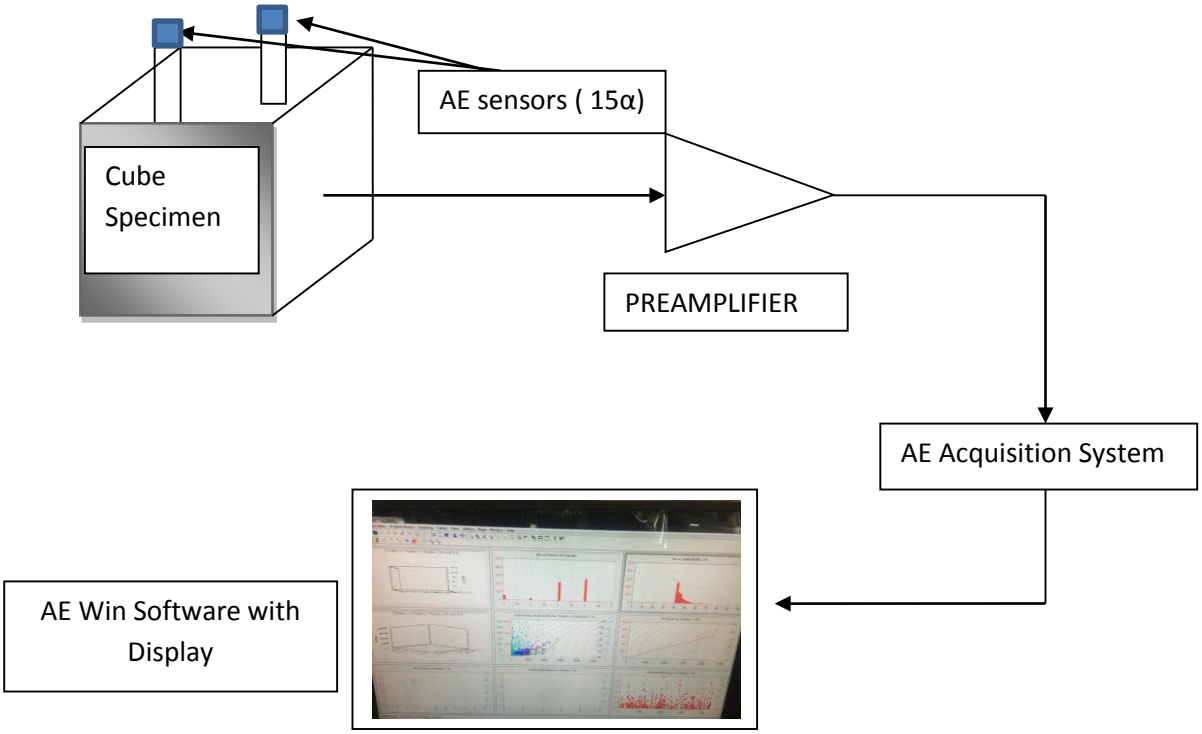

Figure 4.15: Schematic representation of AE monitoring setup

Features of Equipment used are as follows

(a) AE SENSORS

AE sensors are chosen in accordance with their application. Sensors convert mechanical energy of elastic waves detected into electrical signal, hence they function as transducers. AE testing consists of two types of sensors namely resonance (narrow band) and broadband sensors. Where AE features like time of arrival, amplitude and energy are main parameters of study resonant AE sensors are used . They are sensitive to surface waves and resonant frequency plays important role in deciding which AE sensor is to be applied . Broadband sensors respond to a wide range of wave frequency components and are used if frequency desired is unknown or for modal analysis. For the present study R15α sensors were used , specifications of which are as follows:

Table 4.10: Specifications of Sensors Used

S.NO.	R15α
Operating Frequency Range	35-100 KHz

Resonant Frequency	150 KHz
Physical Dimensions	19mm dia x 22.4 mm height
Weight	31 grams
Case Materials	Stainless Steel

Figure 4.16: R15α sensors used in the study

(b) Preamplifier

The signal produced by sensors is further amplified by preamplifier. Preamplifier by Mistras is used which has gain of 40 , 20 and 60 dB and 20-1200 KHz of frequency range .

Figure 4.17: Preamplifier used in the study (Mistras)

(c) AE data acquisition system

It consists of Micro II digital AE system provided by PAC (Physical Acoustics Corporation) shown in the **Figure 4.19** .

Figure 4.18: AE data acquisition system (Micro II , Digital AE system)

4.5.2 AE monitoring methodology

Propagation of elastic waves due to release of localized internal energy constitutes the phenomenon of acoustic emission. Sources of AE activity include crack propagation , plastic deformation and other material degradations. AE sensors convert mechanical energy of elastic waves detected into electrical signal, hence they function as transducers . The signal produced by sensors is further amplified by preamplifier, filtered, detected and measured. Signal voltage is boosted by amplifier to a level which is optimum for its measurement. AE instrument along with stages of amplification has frequency filters which attenuate low frequency background noise and define the frequency range that has to be used . These stages of amplification and filteration are called signal conditioning. The clean signal is then sent to detection circuit which compares amplified signal with user defined threshold voltage . Digital pulse is generated by the comparator when signal voltage rises above threshold voltage. Hence comparator generates additional pulses as the signal oscillates above and below the threshold level.

4.6 DESTRUCTIVE TESTING

4.6.1 Compressive strength of concrete

4.6.1.1 Setup , specimen and methodology

Cubes of size 150mm x 150mm x 150mm were cast. After 24 hours the moulds were removed and test specimens are put in water for curing. The specimens were tested by UTM after 3,7 , 28 and 56 days of curing. Load was applied gradually at the rate of 140 kg/cm^2 per minute till the specimens failed. Load at the failure divided by area of specimen gave the compressive strength of concrete.

$\sigma = P / A$ (4.1)

Where σ = Compressive Strength (N/mm^2)

P = Maximum load (N)

A = Cross section area of cube (mm^2)

(a) Specimen placed in UTM

(b) Sample At Failure

Figure 4.19: Compression testing of cube using UTM

4.7 CHARACTERISATION USING SCANNING ELECTRON MICROSCOPY (SEM) and ENERGY DISPERSIVE SPECTROSCOPY (EDS)

4.7.1 General

Images of samples are generated at high magnification. Images formed by instrument are those due to electrons instead of light thus high magnification photographs are formed . Elements present in particles up to size of one micrometer are identified by EDS detector and results are in the form of black and white images .

Limitations : In case of organic samples images are not clear as they do not generate lot of signals . In case good images above 5000 X magnification are to be obtained the sample must be conductive or it should have sputter coating with thin layer of metal .

4.7.2 Setup and specimen details

Sample constituted of broken pieces after compression testing at 3 and 28 days of curing . Sample was mounted on the pin mount made of Aluminum and shown in **Figure 4.21.**

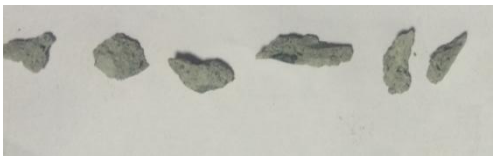

(a) Samples Selected for Testing

(b) Samples mounted

Figure 4.20: Samples for SEM/EDS testing showing samples attached with sticky conducting tape. The copper tape affixed to the top of the sample insures a conductive path to ground .

Sample Grounding

In order to prevent the distortion of image, the electron beam needs to be prevented from charging the sample for which the sample has to be electrically connected to the sample holder . It was done with a conductive sticky double sided copper tape, in case the sample is an insulator it is coated with conductive Au/Pd or Carbon material.

Sample Coating

Deposition system is shown in the **Figure 4.22** with Gold/Palladium target and a sputter deposition rate of about 38 Angstroms per minute. Enough metal was applied in about 1.0-1.5 minutes of sputtering in order to conduct the SEM electrons to ground and prevent charging .

Figure 4.21: Deposition system for coating insulating SEM samples

4.7.3 Methodology

Electrons penetrate the thin sample, collide with its atoms and pass through it and are further detected by diode detectors, thus producing high resolution images both in dark and bright modes with high signal to noise ratio and sharp contrast.

4.8 CLOSING REMARKS

This chapter discusses the characteristics of materials used for making concrete and the supplementary cementitious material used which is silica fume. The layout of experimental program with the details of specimens used and methodology are discussed.

CHAPTER 5

RESULTS AND DISCUSSIONS

The Chapter covers the results obtained by performing different experiments on control concrete and concrete containing silica fume for determining setting and hardening characteristics.

5.1 DESTRUCTIVE TESTING

5.1.1 Compressive strength test

Effect of silica fume (SF) on compressive strength

Figure 5.1 shows the effect of SF on compressive strength of M20 Grade concrete mixes S(0%SF), S-1 (3% SF), S-2(6% SF), S-3 (10% SF) and S-4(12% SF) at the age of 3,7, 28 and 56 days . Percentage replacements were decided with help of previous research carried in this field which show that 10-15 % SF is optimum replacement of cement as further no significant to strength is observed , this may be attributed to extremely fine particle of silica fume which might lead to agglomeration and therefore lead to opposite results (Sanjuan et al ., 2015 and Zhang et al., 2016).

From the compressive strength test results following observations were made:

a) From **Table 5.1** the compressive strength of control concrete mix (S) at 3 days was 10.7 MPa and that of other mixes S1 (3% SF), S2 (6% SF), S3 (10% SF) and S4 (12% SF) were 15.67, 25.36, 25.36 and 39.315 MPa with the percentage increase of 7.28% , 9.15% , 41.57% and 42.31% respectively .
b) Similarly it was found that 7 days compressive strength increased by 5.87%, 6.74%, 18.95% and 24.82% for mixtures S1 (3% SF), S2 (6% SF), S3 (10% SF) and S4 (12% SF) respectively than control mix (S) .
c) At 28 days, increase in strength was 3.06%, 3.87%, 7.66% and 7.31% for S1, S2, S3 and S4 mixes, when compared with S respectively.
d) Percentage increase in compressive strength observed for mixes S1, S2, S3 and S4 were 3.06, 3.87,7.66 and 7.31% respectively than mix S (42.8MPa) at the age of 56 days.
e) Thus it is concluded that with increasing percentage replacement of cement with silica fume up to a maximum of 12%, the strength increased at all the ages .

f) Further it was observed that mixes containing 10% and 12% silica fume exhibited maximum strength as well as percentage increase in compressive strength was also maximum for these two mixes at all the ages which can be seen in **Table 5.2 and Figure 5.1 and 5.2 .**

g) Strength enhancement of SF concrete is related to more spherical shape, smooth texture , fine particles and higher amorphous silicon dioxide content which is highly reactive pozzolanic material as compared to cement particles. Weakest part of hardened concrete system is interfacial transition zone and silica fume helps improve it. SF when added to concrete improves cement – aggregate bond by reducing interfacial transition zone thickness as well as by reduction of orientation of $Ca(OH)_2$ portlandite crystals. Consequently besides chemical formation of C-S-H gel microstructure change i.e. $Ca(OH)_2$ orientation and transition zone thickness justify the strength enhancement.

Table 5.1: Compressive strength of different samples of concrete at different ages .

		Compressive Strength (MPa)			
Age of concrete (in days)	**S (Control concrete)**	**S1 (3% SF)**	**S2 (6 % SF)**	**S3 (10 % SF)**	**S4 (12 % SF)**
3	10.7	11.48	11.68	15.149	15.227
7	15.67	16.59	16.727	18.64	19.56
28	25.36	26.46	26.8	30.73	30.33
56	39.315	40.52	40.84	42.33	42.19

Also the percentage increase in compressive strength decreased at all ages for all the replacement levels. This percentage rate of strength development reduces with age this may be attributed to formation of compact layer of reaction product i.e. C-S-H gel in SF concrete which inhibits the diffusion of ions and hence reaction of SF with $Ca(OH)_2$. Another explanation is the concentration of $Ca(OH)_2$ and alkalis decline (Sanjaun et al., 2015) leading to a drop in pH and retardation of hydration of cement.

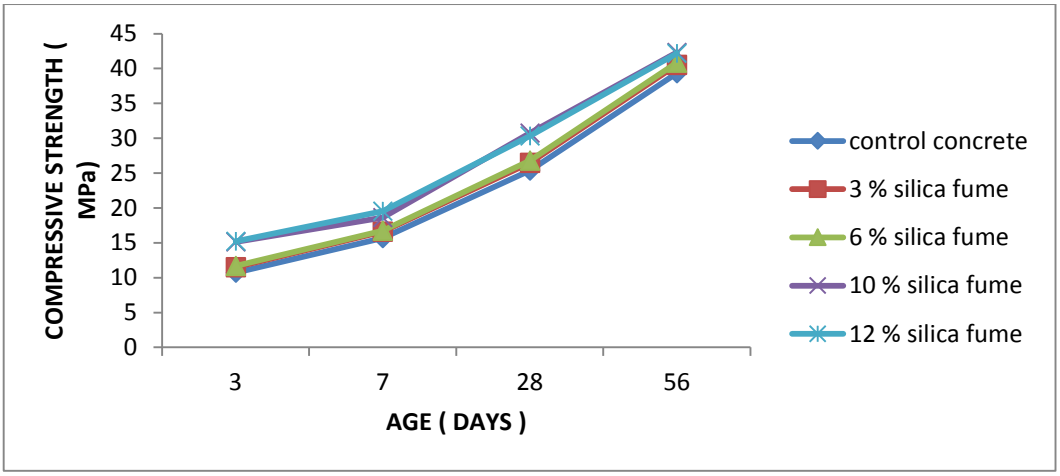

Figure 5.1: Graphs depicting variation of compressive strength vs age of concrete

Table 5.2: Percentage increase in compressive strength with varying replacement of SF in concrete at different ages

		Percentage Increase in Compressive Strength			
Age of concrete(in days)	**Control Concrete (Reference)**	**3% SF**	**6 % SF**	**10% SF**	**12 % SF**
3	0	7.28	9.15	41.57	42.31
7	0	5.87	6.74	18.95	24.824
28	0	4.33	5.67	21.17	19.59
56	0	3.06	3.87	7.66	7.31

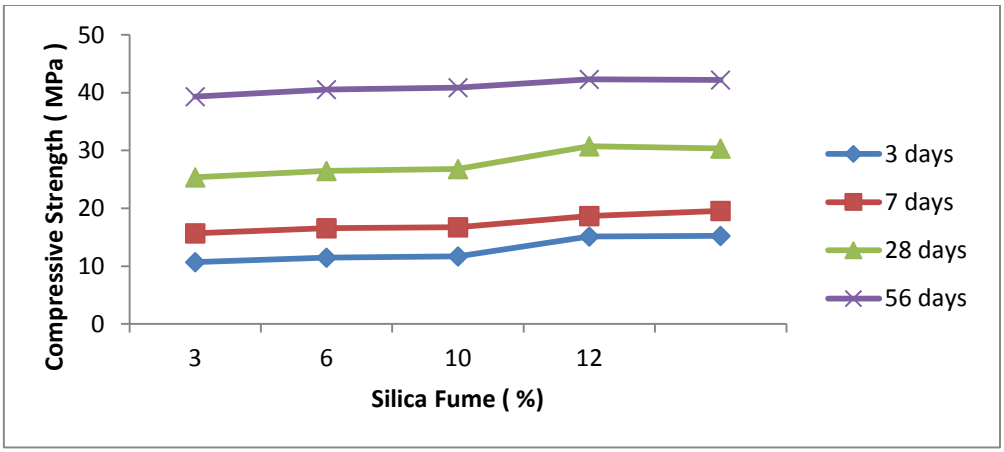

Figure 5.2: Compressive strength vs percentage replacement of cement by silica fume at different ages of concrete

5.2 CHARACTERISATION USING SEM / EDS RESULTS

5.2.1 SEM analysis

SEM images of cement paste and aggregates of control concrete and concrete containing 3%, 6%, 10% and 12% silica fume were taken at 3 days and 28 days. **Figure 5.3 and 5.4** show the results of control and other specimens at 3 days and 28 days and further to determine the chemical composition of SEM images, EDS elemental analysis was carried out as shown in **Figure 5.5** at 3 days and **Figure 5.6** at 28 days.

Microstructure of control concrete at 3 days

Figure 5.3 (a) shows SEM images between aggregate and paste; the aggregate surface was covered by small amounts of C-S-H gels and were irregularly structured, the matrix is porous and non- uniform. Ettringite needle crystals which were porous material and pores were visible; further $Ca(OH)_2$ portlandite crystals were seen.

Microstructure of concrete containing various percentages of silica fume at 3 days

As the percentage replacement of cement by silica fume is increased from 3 to 12 % the microstructure became dense and uniform which was due to CH crystals being consumed in pozzolanic reaction between silica fume and $Ca(OH)_2$ in order to produce C-S-H gels. Hence less porosity, dense and uniform development of matrix.

Further the high specific surface area of amorphous silica fume results in lesser bleeding and wall effect is less critical in samples containing silica fume. (Scrivener et al., 2004) Whereas in case of control concrete specimens have water filled spaces (Bentur and Cohen, 1987) surround aggregates in fresh and hardened stages.

Microstructure of control concrete at 28 days

Figure 5.4 (a) shows SEM images**.** Apart from C-S-H small and large crystals of CH and pores were visible.

Microstructure of concrete containing various percentages of silica fume at 28 days

Figure 5.4 (b, c, d and e) shows SEM images. Large crystals of CH and pores were not observed and denser and compact hydration products appeared.

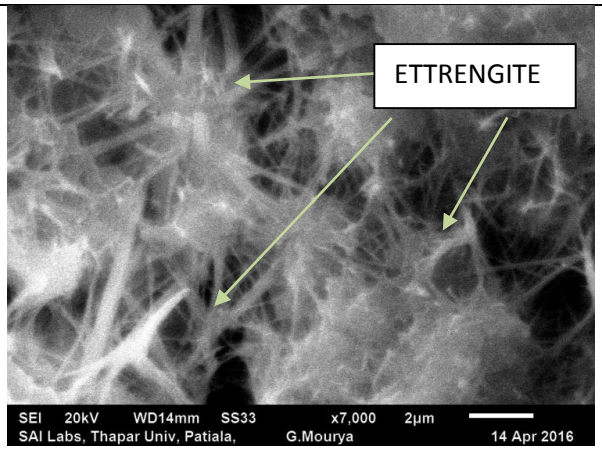
ETTRENGITE
SEI 20kV WD14mm SS33 x7,000 2µm
SAI Labs, Thapar Univ, Patiala, G.Mourya 14 Apr 2016

(A)

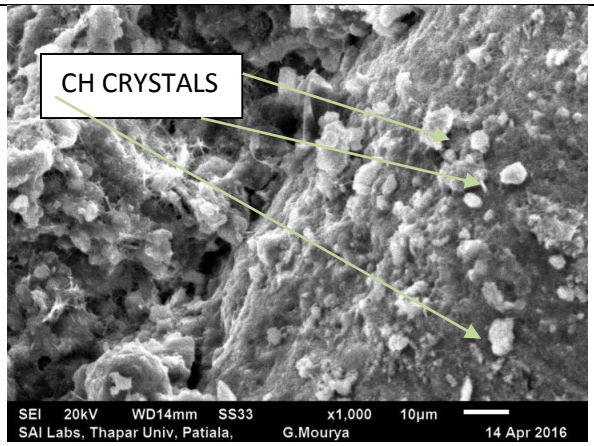
CH CRYSTALS
SEI 20kV WD14mm SS33 x1,000 10µm
SAI Labs, Thapar Univ, Patiala, G.Mourya 14 Apr 2016

(B)

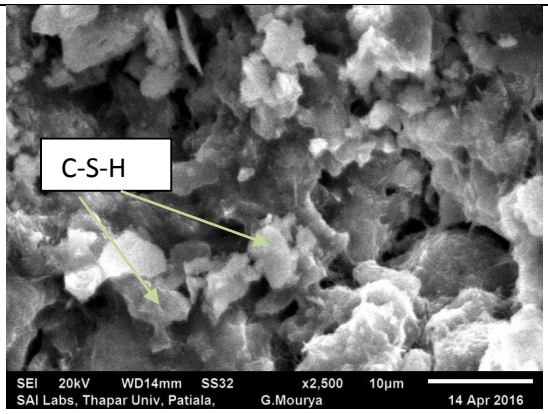
C-S-H
SEI 20kV WD14mm SS32 x2,500 10µm
SAI Labs, Thapar Univ, Patiala, G.Mourya 14 Apr 2016

(C)

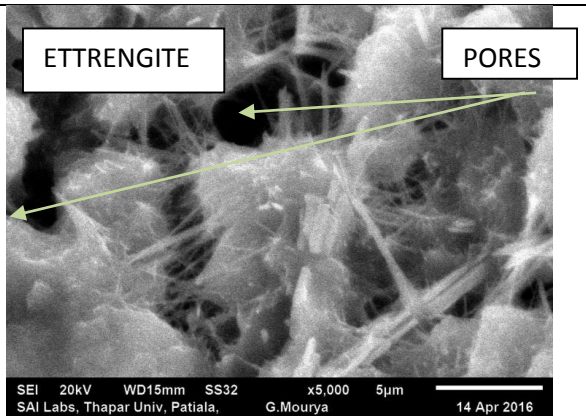
ETTRENGITE
PORES
SEI 20kV WD15mm SS32 x5,000 5µm
SAI Labs, Thapar Univ, Patiala, G.Mourya 14 Apr 2016

(D)

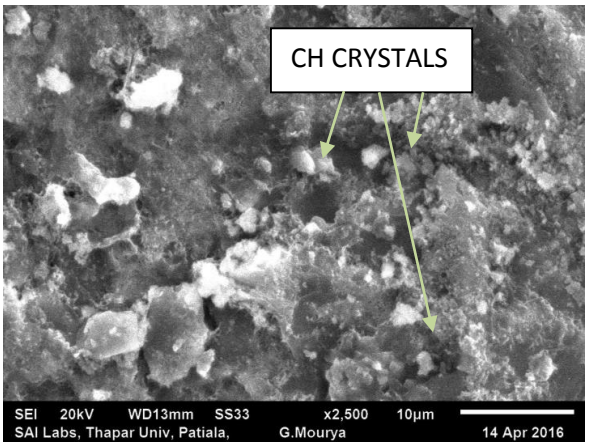
CH CRYSTALS
SEI 20kV WD13mm SS33 x2,500 10µm
SAI Labs, Thapar Univ, Patiala, G.Mourya 14 Apr 2016

(A)

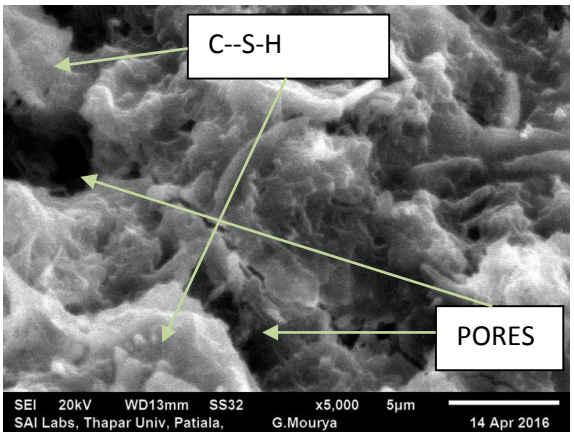
C--S-H
PORES
SEI 20kV WD13mm SS32 x5,000 5µm
SAI Labs, Thapar Univ, Patiala, G.Mourya 14 Apr 2016

(B)

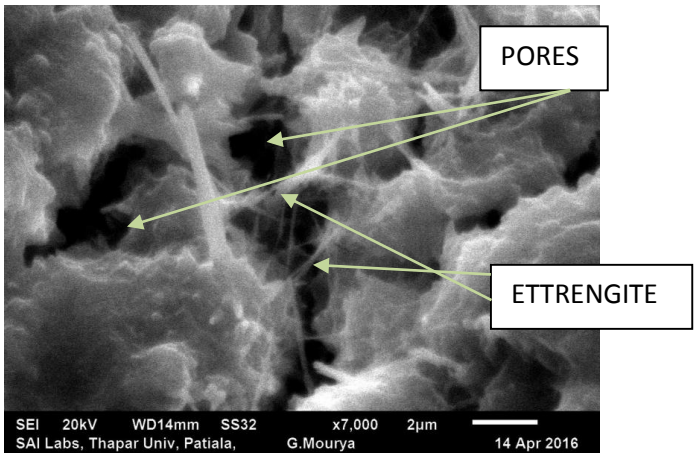
PORES
ETTRENGITE
SEI 20kV WD14mm SS32 x7,000 2µm
SAI Labs, Thapar Univ, Patiala, G.Mourya 14 Apr 2016

(C)

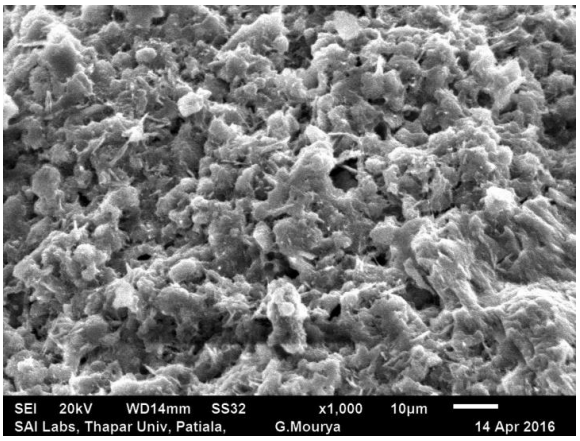
SEI 20kV WD14mm SS32 x1,000 10µm
SAI Labs, Thapar Univ, Patiala, G.Mourya 14 Apr 2016

(D)

(b)

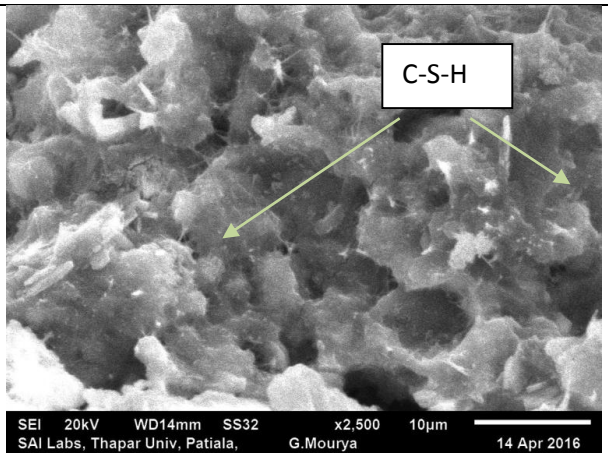
C-S-H
SEI 20kV WD14mm SS32 x2,500 10µm
SAI Labs, Thapar Univ, Patiala, G.Mourya 14 Apr 2016

(A)

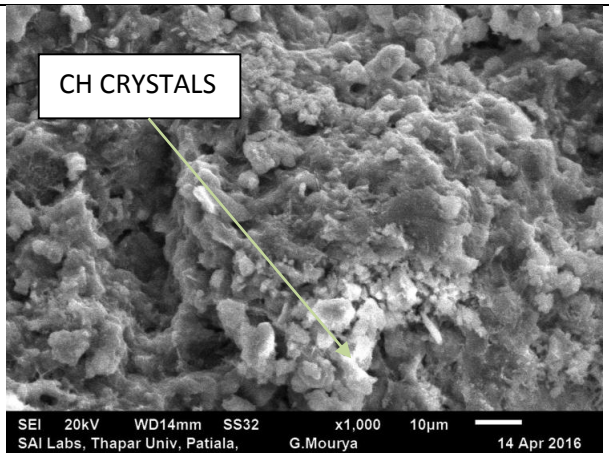
CH CRYSTALS
SEI 20kV WD14mm SS32 x1,000 10µm
SAI Labs, Thapar Univ, Patiala, G.Mourya 14 Apr 2016

(B)

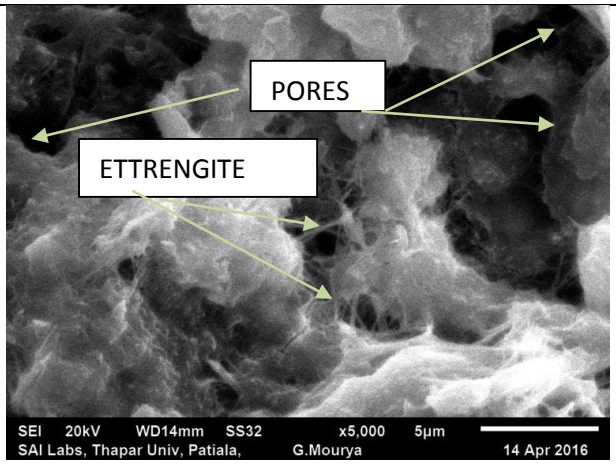
PORES
ETTRENGITE
SEI 20kV WD14mm SS32 x5,000 5µm
SAI Labs, Thapar Univ, Patiala, G.Mourya 14 Apr 2016

(C)

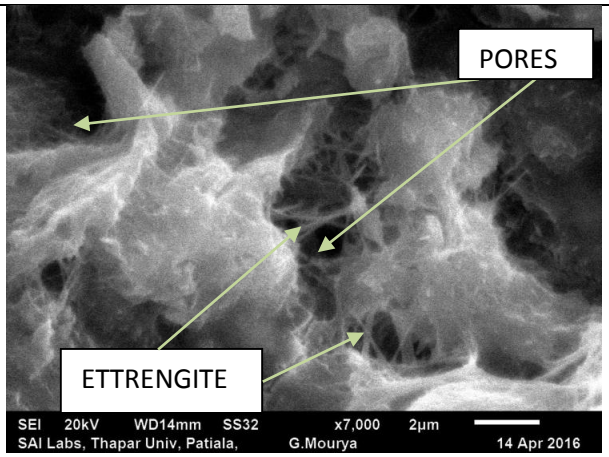
PORES
ETTRENGITE
SEI 20kV WD14mm SS32 x7,000 2µm
SAI Labs, Thapar Univ, Patiala, G.Mourya 14 Apr 2016

(D)

(c)

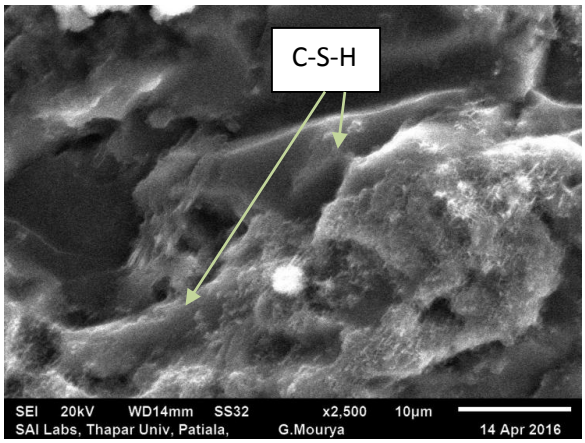
C-S-H
SEI 20kV WD14mm SS32 x2,500 10µm
SAI Labs, Thapar Univ, Patiala, G.Mourya 14 Apr 2016

(A)

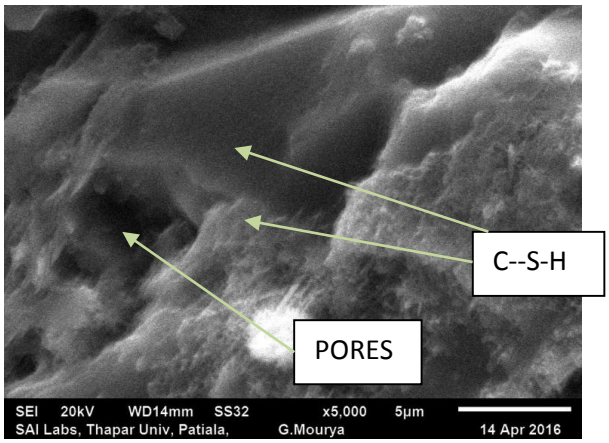
C--S-H
PORES
SEI 20kV WD14mm SS32 x5,000 5µm
SAI Labs, Thapar Univ, Patiala, G.Mourya 14 Apr 2016

(B)

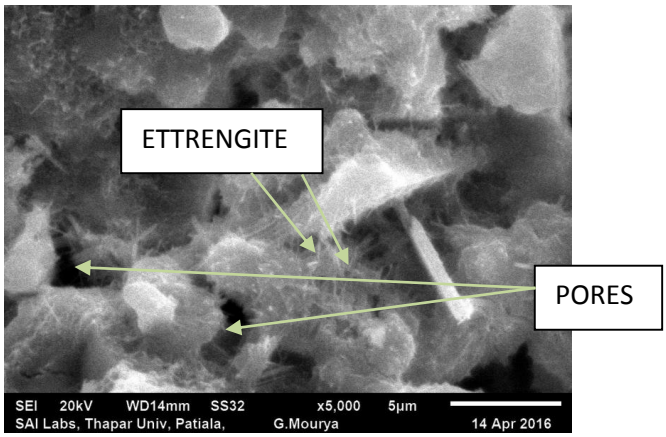
ETTRENGITE
PORES
SEI 20kV WD14mm SS32 x5,000 5µm
SAI Labs, Thapar Univ, Patiala, G.Mourya 14 Apr 2016

(C)

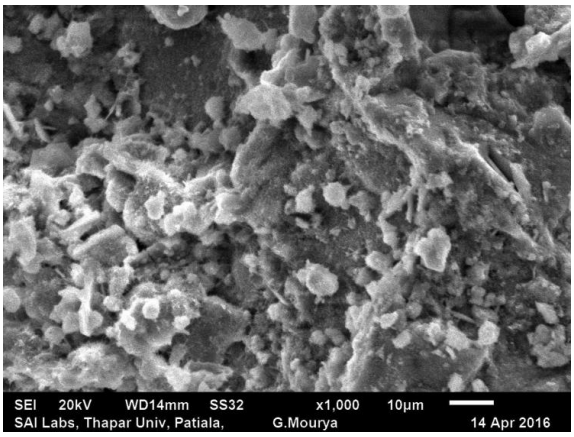
SEI 20kV WD14mm SS32 x1,000 10µm
SAI Labs, Thapar Univ, Patiala, G.Mourya 14 Apr 2016

(D)

(d)

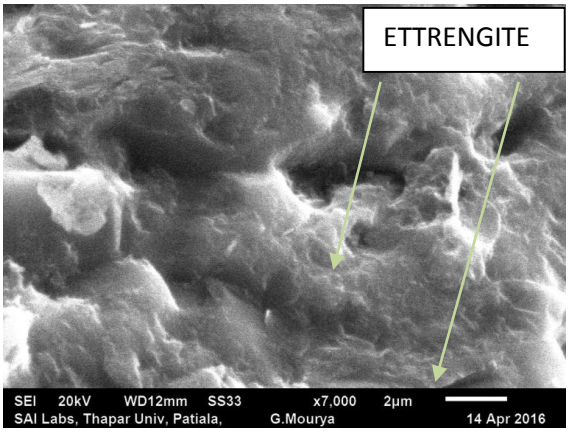
ETTRENGITE
SEI 20kV WD12mm SS33 x7,000 2µm
SAI Labs, Thapar Univ, Patiala, G.Mourya 14 Apr 2016

(A)

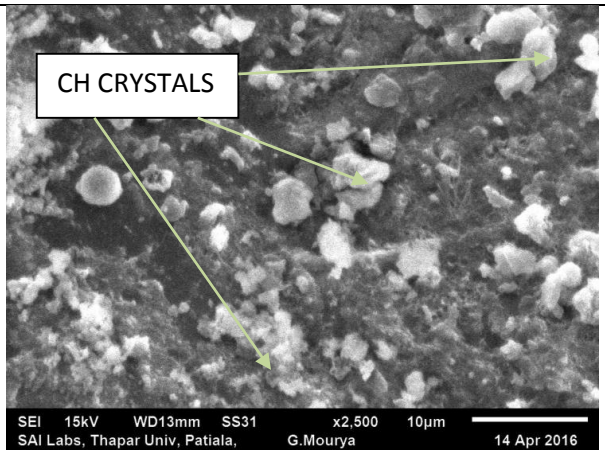
CH CRYSTALS
SEI 15kV WD13mm SS31 x2,500 10µm
SAI Labs, Thapar Univ, Patiala, G.Mourya 14 Apr 2016

(B)

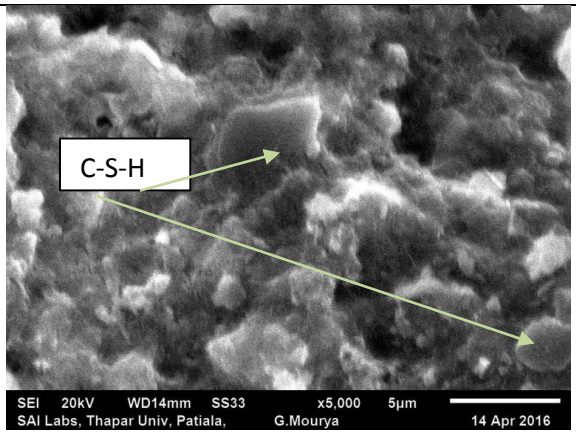

(C)

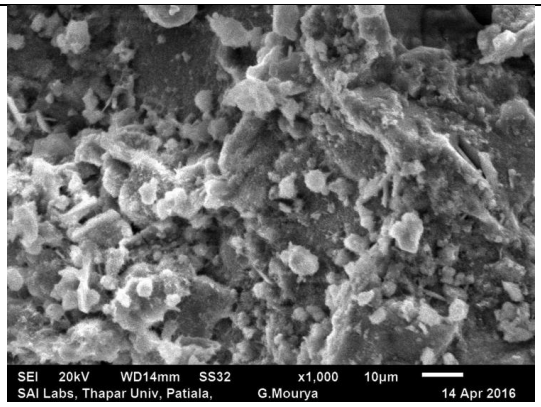

(D)

(e)

Figure 5.3: **SEM images of various samples at 3 days of curing (a) control concrete (S) , (b) 3% silica fume (S1) , (c) 6% silica fume (S2) , (d) 10% silica fume (S3) and (e) 12% silica fume (S4)**

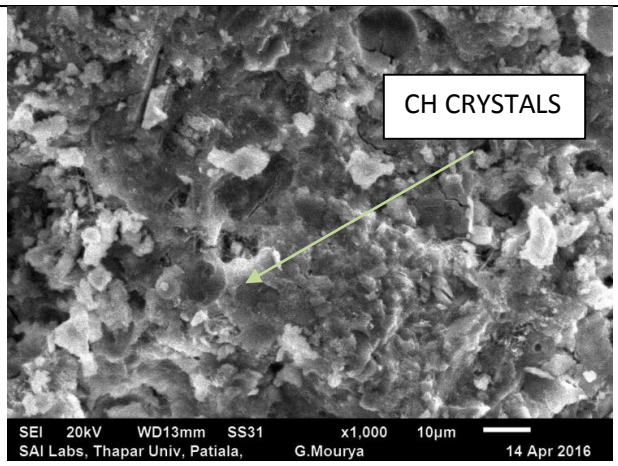

(A)

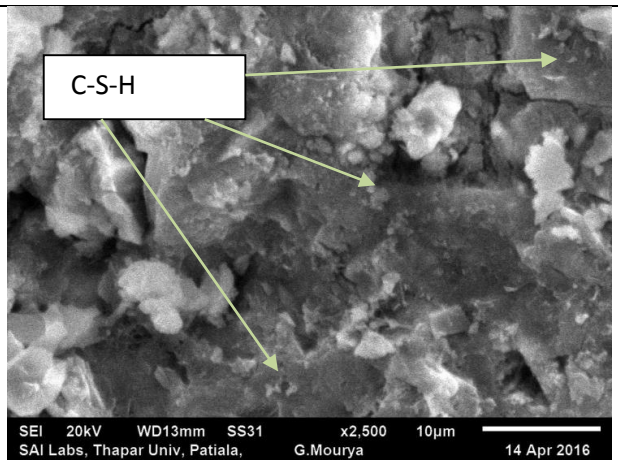

(B)

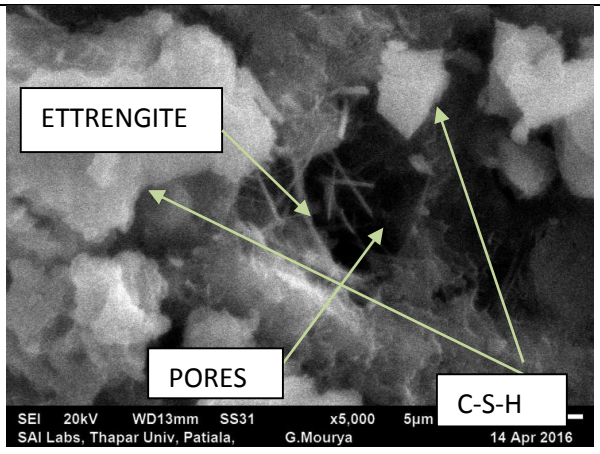

(C)

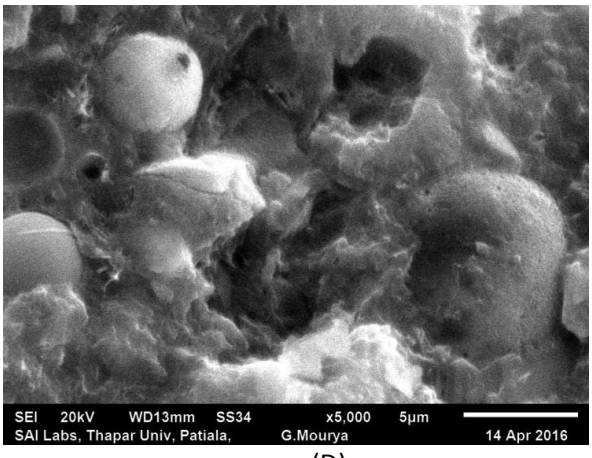

(D)

(a)

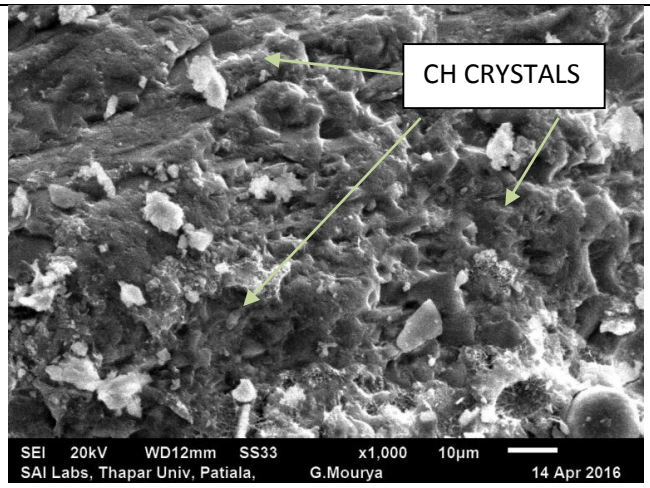
CH CRYSTALS
SEI 20kV WD12mm SS33 x1,000 10µm
SAI Labs, Thapar Univ, Patiala, G.Mourya 14 Apr 2016

(A)

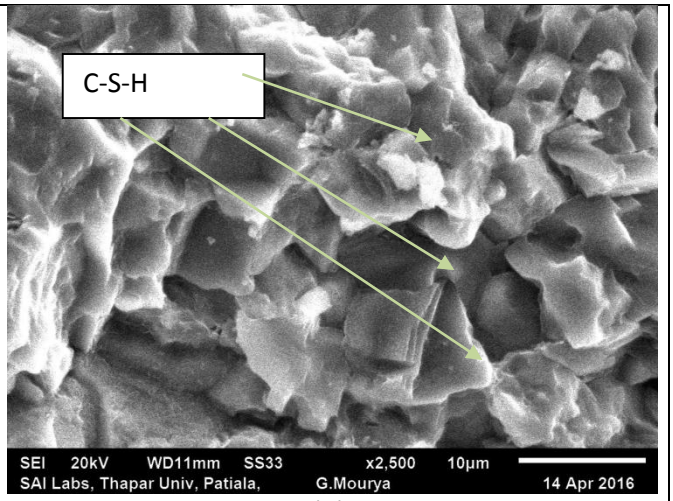
C-S-H
SEI 20kV WD11mm SS33 x2,500 10µm
SAI Labs, Thapar Univ, Patiala, G.Mourya 14 Apr 2016

(B)

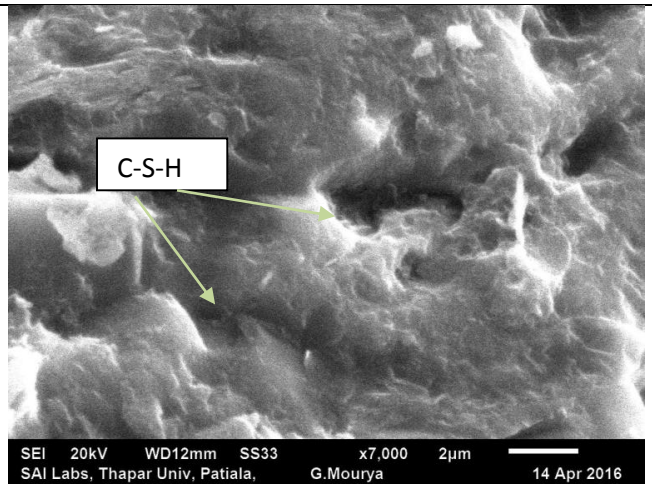
C-S-H
SEI 20kV WD12mm SS33 x7,000 2µm
SAI Labs, Thapar Univ, Patiala, G.Mourya 14 Apr 2016

(C)

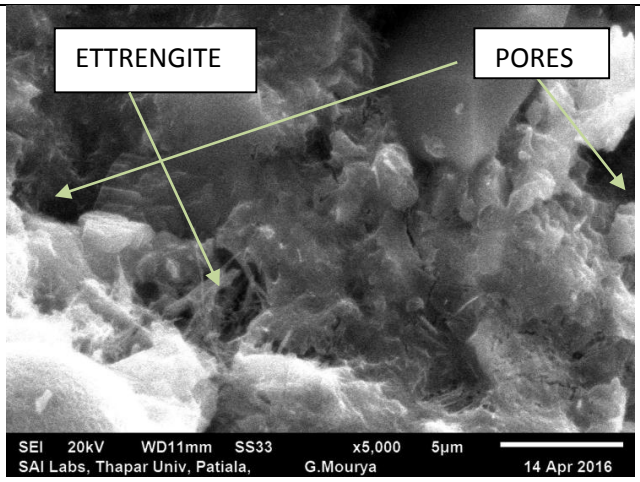
ETTRENGITE
PORES
SEI 20kV WD11mm SS33 x5,000 5µm
SAI Labs, Thapar Univ, Patiala, G.Mourya 14 Apr 2016

(D)

(b)

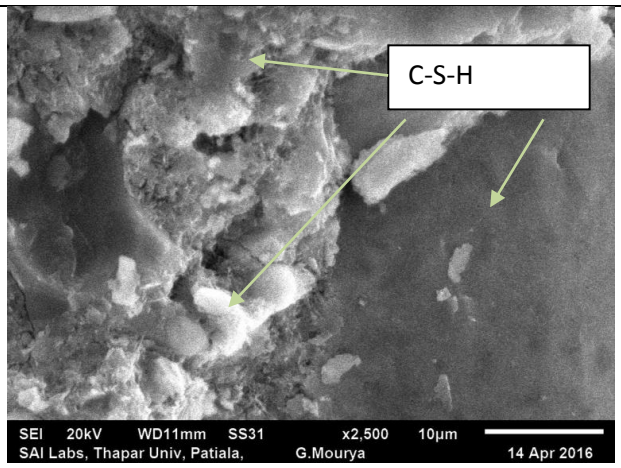
C-S-H
SEI 20kV WD11mm SS31 x2,500 10µm
SAI Labs, Thapar Univ, Patiala, G.Mourya 14 Apr 2016

(A)

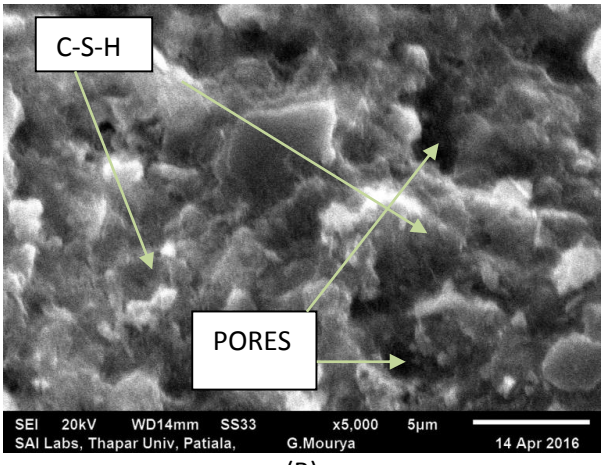
C-S-H
PORES
SEI 20kV WD14mm SS33 x5,000 5µm
SAI Labs, Thapar Univ, Patiala, G.Mourya 14 Apr 2016

(B)


C-S-H
SEI 20kV WD11mm SS31 x1,000 10µm
SAI Labs, Thapar Univ, Patiala, G.Mourya 14 Apr 2016

(C)

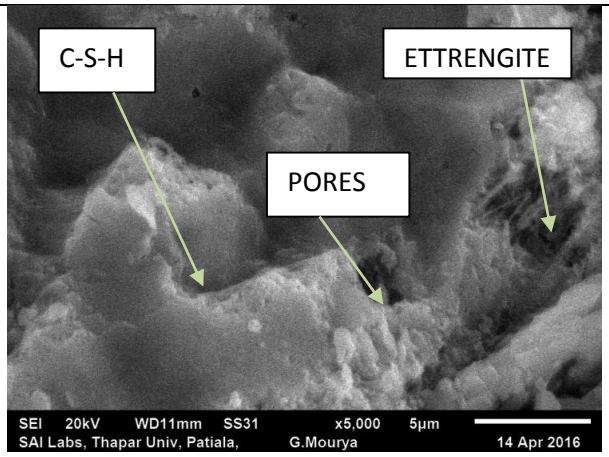
C-S-H
ETTRENGITE
PORES
SEI 20kV WD11mm SS31 x5,000 5µm
SAI Labs, Thapar Univ, Patiala, G.Mourya 14 Apr 2016

(D)

(c)

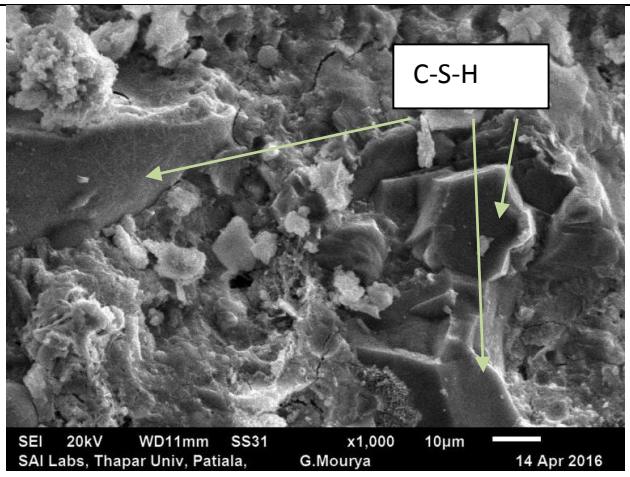
C-S-H
SEI 20kV WD11mm SS31 x1,000 10µm
SAI Labs, Thapar Univ, Patiala, G.Mourya 14 Apr 2016

(A)

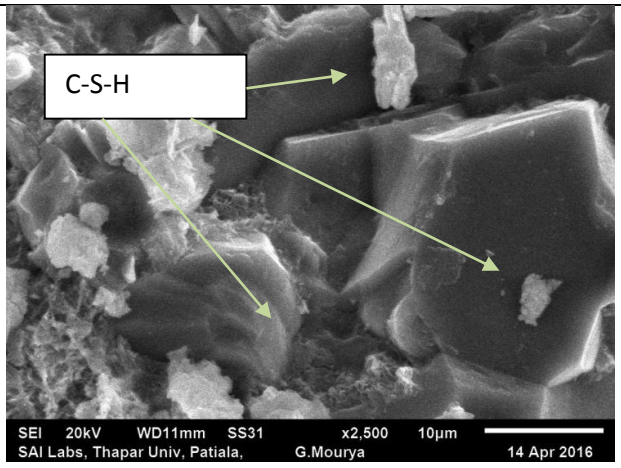
C-S-H
SEI 20kV WD11mm SS31 x2,500 10µm
SAI Labs, Thapar Univ, Patiala, G.Mourya 14 Apr 2016

(B)


C-S-H
SEI 20kV WD11mm SS34 x5,000 5µm
SAI Labs, Thapar Univ, Patiala, G.Mourya 14 Apr 2016

(C)

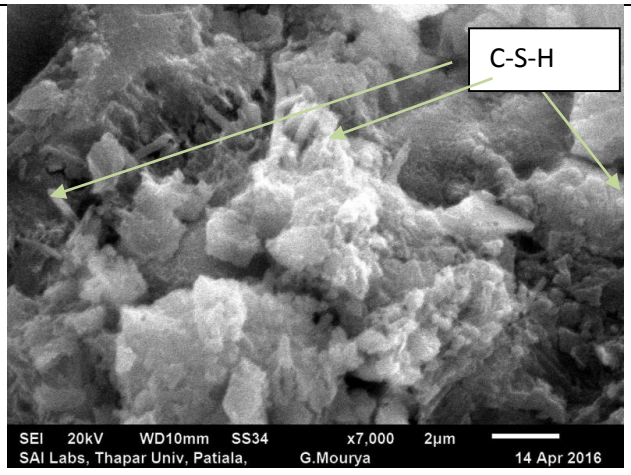
C-S-H
SEI 20kV WD10mm SS34 x7,000 2µm
SAI Labs, Thapar Univ, Patiala, G.Mourya 14 Apr 2016

(D)

(d)

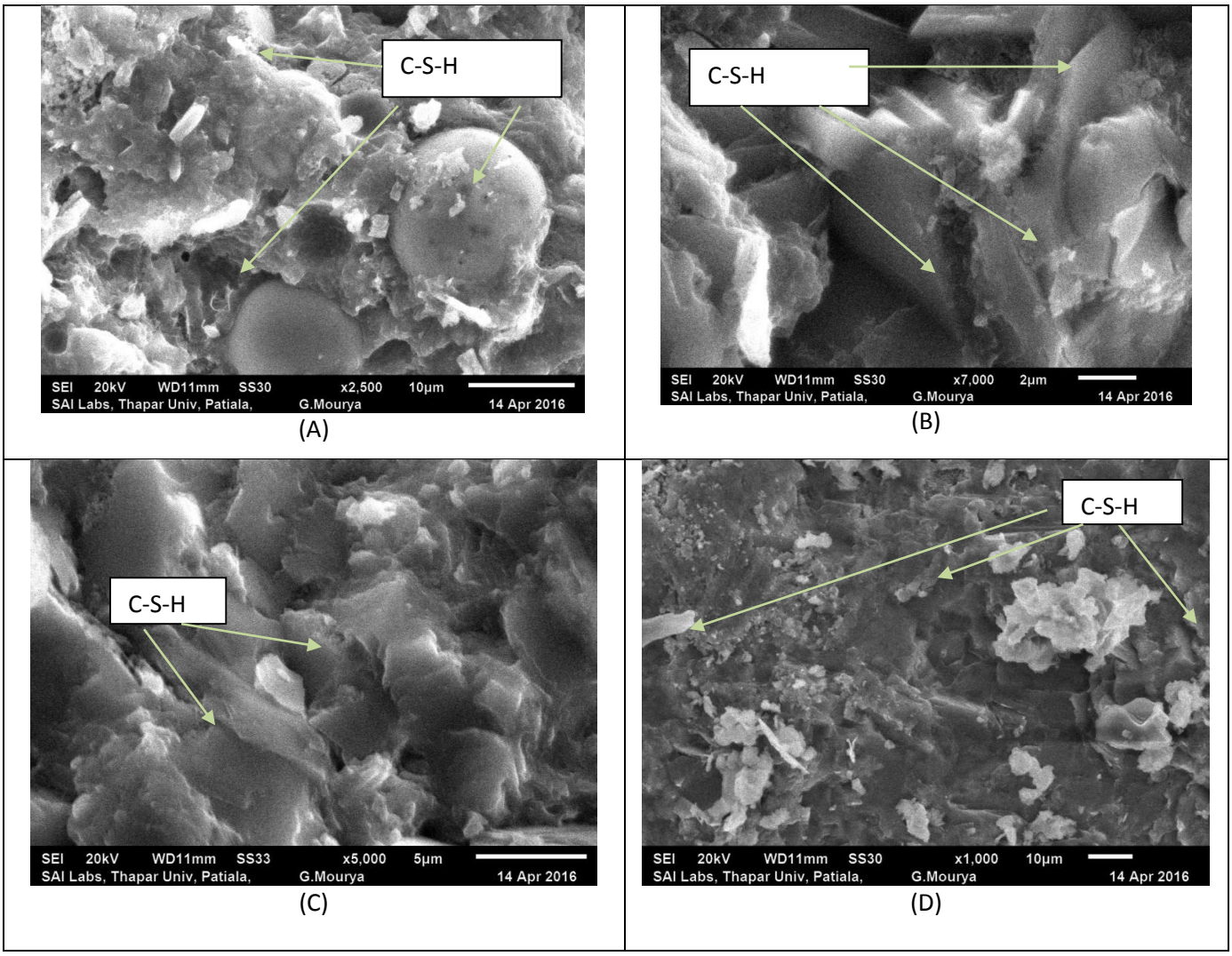

(e)

Figure 5.4: **SEM images of various samples at 28 days of curing (a) control concrete (S) , (b) 3% silica fume (S1) , (c) 6% silica fume (S2) , (d) 10% silica fume (S3) and (e) 12% silica fume (S4)**

5.2.2 EDS results

Table 5.3 and Figure 5.5 represents approximate oxide composition of various samples at 3 days of curing using EDS analysis and **Table 5.4 and Figure 5.6** represents the same at 28 days of curing. At various points the composition using EDS was found and the results were averaged.

Following observations were made :

i. At 3 days of curing it was observed that control specimen S (0% SF) had Ca/Si ratio of 1.59 whereas specimens S1 (3% SF); S2 (6% SF); S3 (10% SF) and S4 (12% SF) had Ca/Si ratio of 1.42, 1.142, 1.108 and 0.84 respectively.

ii. At 28 days of curing the Ca/Si fell from all specimens. From **Table 5.4** the values of S (0%); S1 (3%SF), S2 (6% SF); S3 (10%SF) and S4 (12% SF) were 1.16, 0.793, 0.527, 0.28 and 0.124 respectively.

iii. From **Table 5.3**, the percentage reduction of Ca/Si values from 3 days to 28 days of curing is presented for all specimens. It was observed that

a) Ca/Si value dropped for all specimens from 3 to 28 days of curing.

b) As the percentage replacement of cement by silica fume increased, the percentage reduction in Ca/Si values increased; hence in 12% silica fume (S4) specimens maximum percentage reduction of 85.23 was observed.

The observations are attributed to the fact that in early stages $Ca(OH)_2$ is present and C-S-H gel which was formed is rich in Ca and in control concrete at later stages as the reaction proceeded Ca present was consumed in the reaction and hence Ca / Si ratio decreased , whereas in case of samples containing silica fume , SiO_2 reacts with the $Ca(OH)_2$ and its content reduced which lead to C-S-H gel which were rich in Si and Ca /Si ratio reduced . This validates with the previous research (Muller et al., 2015 ; Rossen et al. 2015 ; Bach et al., 2012 ; Lothenbach ,2014). Thus due to reaction of $Ca(OH)_2$ with SiO_2 lead to consumption of calcium and hence loss of calcium from C-S-H . Hence changes in pore solution occurs as calcium concentration as well as pH decrease with increase in levels of silica concentration (Bach et al. 2012 ; Lothenbach, 2014).

Table 5.3: **Composition of various samples at 3 days of curing using EDS analysis**

	Control Concrete	**3 % SF**	**6 % SF**	**10 % SF**	**12 % SF**
CaO	37.56	45.19	36.26	36.84	38.59
SiO_2	23.61	31.8	31.74	33.24	41.1
Ca/Si	1.59	1.42	1.142	1.108	0.84

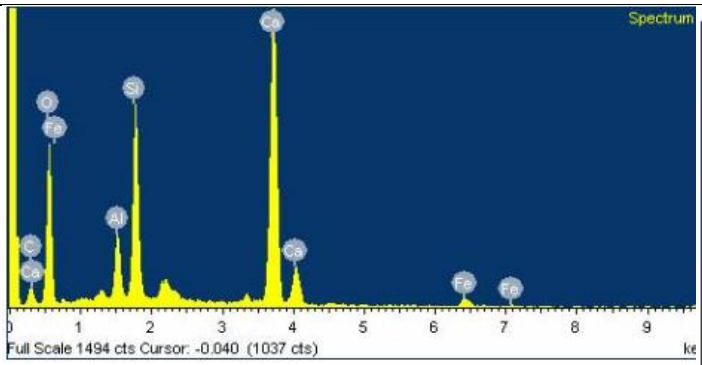

Element	Weight%	Atomic%	Compd%	Formula
C K	7.99	13.51	29.29	CO2
Al K	3.69	2.77	6.96	Al2O3
Si K	11.04	7.97	23.61	SiO2
Ca K	26.85	13.59	37.56	CaO
Fe K	2.00	0.73	2.57	FeO
O	48.44	61.43		
Totals	100.00			

(a) Control Concrete (S)

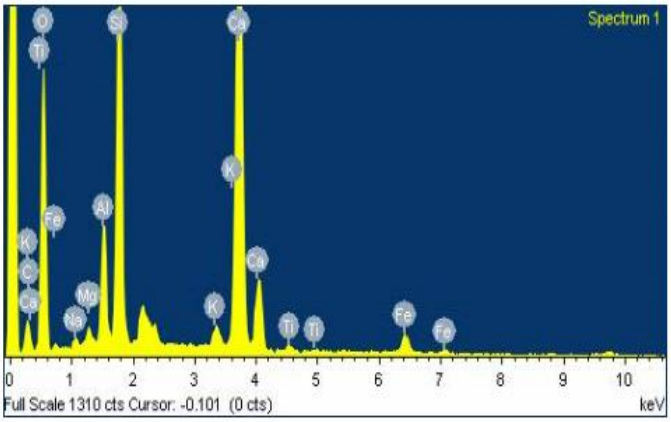

Element	Weight%	Atomic%	Compd%	Formula
C K	1.97	3.76	7.20	CO2
Na K	0.62	0.62	0.83	Na2O
Mg K	0.61	0.57	1.00	MgO
Al K	4.28	3.64	8.09	Al2O3
Si K	14.87	12.15	31.80	SiO2
K K	1.01	0.59	1.21	K2O
Ca K	32.30	18.50	45.19	CaO
Ti K	0.57	0.27	0.95	TiO2
Fe K	2.89	1.19	3.71	FeO
O	40.90	58.70		
Totals	100.00			

(b) 3 % Silica Fume (S1)

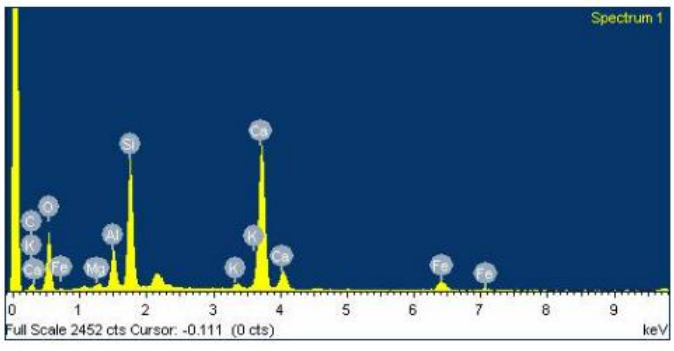

Element	Weight%	Atomic%	Compd%	Formula
C K	4.32	7.80	15.82	CO2
Mg K	0.63	0.56	1.04	MgO
Al K	4.33	3.49	8.19	Al2O3
Si K	14.84	11.47	31.74	SiO2
K K	0.85	0.47	1.03	K2O
Ca K	25.91	14.03	36.26	CaO
Fe K	4.61	1.79	5.93	FeO
O	44.51	60.39		
Totals	100.00			

(c) 6 % Silica Fume (S2)

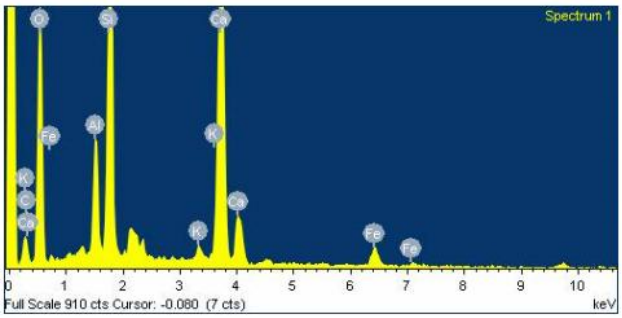

Element	Weight%	Atomic%	Compd%	Formula
C K	3.84	6.97	14.07	CO2
Al K	4.80	3.88	9.08	Al2O3
Si K	15.54	12.07	33.24	SiO2
K K	0.70	0.39	0.84	K2O
Ca K	27.58	15.01	38.59	CaO
Fe K	3.25	1.27	4.18	FeO
O	44.29	60.40		
Totals	100.00			

(d) 10 % Silica Fume (S3)

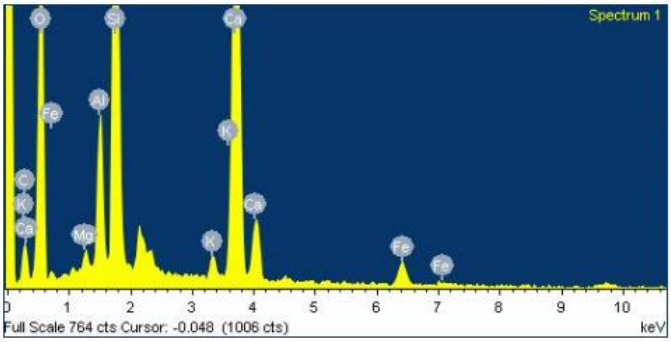

Element	Weight%	Atomic%	Compd%	Formula
C K	1.20	2.25	4.38	CO2
Mg K	0.65	0.60	1.07	MgO
Al K	4.75	3.98	8.98	Al2O3
Si K	20.36	16.36	43.56	SiO2
K K	1.08	0.62	1.30	K2O
Ca K	26.33	14.83	36.84	CaO
Fe K	3.01	1.22	3.87	FeO
O	42.63	60.14		
Totals	100.00			

(e) 12 % Silica Fume (S4)

Figure 5.5: **Composition of various samples at 3 days of curing using EDS analysis (a) control concrete (S) , (b) 3% silica fume (S1) , (c) 6% silica fume (S2) , (d) 10% silica fume (S3) and (e) 12% silica fume (S4)**

Table 5.4 : **Composition of various samples at 28 days of curing using EDS analysis**

	Control Concrete	**3% SF**	**6% SF**	**10% SF**	**12% SF**
CaO	35.78	25.92	21.31	10.55	9.07
SiO_2	30.78	32.67	40.7	37.58	72.77
Ca/Si	1.16	0.793	0.527	0.28	0.124

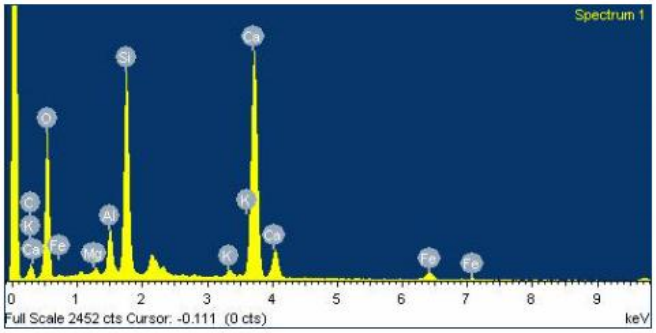

Element	Weight%	Atomic%	Compd%	Formula
C K	6.31	10.89	23.11	CO2
Mg K	0.55	0.47	0.91	MgO
Al K	3.11	2.39	5.87	Al2O3
Si K	14.39	10.62	30.78	SiO2
K K	0.62	0.33	0.75	K2O
Ca K	25.57	13.23	35.78	CaO
Fe K	2.18	0.81	2.81	FeO
O	47.28	61.27		
Totals	100.00			

(a) Control Concrete (S)

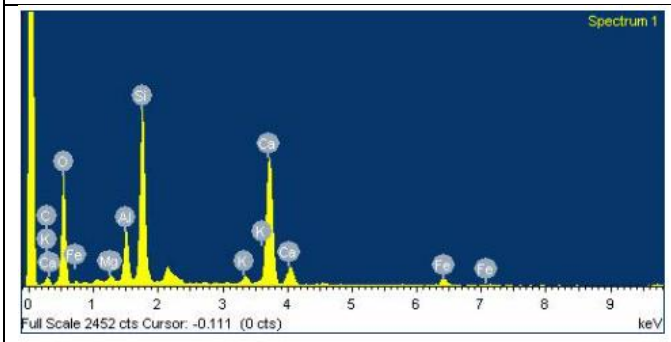

Element	Weight%	Atomic%	Compd%	Formula
C K	7.62	12.60	27.93	CO2
Mg K	0.61	0.50	1.01	MgO
Al K	4.34	3.19	8.19	Al2O3
Si K	15.27	10.80	32.67	SiO2
K K	0.91	0.46	1.10	K2O
Ca K	18.52	9.18	25.92	CaO
Fe K	2.47	0.88	3.18	FeO
O	50.25	62.38		
Totals	100.00			

(b) 3 % Silica Fume (S1)

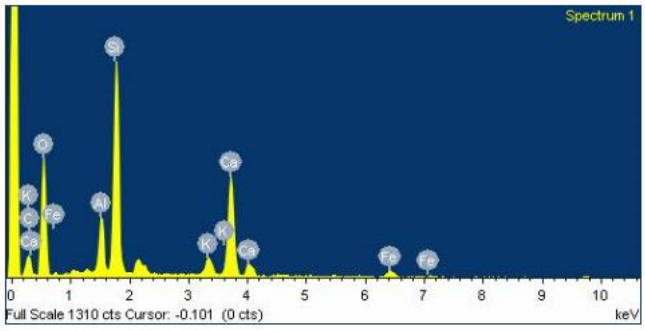

Element	Weight%	Atomic%	Compd%	Formula
C K	6.30	10.53	23.10	CO2
Al K	4.83	3.59	9.13	Al2O3
Si K	19.03	13.59	40.70	SiO2
K K	2.15	1.10	2.59	K2O
Ca K	15.23	7.62	21.31	CaO
Fe K	2.46	0.88	3.16	FeO
O	49.99	62.68		
Totals	100.00			

(c) 6 % Silica Fume (S2)

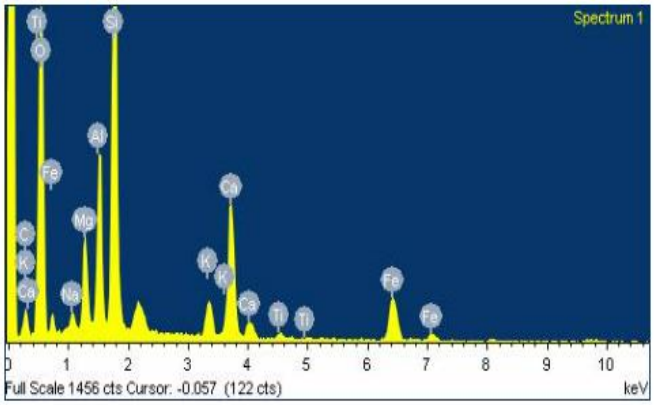

Element	Weight%	Atomic%	Compd%	Formula
C K	5.80	9.71	21.27	CO2
Na K	1.00	0.88	1.35	Na2O
Mg K	3.64	3.01	6.04	MgO
Al K	6.20	4.62	11.71	Al2O3
Si K	17.57	12.57	37.58	SiO2
K K	1.81	0.93	2.18	K2O
Ca K	7.54	3.78	10.55	CaO
Ti K	0.36	0.15	0.61	TiO2
Fe K	6.77	2.44	8.71	FeO
O	49.30	61.92		
Totals	100.00			

(d) 10 % Silica Fume (S3)

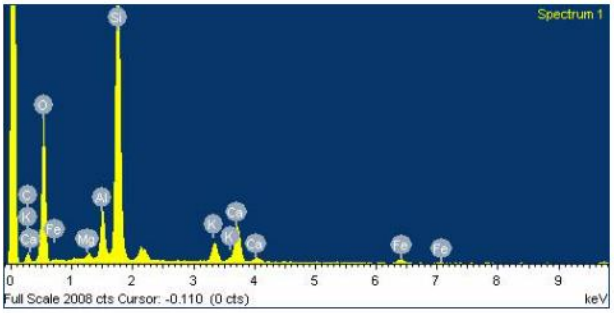

Element	Weight%	Atomic%	Compd%	Formula
C K	0.68	1.19	2.51	CO2
Mg K	0.62	0.54	1.03	MgO
Al K	4.42	3.43	8.35	Al2O3
Si K	34.02	25.35	72.77	SiO2
K K	3.21	1.72	3.87	K2O
Ca K	6.48	3.39	9.07	CaO
Fe K	1.86	0.70	2.39	FeO
O	48.70	63.70		
Totals	100.00			

(e) 12 % Silica Fume (S4)

Figure 5.6: Composition of various samples at 28 days of curing using EDS analysis (a) control concrete (S) , (b) 3% silica fume (S1) , (c) 6% silica fume (S2) , (d) 10% silica fume (S3) and (e) 12% silica fume (S4)

Table 5.5: Percentage reduction in Ca / Si for various specimens from 3 days to 28 days of curing

Age → /Specimen ↓	3 Days	28 Days	% Reduction
Control Concrete	1.59	1.16	27
3 % SF	1.42	0.793	44.15
6 % SF	1.142	0.527	53.85
10 % SF	1.108	0.28	74.72
12 % SF	0.93	0.124	85.23

5.3 ULTRASONIC PULSE VELOCITY (UPV) INVESTIGATIONS

5.3.1 Setting in control concrete samples

Figure 5.7 shows the velocity time graph in case of Control Concrete (S);

(a) **Initial Setting**: UPV increased with time in all the samples; as the microstructure became dense, waves get clear path to travel hence the time of travel reduced with age, distance of travel remaining constant (i.e. 150 mm) and velocity increased with setting of concrete.

(b) **Final Setting**: Once concrete solidifies, the distance of travel being constant, time of travel becomes constant and so does the UPV value. Steady value of UPV indicates final setting of concrete as indicated in **Figure 5.7**.

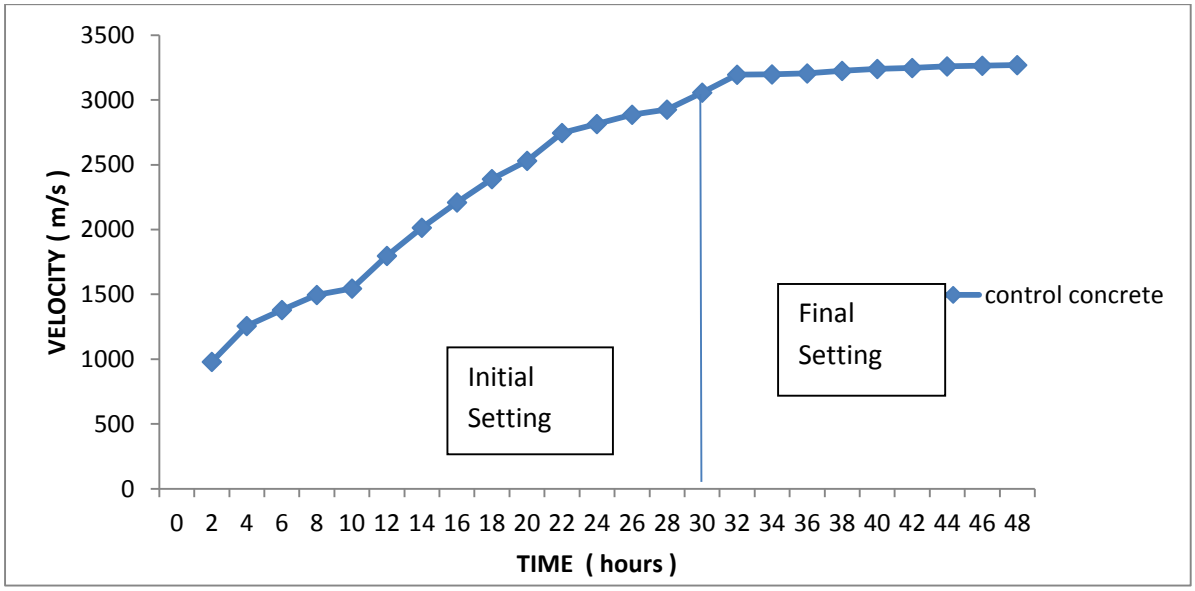

Figure 5.7: Variation of UPV with age (Control Concrete)

5.3.2 Setting in samples containing silica fume

From **Figure 5.8** following observations are made with replacement of silica fume in concrete

a) With increased dosage of silica fume, due to higher fineness, the hydration is faster leading to higher values of ultrasonic pulse velocity as compared to control concrete at all ages in all samples containing silica fume .The highest values of UPV are observed in samples containing 10% and 12% silica fume.

b) With increase in addition of SF the durations of initial and final setting reduced. In case of control concrete sample initial setting lasted for 8- 10 hours whereas in case of 6% SF it lasts for only 4-6 hours , for 10% and 12 %

SF it ended in 2-3 hours pointing towards earlier and rapid initial setting with increase in addition of SF.

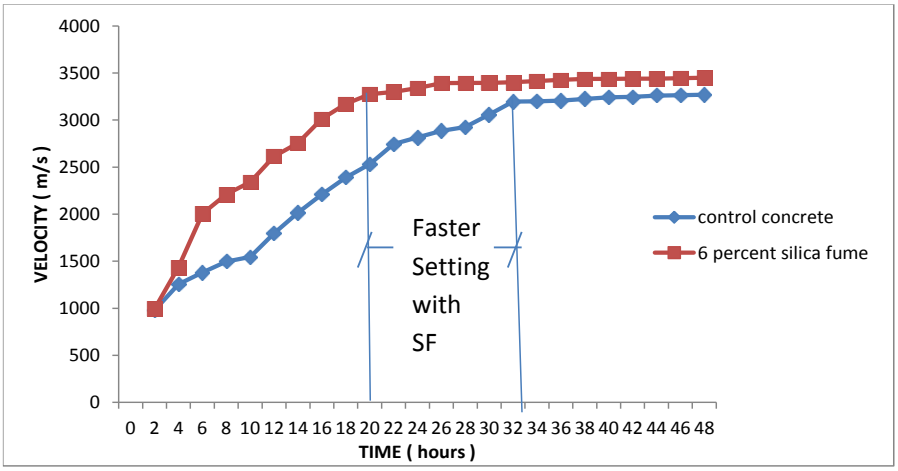

(a)

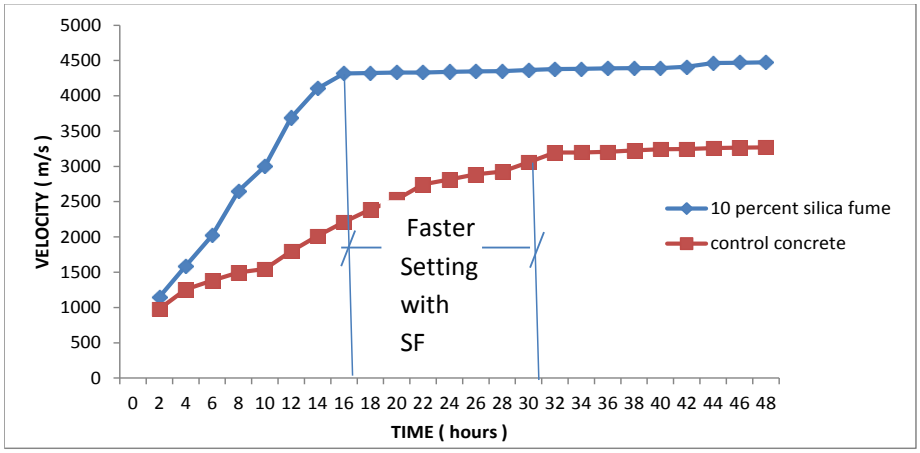

(b)

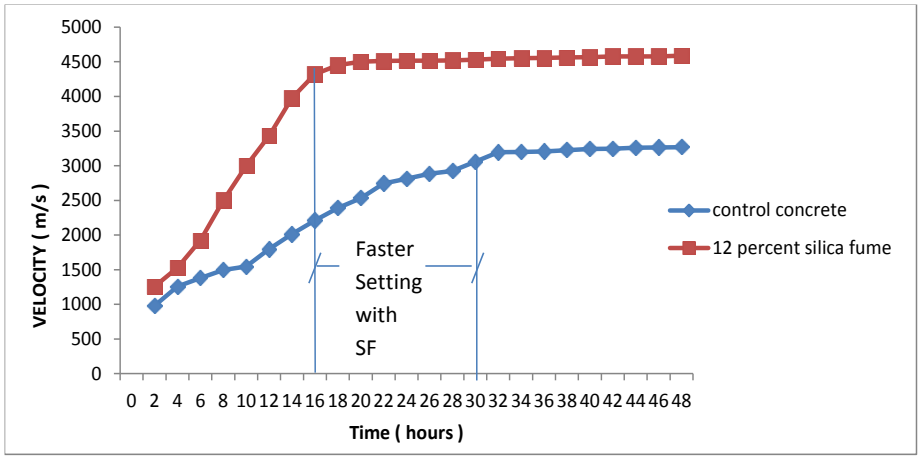

(c)

Figure 5.8: Comparison of variation of ultrasonic pulse velocity with age, (a) control concrete v/s 6% silica fume, (b) control concrete v/s 10% silica fume, (c) control concrete v/s 12% silica fume

Change in initial setting period is picked up by UPV with increase in addition of SF IN concrete. But detailed mechanism of setting of concrete as well as SF modified is not indicated by UPV. Hence, other NDT of UGW and AE are also applied to monitor setting of concrete and modified concrete.

5.4 ULTRASONIC GUIDED WAVE (UGW) INVESTIGATIONS

Ultrasonic pulse transmission signals were recorded using both L(0,1) and L(0,7) modes at an interval of 2 hours for 48 hours until the pulse transmission vanished after 48 hours. The tests were conducted on cube specimens of size 150mm x 150mm x 150mm with 25 mm diameter holes on two opposite faces in order to embed mild steel bar of 25 mm diameter and 300 mm length. A pulse transmission signature i.e. Voltage–Time signals (**Figure 5.9**) were captured immediately after preparing concrete mould and at regular two hours interval for 48 hours.

Figures 5.10 and 5.11 show the pulse transmission signatures at different intervals using L(0,7) at 0.1MHz and L(0,1) at 0.1MHz respectively. Peak to peak voltage amplitudes (pk –pk) of the signals were calculated from the signatures obtained and further normalized which are reported as pk-pk voltage ratio (R). A plot of pk-pk voltage ratio Vs age of concrete at different durations of setting of concrete is plotted for both the selected modes . It was observed that using L(0,1) at 0.1MHz **(Figure 5.11)** a continuous drop in pk-pk voltage amplitude of the signals with increasing age of concrete occurred.

This is due to the bond between embedded rebar and surrounding concrete improves as the concrete sets thus leading to increase in leakage of energy into surrounding concrete, causing fall in signal strength. But with 1 MHz (**Figure 5.10)** frequency it was seen that no drastic change in voltage amplitude occurred throughout the 48 hours of pouring concrete. This difference in detection of setting process due the two modes can be explained by their energy distribution profiles **(Figure 4.13 and 4.14)**. In case of L(0,7) mode it has negligible surface component, radial distribution of displacement and strain energy density is concentrated in the core area of bar, therefore signal is sensitive to deteriorations and irregularities inside the bar rather than its surface. Whereas L (0,1) is referred as surface seeking mode as it has significant surface component and is sensitive to interface changes such as bond development

between rebar and concrete due to setting of concrete. Hence on the basis of **Figure 5.10 and 5.11** the L(0,1) at 0.1MHz was selected further for monitoring early age setting of silica fume concrete.

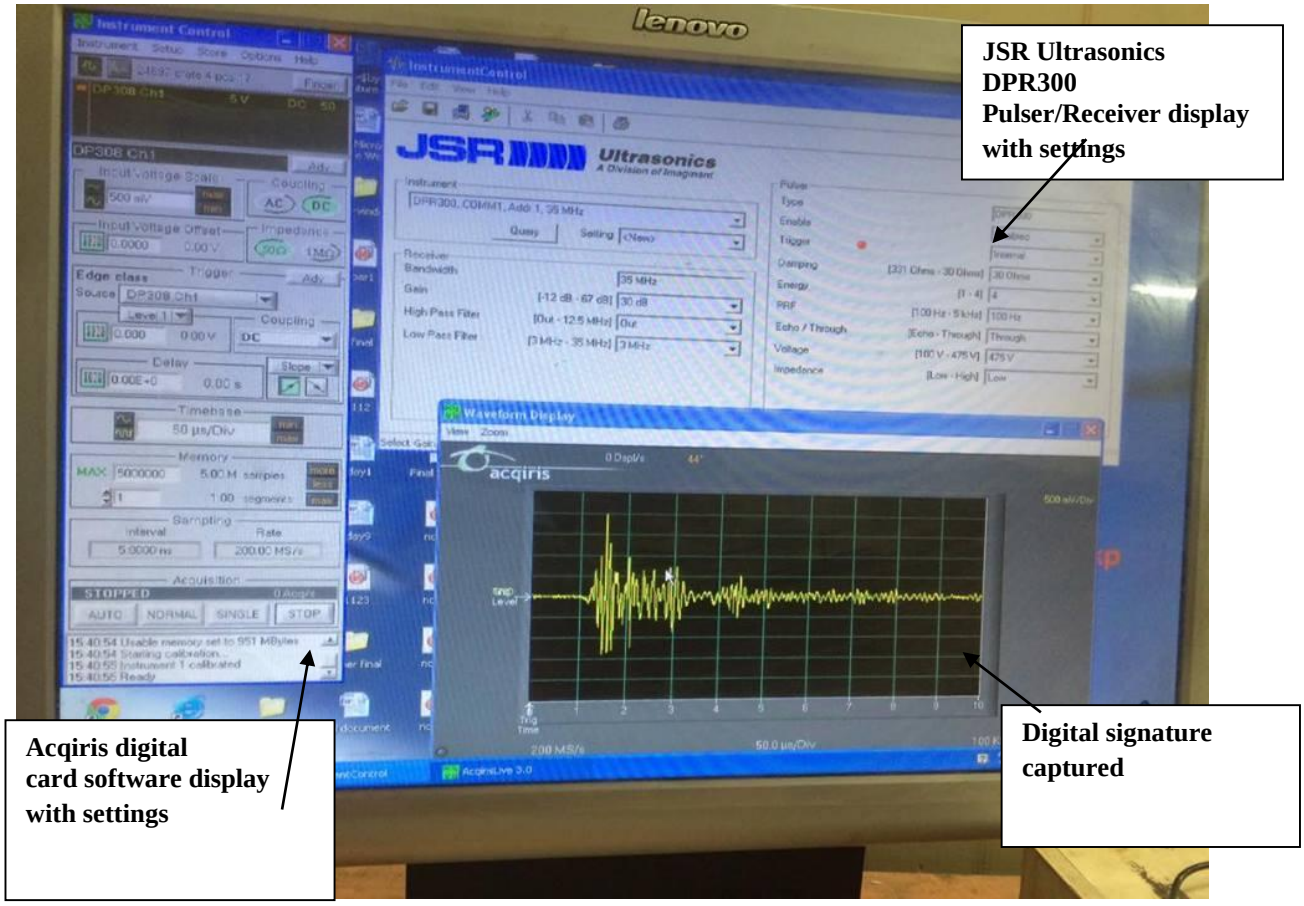

Figure 5.9: Image of captured waveform

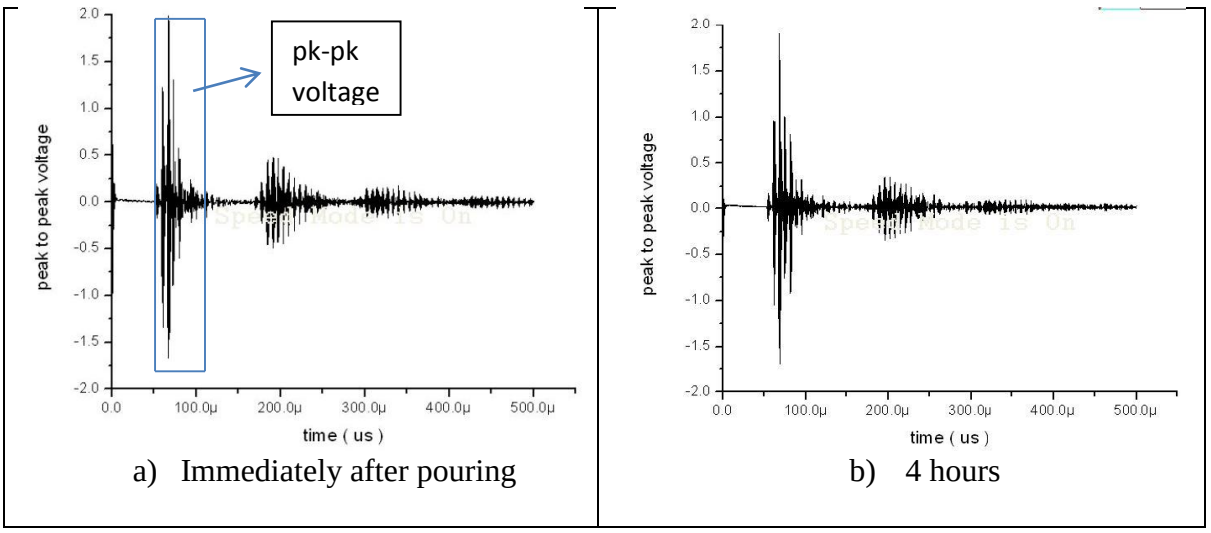

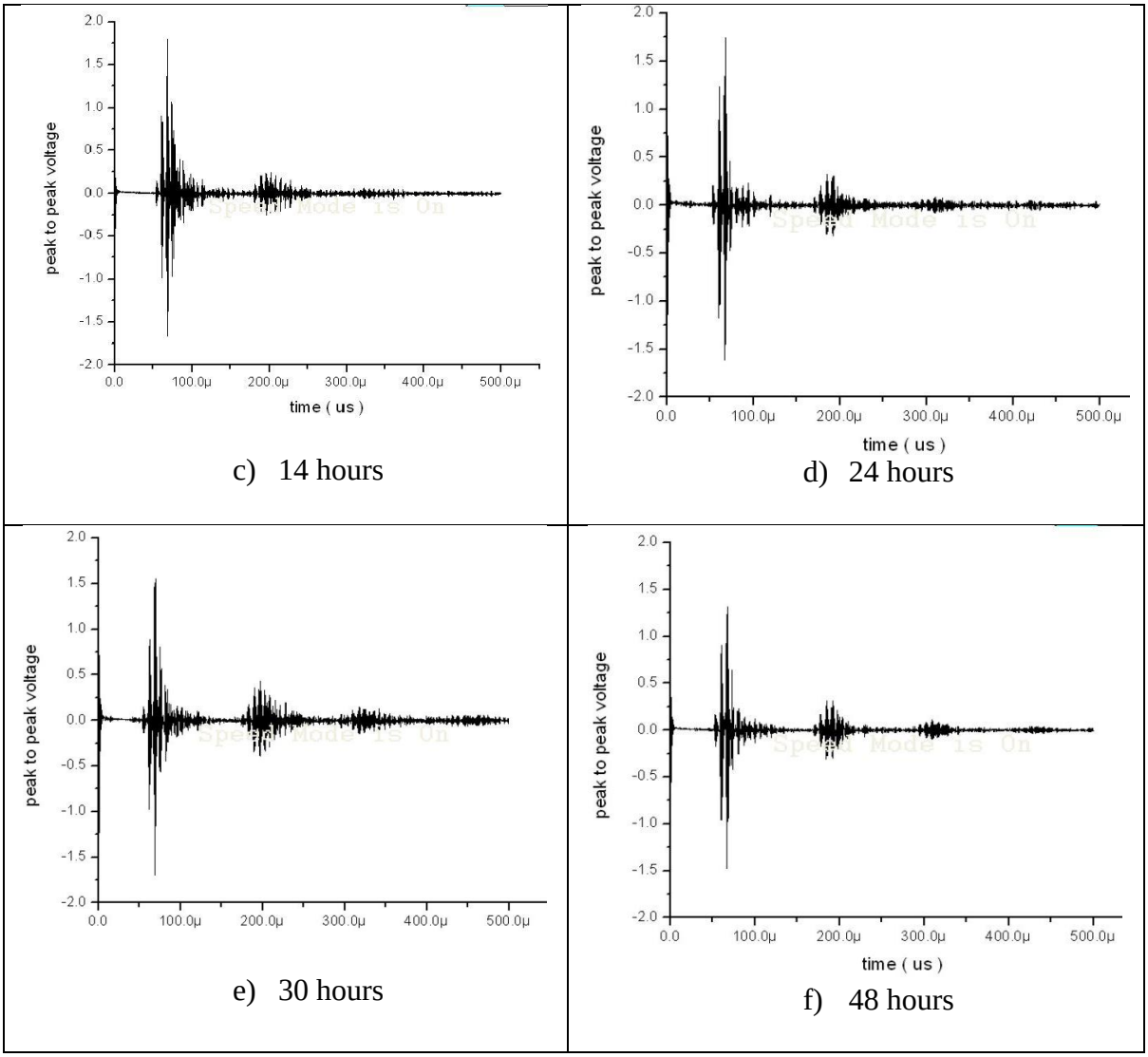

Figure 5.10: Voltage – Time signatures of control concrete (S) specimen using L (0,7) at 1MHz

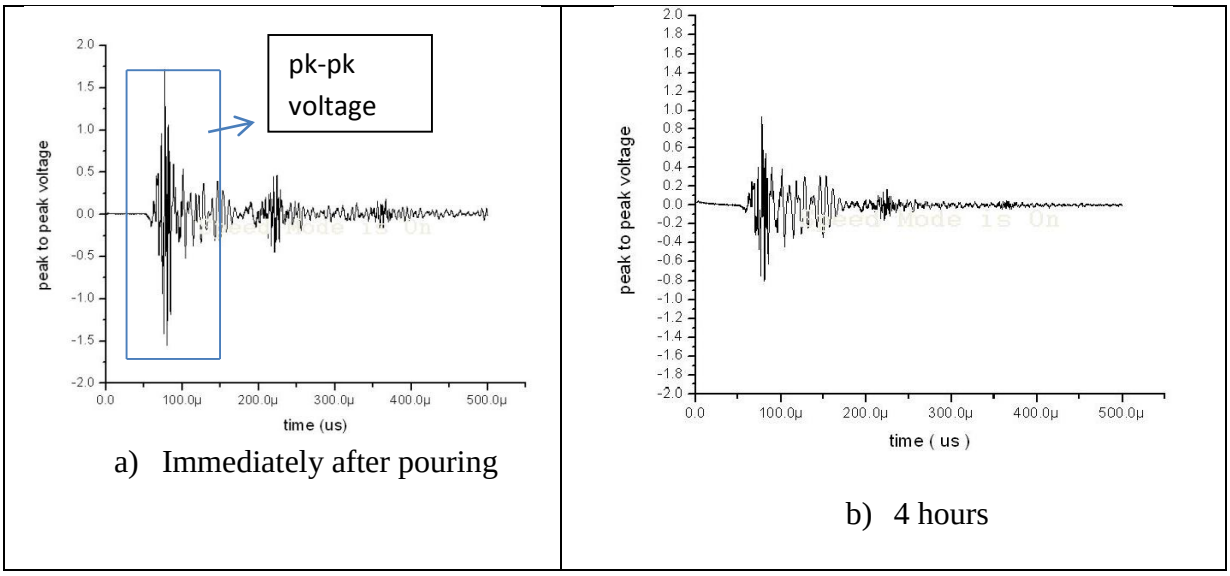

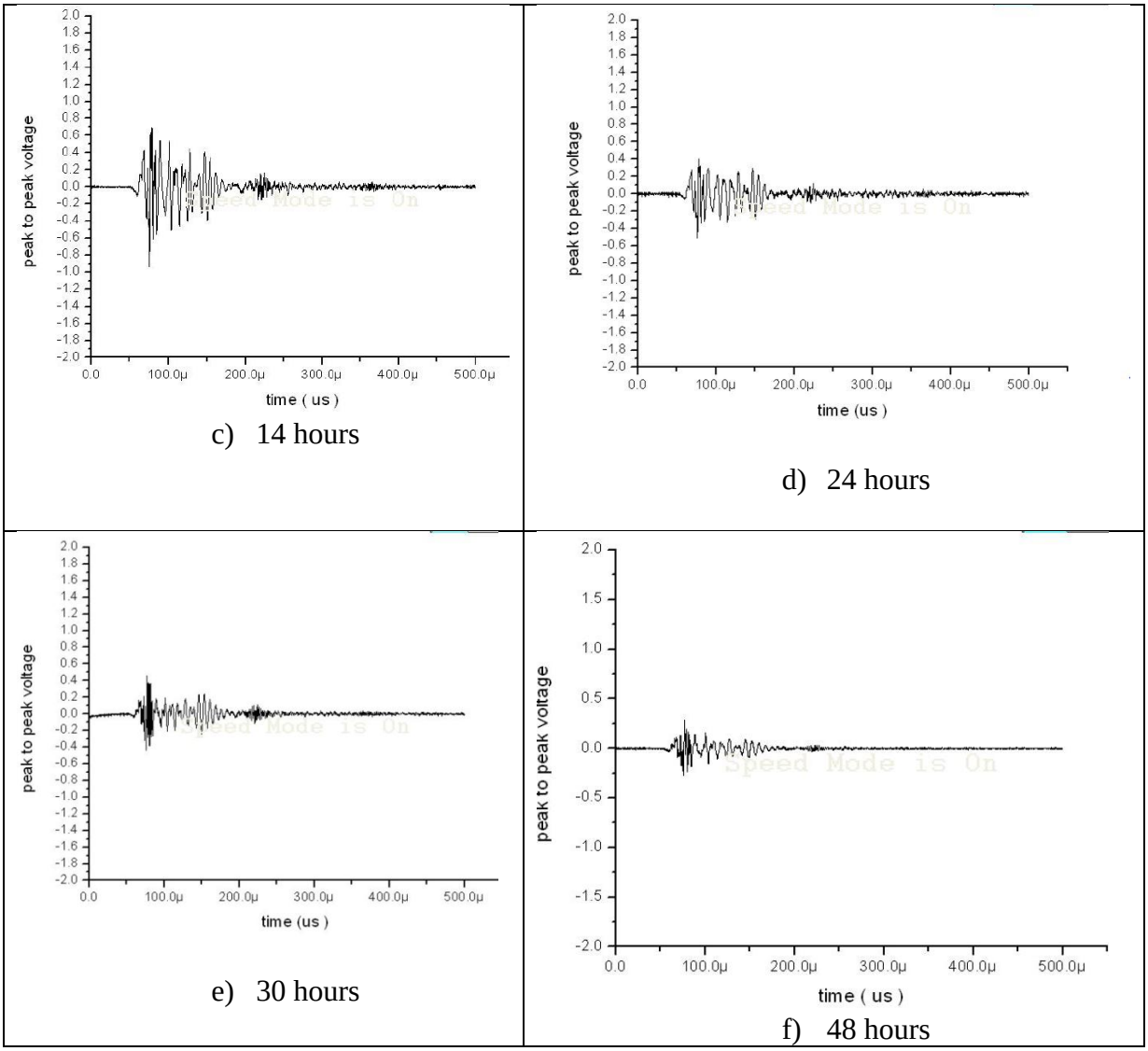

Figure 5.11: Voltage – Time signatures of control concrete (S) specimen using L(0,1) at 0.1MHz

5.4.1 Setting in control concrete (S)

Figure 5.12 (a) shows the trend in signals of L(0,1) obtained in S (control concrete). Following observations have been made in control concrete setting using GW:

a) Setting Process of concrete is characterized by two visible phases: Semi-solid Phase which lasts for 22-24 hours during which there is rapid reduction in peak to peak voltage value of signal (R) indicating bond development between steel and concrete. Concrete hardens leading to increased leakage of signal from steel bar to concrete and hence drop in signals.

b) Solid phase after 24 hours during which a signal n incremental change is observed and marks the solidification of concrete. This phase is referred to as solid phase.

c) In initial 4-5 hours pk-pk voltage signature with significant fall in R indicates faster bond development.

d) Whereas from 5-24 hours R dropped nominally indicating gradual development of bond. Hence leakage of signal energy into surrounding concrete indicates solidification of concrete. During this stage concrete undergoes a change of phase from fluid to semi-solid, marks the Transition Phase of concrete.

e) After 24 hours and till 48 hours drop in R is very insignificant indicating solidification of concrete hence slow drop in voltage and almost negligible leakage into concrete indicating that bond development and setting of concrete is almost complete in 1- 1 ½ day. This zone is referred as **Solid Phase**.

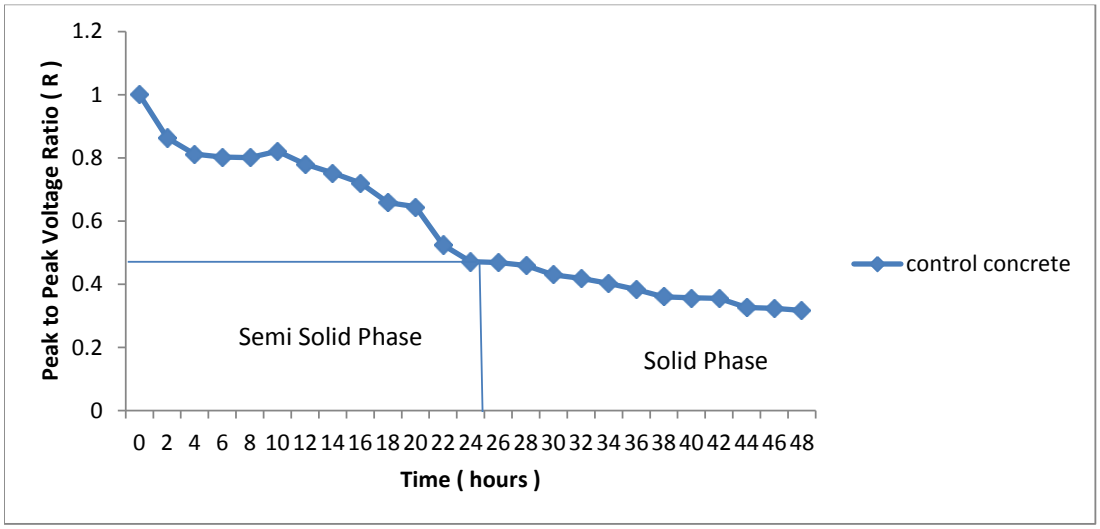

(a)

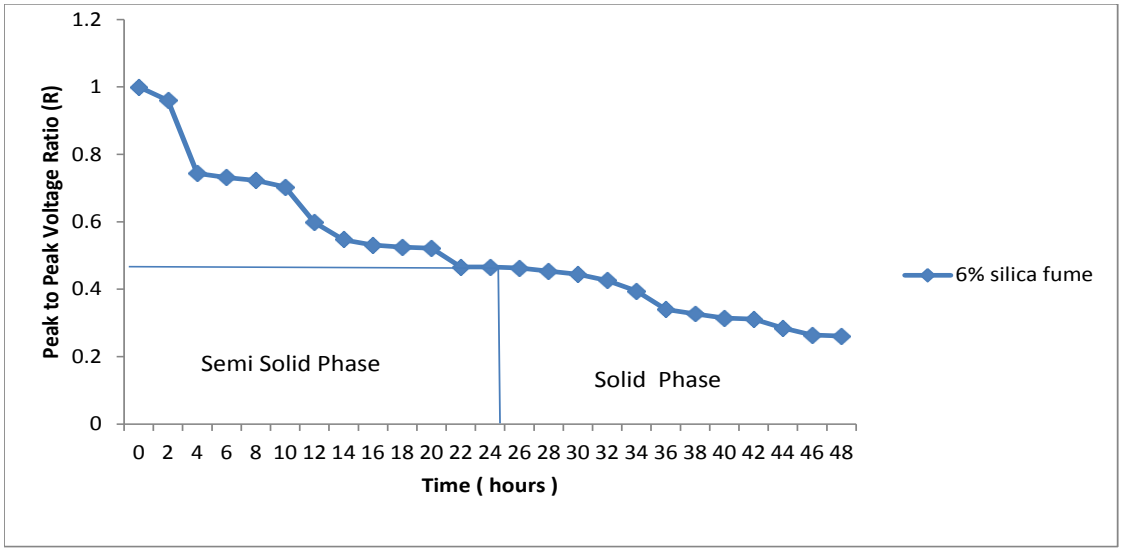

(b)

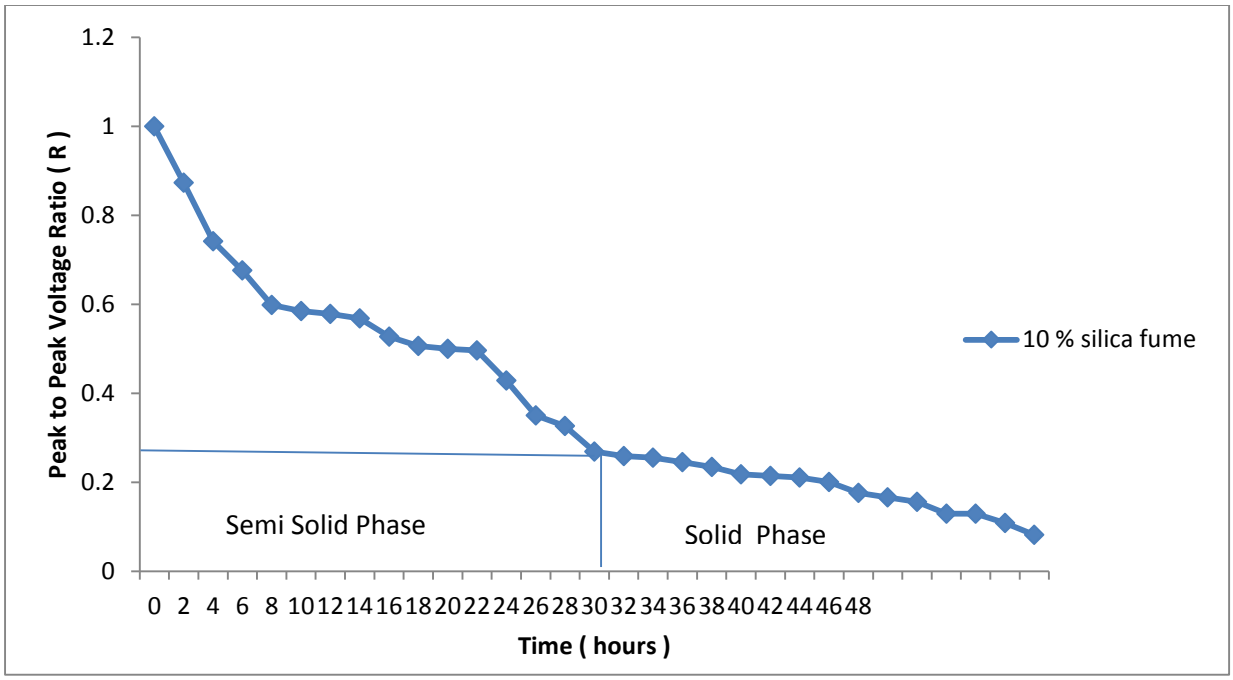

(c)

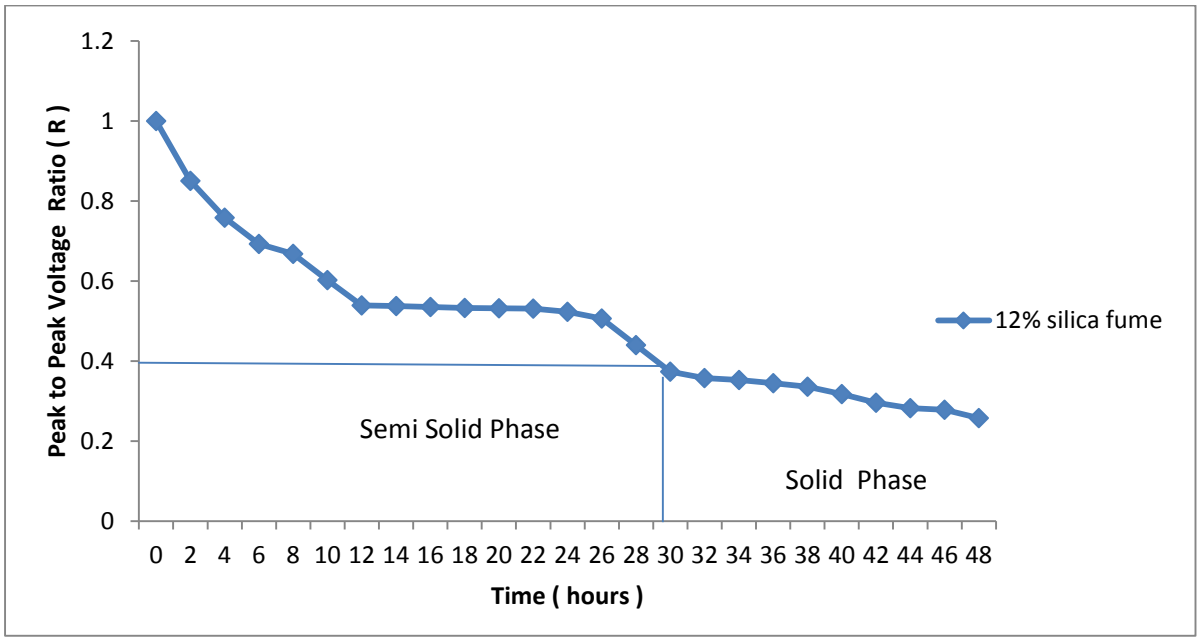

(d)

Figure 5.12: UPT monitoring with L(0,1) mode at 0.1 MHz, (a) control concrete, (b) 6% silica fume, (c) 10% silica fume, (d) 12% silica fume

5.4.2 Setting in samples with SF replacement

a) The fall in transmitted signal strength was observed in all the samples (control as well as samples with replacement) which was attributed to improvement in the

development of bond , as concrete solidifies its acoustic impedance goes closer to that of steel thus increase in leakage of energy from bar to concrete hence fall in signal strength .

b) From **Figure 5.12 (b , c and d)** it was observed that control concrete (S) and 6% SF concrete (S1) sets slowly than concrete containing 10 % and 12 % silica fume . The pattern was well validated by compressive strength test results as discussed in later sections .

c) As discussed earlier the initial fluid zone lasts for 4-6 hours in control concrete whereas concrete containing 6%, 10% and 12% silica fume setting is faster and solidification starts after 2 hours indicating early setting of concrete containing silica fume.

d) The semi-solid phase lasts for 24 hours in control concrete and 6% silica fume whereas in concrete with 10% and 12% replacement of silica fume it lasts till 30-32 hours indicating early age setting going on for longer durations on higher replacement of silica fume. Thereafter no drastic change in signal is observed in solid phase in 10% and 12% SF samples indicating that setting is almost over in 30-32 hours as against 48 hours in control concrete as well as 6% SF samples.

e) Another observation in Semi Solid phase is rapid fall in the signal with 10% and 12% silica fume replacement which continues for 7 hours and 11 hours respectively in both samples. Further fall in signal strength is gradual. On the other hand, control concrete sample and 6% silica fume, R continuously fell indicating rapid solidification till 24 hours. Further from 24 hours onward the fall in signal is slow.

5.5 ACOUSTIC EMISSION INVESTIGATIONS

AE signals were picked up using the AE sensors , recorded using AE win software and are displayed in form of various parameters like Number of AE Hits, Amplitude, Energy and Signal Strength of AE hits, etc. Out of the various AE parameters recorded during the 48 hours of monitoring, only few parameters namely Cumulative Counts, Cumulative Signal Strength and Cumulative Energy have been used to analyse the process of setting and hardening of concrete with and without replacement of silica fume in this research.

5.5.1 Variation in cumulative AE counts

ASTM E 1316 defines count as the number of times acoustic emission signal exceeds a preset threshold during any selected portion of a test. Total number of count is common parameter used for acoustic emission data interpretation.

Figure 5.13 (a and b) shows variation of cumulative AE counts with time in case of control concrete samples (S) in which sensors were placed on concrete directly **(a)** and sensors placed on steel bars **(b)** . The graph rises with almost same slope throughout 48 hours examination of specimen in case sensors are placed directly on concrete. Thus various stages of setting and hardening could not be determined clearly from the graph obtained. Thus the process of setting and hardening is better explained by AE sensors placed on 12 mm diameter steel bars embedded vertically in concrete cube. They detect AE activity through the bond development between steel bar and concrete and will be further used for AE parameter measurement. Therefore, AE sensors put on embedded steel bar in concrete will be used further in this research to understand the phenomenon of setting and hardening of concrete and SF modified concrete.

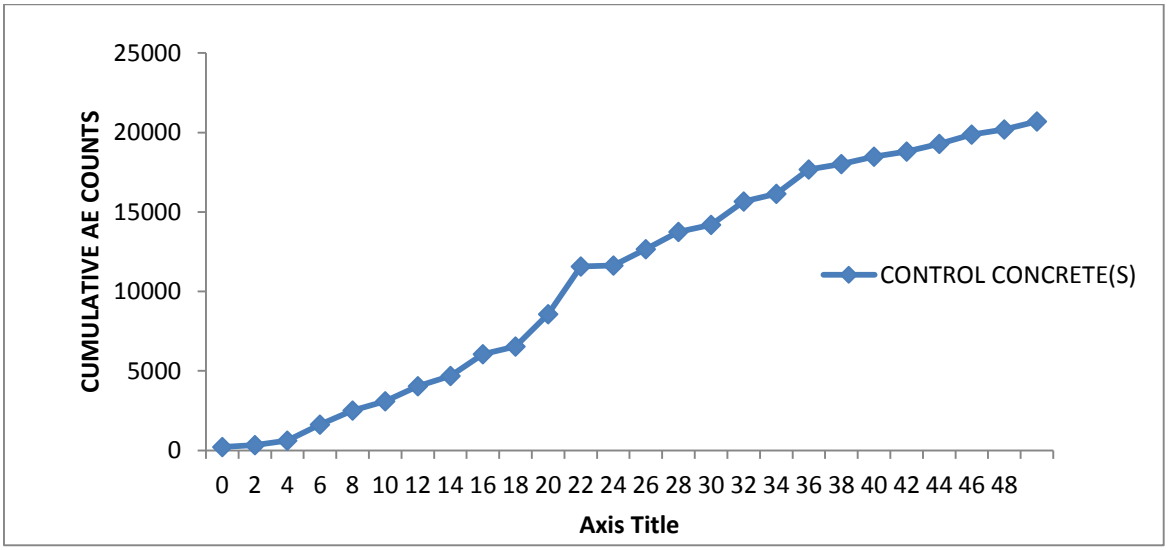

(a)

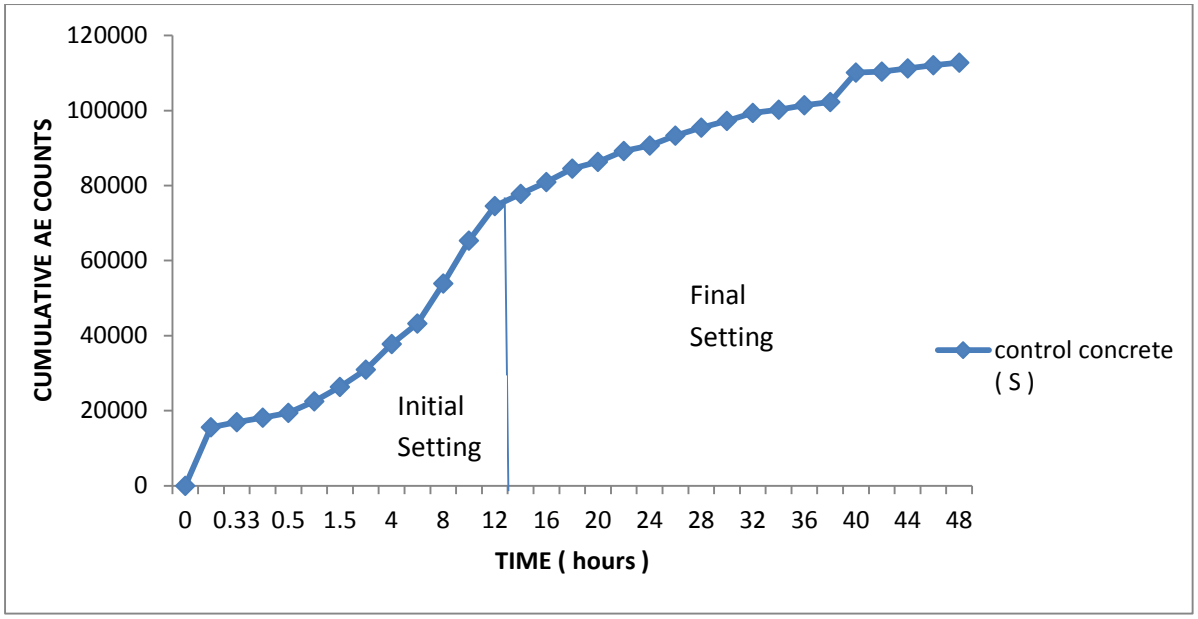

(b)

Figure 5.13: AE parameter cumulative AE counts v/s Time for control concrete (S) ; (a) AE sensors placed directly on concrete ; (b) AE sensors placed on steel bars in concrete

5.5.2 Monitoring setting with cumulative AE counts

(A) Setting in control concrete (sample S)

Figure 5.13 (b) represents cumulative counts of AE signals with age of concrete for control concrete samples. The following observations were made from this study.

a) ***Initial Setting Phase*: Figure 5.13 (b)** shows steep rise indicating significant AE activity pointing towards bond development between steel bar and concrete. This suggests active setting of concrete influencing AE activity in bar where AE sensor has been placed. This stage lasts for 12 hours in control concrete samples. The rise in the parameters can be attributed to the formation of products of hydration , porosity and water absorption by capillary pores . As the concrete sets smaller bubbles are formed in the pores and as it stiffens the initial water which was consumed in chemical shrinkage absorbs water from the top surface and eliminates cavitation due to the bubbles formed . Thus this consumption of water leaves behind capillary pores . Hence in addition with formation of products of hydration this drying process generates acoustic activities (Lura et al ., 2009 ; Chotard et al, 2001 ; Skal'skyi et al, 2004)

b) ***Final Setting Phase*:** Slow rise indicting active setting has already taken place in initial 12 hours and setting slows further and concrete has reached stages of final setting. This is indicated by slow AE activity counts. As the concrete attains strength the rate of increase of the parameters of AE signal reduces this is because the products of hydration take up the space and fill the pores, concrete becomes compact and cement is protected by layer of hydration products and the process of crystal structure formation is decelerated.

c) ***Solidification Phase:*** The increase in cumulative counts is almost steady indicating marginal increase in AE activity and pointing towards solidification of concrete.

(B) Setting in samples with silica fume replacement

a) **From 5.14** it was concluded that control concrete (S) and 6% SF concrete (S1) sets slowly than concrete containing 10% and 12% silica fume. The pattern was well validated by compressive strength test results and SEM/EDS analysis as discussed in later sections.

b) The durations of initial and final setting zone reduced from 12 to 2-3 hours for 10% SF and 12% SF samples as compared to Control Concrete and 6% SF due to early hydration in former samples which was attributed to high reactivity of silica fume because of its fine size, pore refinement and chemical reaction with $Ca(OH)_2$.

c) The setting patterns of sample S3 (10 % SF) and S4 (12 % SF) were different from those of S (Control Concrete) and S2 (6 % SF) as steep slope was observed for former specimens, moreover with high values of all AE parameters at every age which was attributed to the fast reaction of silica fume which lessen the duration of solidification process.

d) Large values of counts in comparison to control concrete indicate large AE activity initially and faster setting in silica fume concrete rather than control concrete.

e) **Figure 5.14** indicates faster initial setting with steep slope up to 20 hours and then negligible AE activity. Almost all setting has taken place in first 20 hours in 12%, 10% silica fume samples which is also reflected by large cumulative signal strength values in 6%, 10% and 12% silica fume replacement samples in comparison to control concrete.

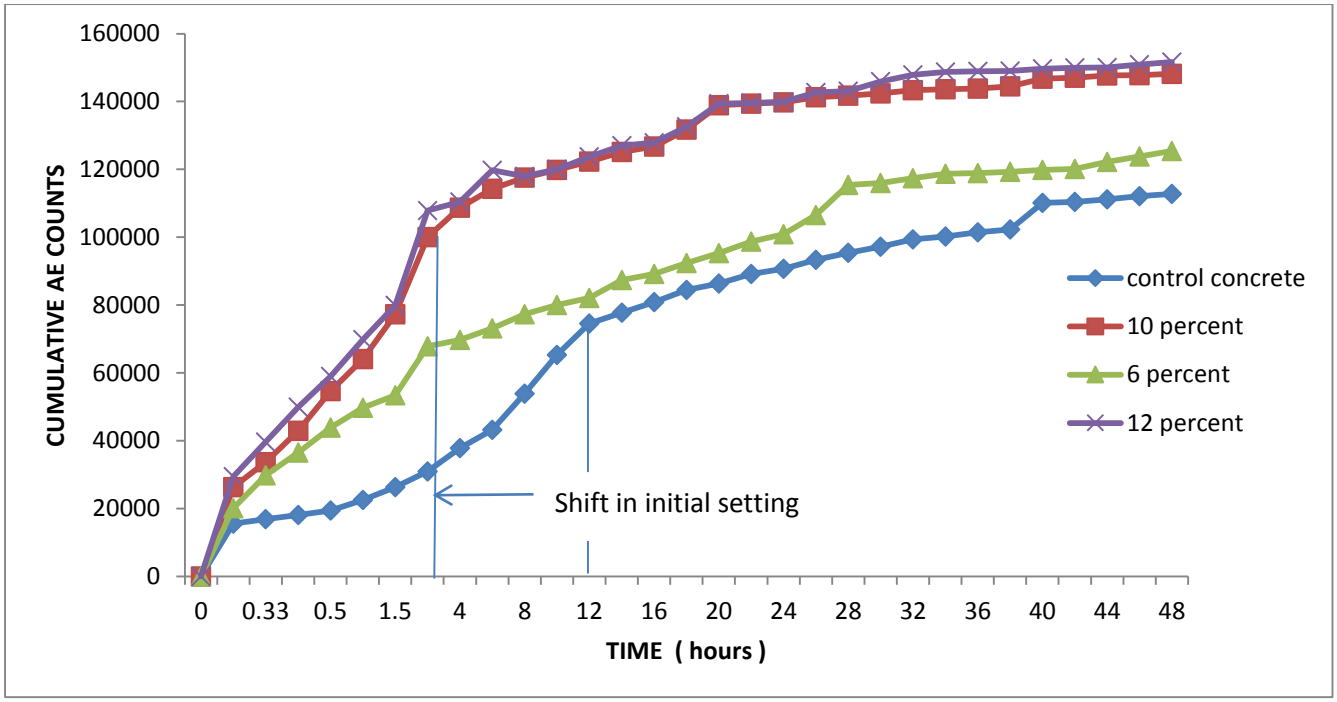

Figure 5.14: Comparison of variation of AE parameter cumulative AE counts v/s time in control concrete , 6 % silica fume , 10 % silica fume and 12 % silica fume

5.5.3 Cumulative AE signal strength

The ASTM E 1316 defines signal strength as measured area of the rectified AE signal. Its units are volt- of energy released by the specimen. It is a function of duration and amplitude of signal. Fowler et al. (1989) expressed signal strength as follows:

$$S_o = \frac{1}{2}\int_{t1}^{t2} f_+(t)\,dt + \frac{1}{2}\int_{t1}^{t2} f_-(t)\,dt \qquad (5.1)$$

Where S_0 = Signal strength

f_+ = positive signal envelope function

f_- = negative signal envelope function

t_1 = time at first threshold crossing

t_2 = time at last threshold crossing

(A) Setting in Control Concrete (sample S)

Figure 5.15 represents cumulative signal strength of AE signals with age of concrete for control concrete samples . The following observations were made:

a) From **Figure 5.15** the rise in cumulative signal strength is steep which is attributed to hydration products formation and water absorption by capillary

pores. This phase of steep rise in cumulative signal strength is termed as initial setting phase which lasts for 12 hours in samples of control concrete. This phase represents active setting of concrete and hence AE activity in steel bar due to bond development between bar and concrete.

b) As concrete attains strength AE activity slows down and so does the rise in cumulative signal strength. As the hydration products take up space pore filling occurs which leads to formation of protected layer of products of hydration and hence lesser AE activity.

c) Solidification of concrete is marked by marginal increase in cumulative signal strength.

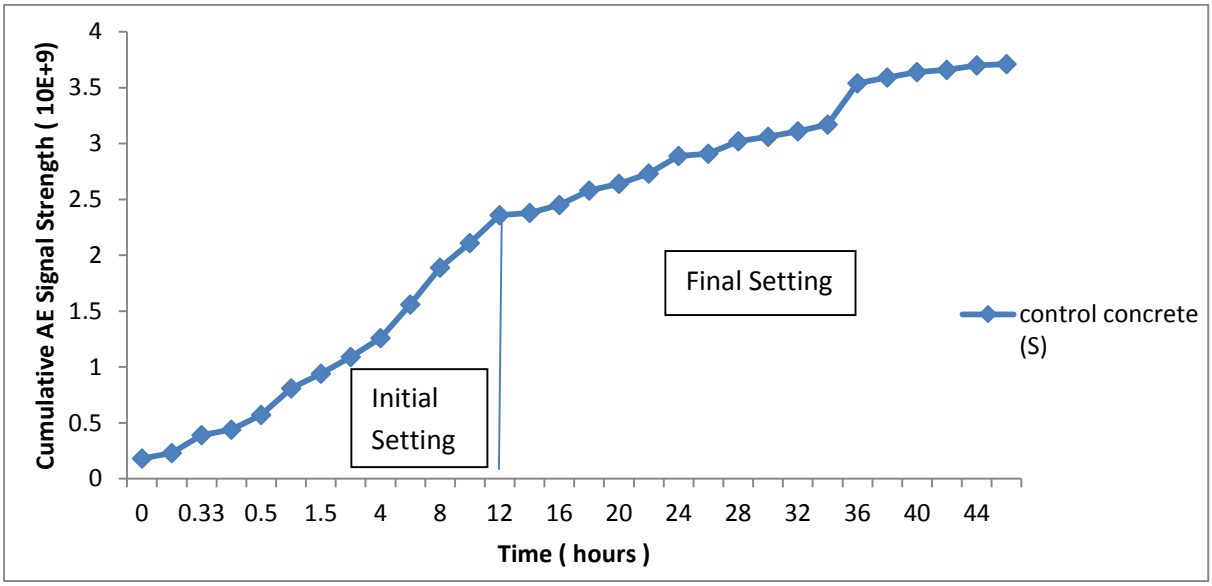

Figure 5.15: AE parameter cumulative AE signal strength v/s Time for control concrete (S)

(B) Setting in samples with silica fume replacement

a) Control concrete and 6% silica fume replacement concrete set slowly as shown in **Figure 5.16** in comparison to 10% and 12% replacement silica fume which was indicated by longer durations of initial and final setting zone in case of control concrete and 6% silica fume replacement concrete.

b) The rise in cumulative signal strength is much steeper in case of 10% and 12% silica fume replacement as compared to the other. Moreover higher values of cumulative signal strength were obtained in 10% and 12% silica fume replaced samples.

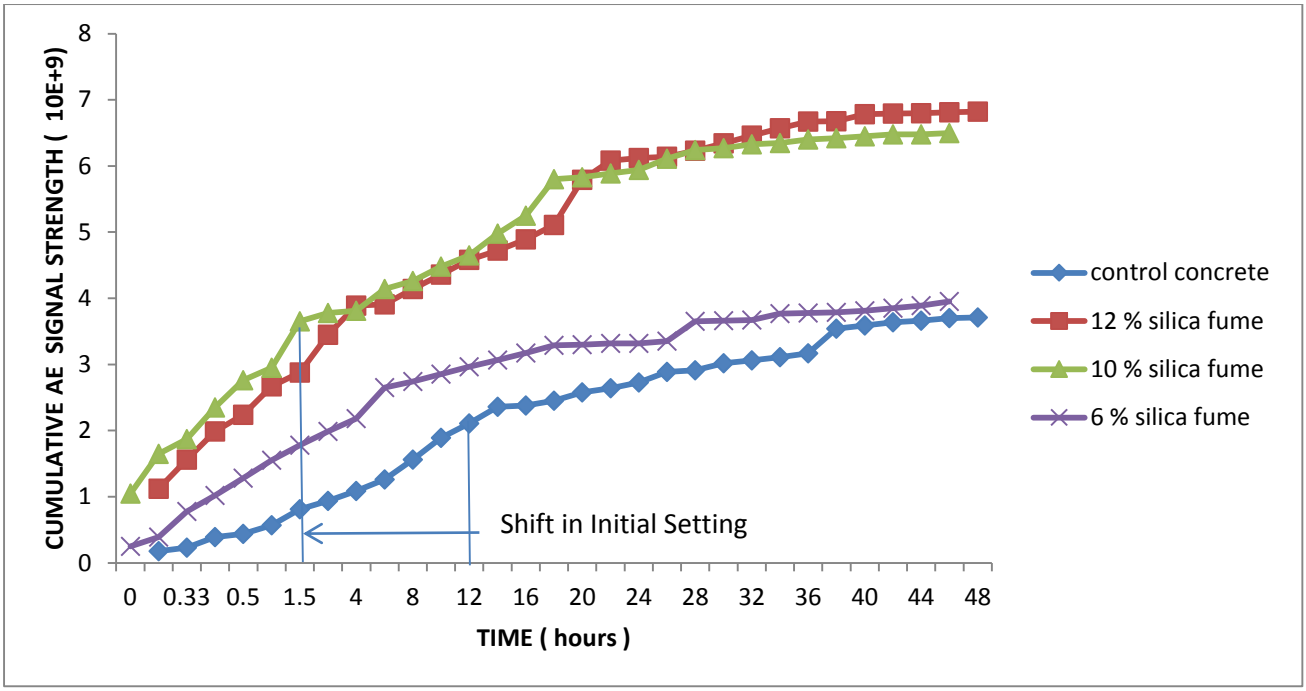

Figure 5.16: Comparison of variation of AE parameter cumulative AE signal strength v/s time in control concrete , 6% silica fume , 10% silica fume and 12% silica fume

5.6 COMPARISON OF VARIOUS NDT TECHNIQUES FOR MONITORING SETTING OF CONCRETE AND SF MODIFIED CONCRETE

- UPV – Change in initial setting period is picked up by UPV with increased addition of SF in concrete. Higher values of UPV and reduced durations occur in case of SF modified concrete. But detailed mechanism of setting of concrete as well as SF modified is not indicated by UPV.
- UGW – The setting process was studied using surface seeking L(0,1) Mode at 0.1MHz. The fall in transmitted signal was observed which was attributed to improvement in development of bond between steel and concrete

  The phases were well identified using UGW and semi-solid phase continued upto 24 hours in case of control concrete.
- AE – The cumulative AE counts studied in this research accounts to energy changes taking place in the system and not entirely to the band development between steel and concrete. Thus the rise in cumulative AE counts very well demarcates different phases of setting and hardening process. Initial setting is upto 12 hours, which is near to practical observations.

- A judicious combination of all the three NDT techniques gives a good indication of the setting mechanism in concrete as well as SF modified concrete.
- Visible changes in NDT parameters were observed with SF addition, so NDT techniques work well with modified concrete.

5.7 CORRELATION OF DESTRUCTIVE TESTING WITH NDT AND SETTING OF CONCRETE

Destructive Testing gives no indication of initial setting in 24 hours and three days. No setting is judged using destructive testing. NDT parameters show remarkable change in parameters UGW the pk-pk voltage ratio (R) falls as the bond between steel and concrete develops and the rate of change of fall marks various stages of setting and hardening process. Similarly AE parameters increase with the age of concrete and the rate of increase of AE parameters demarcate various stages of setting and hardening of concrete as well as modified SF concrete. Hence for destructive testing a minimum of 3-7 days period is required whereas NDT parameters give an indication of quality of concrete within few hours of casting. So if the mixture is not good, it can be redesigned.

5.8 CORRELATION OF SEM/EDS ANALYSIS WITH NDT AND DESTRUCTIVE TESTS

The microstructural SEM/EDS analysis well validates the compressive strength results of control concrete and SF modified concrete. With increase in replacement levels of silica fume the strength increase at all ages and corresponding pores, ettringites and Ca/Si ratio reduces with age of concrete. The hydration products formed increased and so does the compressive strength. From SEM images with increase in replacement level of silica fume the bond becomes better due to decrease in pores and because of rapid hydration of silica fume particles the rate of setting is faster which well validates the UGW and AE results.

5.9 CLOSING REMARKS

This chapter shows the results obtained by ultrasonic guided waves , acoustic emission , ultrasonic pulse velocity under non – destructive techniques and compressive strength with SEM/EDS analysis for destructive techniques for control concrete and concrete containing various different percentages of silica fume.

CHAPTER 6

CONCLUSIONS AND SCOPE OF FUTURE WORK

6.1 GENERAL

Non – Destructive Tests namely Ultrasonic Pulse Velocity , Ultrasonic Guided Waves and Acoustic Emission were carried out to monitor setting and hardening of concrete containing 3%, 6%, 10% and 12% Silica Fume as replacement of Cement . The results were validated with compressive strength tests and SEM/EDS analysis. These destructive tests proved the pattern obtained by various samples. As the rate of increase of strength in 10% and 12% silica fume samples was much higher than 3% and 6% silica fume samples with reference to control concrete similar is the pattern obtained in UPV, UGW and AE tests. SEM/EDS analysis also confirms the behavior of various SF replacements in concrete. As the content of calcium hydroxide ettringites and pores (size and content) decreased at three days in samples containing 10% and 12% silica fume to large extent than in case of 3% and 6%.

Ultrasonic Pulse Velocity Investigations

- The velocity increased in all the samples of concrete.
- The increase in velocity is attributed to the development of dense microstructure.
- With addition of silica fume the duration of stages defined decreased due to rapid hydration process of silica fume samples.
- The values of velocities obtained in 10% and 12% silica fume samples were higher than rest of the samples.

Ultrasonic Guided Waves Investigations

- Ultrasonic Guided Wave Technique using L (0,1) mode at 0.1 MHz has been proved to be efficient in monitoring setting and hydration of concrete containing different replacements levels of cement by silica fume. Whereas with L(0,7) mode at 1 MHz no major change in voltage amplitude was observed throughout the 48 hours of testing .
- Fall in transmitted signal strength was observed in all the samples.
- Change of slopes in curves marked two stages of setting and hardening process namely semi-solid phase and solid phase.

- Fluid zone for control concrete ends in 4-6 hours as against two hours in samples containing silica fume. The semi-solid phase lasts for 24 hours in control concrete and 6% silica fume sample; 30-32 hours for 10% and 12% silica fume respectively.
- Difference in setting patterns was observed due to sharp increase in rate of fall of signal voltage in 10% and 12% silica fume samples as compared to control concrete and 6% silica fume samples.
- The results indicate that rate of pozzolanic reaction is fast in case of samples containing silica fume and concrete solidifies quickly leading to better bond development between concrete and rebar, more leakage of signal from bar to concrete , hence sharp decline in R value.

Acoustic Emission Technique Investigations :

- Acoustic Emission monitoring proved to be efficient in identifying various stages of stetting of concrete which occur after pouring of concrete and it well relates with the setting and hydration phases as identified by Guided Wave Monitoring.
- The acoustic emissions studied include cumulative AE counts and cumulative AE signal strength.
- All the parameters increased with the age of concrete indicating the setting and hardening of concrete.
- Rate of increase of parameters decreased from initial setting zone to final setting zone, being maximum former and minimum in latter.
- The increase in parameters is attributed to formation of hydration products, porosity and water absorption by capillary pores.
- The decrease in rate of increase of parameters is attributed to the fact that products of hydration fill the pores making concrete compact and cement is protected by layer of hydration products.
- Initial setting zone for control concrete lasted for 12 hours against 2-4 hours for 6%, 10%, 12% SF replacements.
- Due to higher reactivity of silica fume the durations of various zones shortens.
- Besides decrease in duration of various zone in case of silica fume concrete samples; steep slope and higher values of various parameters were obtained in 10% and 12% concrete samples which is attributed to higher reactivity of silica fume at 10% and 12 % replacement levels.

A judicious combination of all the three NDT techniques gives a good indication of the setting mechanism in concrete as well as SF modified concrete. Visible changes in NDT parameters were observed with SF addition, so NDT techniques work well with modified concrete. Moreover for destructive testing a minimum of 3-7 days period is required whereas NDT parameters give an indication of quality of concrete within few hours of casting. So if the mixture is not good, it can be redesigned.

REFERENCES

- Achenbach, J.D. (1975) ,Wave Propagation in Elastic Solids. Elsevier, New York.
- Aggelis, D.G., Shiotani, T., and Terazawa, M. (2010a), Assessment of construction joint effect in full-scale concrete beams by acoustic emission activity, Journal of Engineering Mechanics, 136 (7), 906–912.
- Aggelis, D.G., Matikas, T.E., and Shiotani, T.(2010b) , Advanced acoustic techniques for health monitoring of concrete structures. In: Kim, S.H., Ann, K.Y. (Eds.), The Song's Handbook of Concrete Durability,Middleton Publishing Inc.,331–378.
- Aggelis, D.G., Barkoula, N.M., Matikas, T.E., Paipetis and A.S.(2010c), Acoustic emissionmonitoring of degradation of cross ply laminates, Journal Acoustical Society of America,127 (6), EL246–EL251.
- Aggelis, D. G. (2011) , Classification of cracking mode in concrete by acoustic emission parameters. Mechanics Research Communications, 38(3), 153–157.
- Alaa, M.R. , El_Din, H.S.H. , Khalid and M.Y. (2009) , Compressive strength of concrete mixtures with binary and ternary cement blends , Building Research Journal , 57 (2) ,107–130.
- Amziane S., Perrot A., and Lecompte T. (2008), A novel settling and structural build-up measurement method , Measurement Science Technology , 19 (10) , 105–702.
- ASTM E976-10 (2010), Standard guide for determining the reproducibility of acoustic emission sensor response, ASTM ,5.
- Ativitavas, N. (2002), Acoustic Emission Signature Analysis of Failure Mechanisms in Fiber Reinforced Plastic Structures (Ph.D. thesis) , The University of Texas at Austin.
- Bach, T.T.H. , Coumes, C.C.D. , Pochard I., Mercier, C. , Revel, B. and Nonat, A. (2012), Influence of temperature on the hydration products of low pH cements. Cement Concrete Research , 42 ,805–817.
- Beard , M.D. , Lowe , M.J.S. and Cawley , P. (2003) , Ultrasonic Guided Waves for Inspection of grouted tendons and bolts . Journal of Materials in civil engineering . 10.1061/ (ASCE)0899-156115 , 3 (15) , 212-218.

- Bentur , A. , Cohen and M.D. (1987), Effect of condensed silica fume on the microstructure of the interfacial zone in Portland cement mortars . Journal of American Ceramic Society, 70 , 738–743.
- Bhanja, S. and Sengupta, B. (2005) , Influence of silica fume on the tensile strength of concrete , Cement and Concrete Research, 35 (4) , 743–747.
- Biricik, H. and Sarier, N. (2014) , Comparative study of the characteristics of nano silica - , silica fume - and fly ash - incorporated cement mortars, Materials Research, 17(3), 570–582.
- Carette, J. and Staquet, S. (2016), Monitoring the setting process of eco-binders by ultrasonic P-wave and S-wave transmission velocity measurement: Mortar vs concrete, Construction and Building Materials, 110, 32–41.
- Carpinteri, A., Cardone, F. and Lacidogna, G. (2010) , Energy emissions from failure phenomena: mechanical, electromagnetic, nuclear. Experimental Mechanics ,50, 1235–1243.
- Chotard, T.J., Barthelemy, A., Smith, A., Gimet-Breart, N.,Hunger, M., Fargeot, D. and Gault, C. (2001) , Acoustic emission monitoring of calcium aluminate cement setting at the early age , 7(20) , 667-669.
- Chotard, T. J., Smith, A., Codet, N., De Baillencourt, M., Fargeot, D. and Gault, C. (2002), New applications of acoustic emission technique for real-time monitoring of material processes, Journal of Materials Science Letters, 21(16), 1261–1266.
- Clark, G. (1992) , Commentary on QAE source characterization of microcracking in steel. Research in Nondestructive Evaluation , 4(3), 1583-190.
- Daake, H. Von and T., Stephan, D. (2016), Impact of retarders by controlled addition on the setting , early hydration and microstructural development of different cements Impact of retarders by controlled addition on the setting , early hydration and microstructural development of different cements, (July).
- Ding, J. T. and Li, Z. (2002), Effects of metakaolin and silica fume on properties of concrete, ACI Materials Journal, 99(4), 393–398.
- Duan P. , Shui Z. , Chen W. and S. C. (2013), Effects of metakaolin, silica fume and slag on pore structure, 44, 1–6.
- Elfergani, H.A. , Pullin, R. and Holford , K.M. (2013) , Damage assessment of corrosion in prestressed concrete by acoustic emission , Constrution Building Material ,40 ,925–933.

- Enfedaque , A. , Sánchez-Paradela, L. and Sánchez-Gálvez, V. (2010), The effect of silica fume and metakaolin on glass–fibre reinforced concrete (GRC) ageing . Material Construction, 60 (300) , 67–82.
- Ervin, B. L. and Reis, H. (2008), Longitudinal guided waves for monitoring corrosion in reinforced mortar. Measurement Science and Technology, 19(5), 55702.
- Ervin, L. B., Kuchma ,A.D., Bernhard, T.J. and Reis,H. (2009), Monitoring Corrosion of Rebar Embedded in Mortar Using High-Frequency Guided Ultrasonic Waves . Journal of Engineering Mechanics, 135(1) , 9-19.
- Eshmaiel , G. and Sadeghi , P.H. (2009) , The effect of Persian gulf zone exposure on durability of mixes containing silica fume and blast-furnace slag. Construction Building Material , 23 (2) , 644–652.
- Fargeot, D. and Gault, C. (2001), Acoustic emission monitoring of calcium aluminate cement setting at the early age, 667–669.
- Fowler, T.J. and Berkowitzi, P.C. (1995) , Crack Detection in Naval Crane Shafts Using Acoustic Emission. The University of Texas .
- Gabrijel, I., Mikulić, D. and Milovanović, B. (2011), Application of Ultrasonic Measurements for Determination of Setting and Hardening in Cement Paste. Journal of Civil Engineering and Architecture, 5(3), 278–283.
- Ghorbanpoor, A. (1987), Acoustic emission characterization of fatigue crack growth in highway bridge components . PhD thesis , University of Maryland , College Park , Md.
- Ghorbanpoor, A. and Rentmeester, A. T. (1993), NDE of steel bridges by acoustic emission , Proceedings in Structural Engineering in Natural Hazards Mitigation ASCE , 1008-1013.
- Gong, Z., Nyborg, E.O. and Oommen,G. (1992) , Acoustic emission monitoring of steel railroad bridges . Material Evaluation , 883-887.
- Grosse, C.U. and Ohtsu, M. (2008), Acoustic Emission Testing. Springer, Heidelberg.
- Gleize, P.J.P. , Müller, A. and Roman, H.R. (2003), Microstructural investigation of a silica fume–cement–lime mortar , Cement Concrete Composite , 25 (2) , 171–175.
- Haneef, T. K., Kumari, K., Mukhopadhyay, C. K., Rao, B. P. and Jayakumar, T. (2013), Influence of fly ash and curing on cracking behavior of concrete by acoustic emission technique, Construction and Building Materials, 44, 342–350.

- Holford, K.M. (2009) , Acoustic emission in structural health monitoring , Key Engineering Material, 413–414 15–28.
- Hopwood II, T. (1988), Acoustic Emission inspection of steel bridges.Public Works . 66-69.
- Hosam, E.D.S, Alaa, M.R. and Basil, A.E.S. (2010), Durability and strength evaluation of high-performance concrete in marine structure, Construction Building Material , 24 (6) , 878–884.
- Hosam, E.D.S. , Alaa, M.R. and Elsokary, T. (2011), Effect of elevated temperature on physicmechanical properties of blended cement concrete , Construction Building Material , 25 (2) , 1009–1017.
- Huang, M., Jiang L., Liaw P.K., Brooks C.R., Seeley R. and Klarstrom D.L. (1998) Using acoustic emission in fatigue and fracture materials research , JOM-e 50 (11).
- Kamada, T., Uchida, S. and Rokugo, K. (2005) , Nondestructive Evaluation of Setting and Hardening of Cement Paste Based on Ultrasonic Propagation Characteristics, Journal of Advanced Concrete Technology, 3(3), 343–353.
- Kar, A., Ray, I., Unnikrishnan, A. and Davalos, J. F. (2012), Estimation of C-S-H and calcium hydroxide for cement pastes containing slag and silica fume, Construction and Building Materials, 30, 505–515.
- Kim, S., Kwun, H. and Light, G.(2001), Long-range guided wave inspection of structures using the magnetostrictive sensor, Journal of Korean Society, *NDT*, *21*(4), 383–390
- Kundu T. (2007), Advanced Ultrasonic Methods for Material and Structure Inspection , ISTE Ltd.
- Kundu, T. (2014), Ultrasonic and Electromagnetic Waves for Nondestructive Evaluation and Structural Health Monitoring, Procedia Engineering, 86, 395–405
- Kurz, J.H., Finck, F., Grosse, C.U. and Reinhardt, H.W. (2006) , Stress drop and stress redistribution in concrete quantified over time by the b-value analysis, Structural Health Monitoring, (5), 69–81.
- Lai, W. L., Wang, Y. H., Kou, S. C. and Poon, C. S. (2013), Dispersion of ultrasonic guided surface wave by honeycomb in early-aged concrete. NDT and E International, 57, 7–16.

- Liu, S., Zhu, J., Seraj, S., Cano, R. and Juenger, M. (2014), Monitoring setting and hardening process of mortar and concrete using ultrasonic shear waves, Construction and Building Materials, 72, 248–255.
- Lootens, D., Jousset, P., Martinie, L., Roussel N. and Flatt,R.J. (2009), Yield stress during setting of cement pastes from penetration tests, Cement and Concrete Research .39, 401-408.
- Lootens, D. and Bentz, D. P. (2016), On the relation of setting and early-age strength development to porosity and hydration in cement-based materials, Cement and Concrete Composites, 68, 9–14.
- Lothenbach, B. , Rentsch, D. and Wieland, E. (2014), Hydration of a silica fume blended low-alkali shotcrete cement, Physics and Chemistry Earth Parts ABC , 16 (3),70–71 .
- Lovejoy, S.C. (2006), Development of Acoustic Emissions Testing Procedures Applicable to Conventionally Reinforced Concrete Deck Girder Bridges Subjected to Diagonal Tension Cracking (Ph.D. thesis) , Oregon State University .
- Lura, P., Couch, J., Jensen, O. M. and Weiss, J. (2009), Early-age acoustic emission measurements in hydrating cement paste: Evidence for cavitation during solidification due to self-desiccation, Cement and Concrete Research, 39(10), 861–867.
- Mathieson, P.A.R. (1987), Acoustic emissions from fatigue cracks in steels. PhD dissertation, Cranfield Institute of Technology,U.K.
- Matikas, T.E. (2008), Influence of material processing and interface on the fiber fragmentation process in titanium matrix composites, Composite Interfaces ,15 (4), 363–377.
- Miller, T., Hauser, C.J.and Kundu, T. (2002), Nondestructive inspection of corrosion and delamination at the concretesteel reinforcement interface. In: Proceedings of the ASME NDE division symposium, vol. NDE 23, New Orleans, LA, 17–22 November, ASME, New York, USA. 121–128.
- Mindess, S. (2004), Acoustic emission methods. In: Malhotra, V.M., Carino, N.J. (Eds.), CRC Handbook of Nondestructive Testing of Concrete. CRC, Boca Raton, FL.
- Morsy, M.S. , Rashad, A.M. and Shebl, S.S. (2008), Effect of elevated temperature on compressive strength of blended cement mortar. Building and Research Journal , 5 (2–3) , 173–185.

- Muller, A. C. A., Scrivener, K. L., Skibsted, J., Gajewicz, A. M. and McDonald, P. J. (2015), Influence of silica fume on the microstructure of cement pastes: New insights from 1H NMR relaxometry, Cement and Concrete Research, 74(8), 116–125.
- Na, W.B., Kundu, T. and Ehsani, M. (2002), Ultrasonic guided waves for steel bar–concrete interface testing, Materials Evaluation, 60(3), 437–444.
- Na, W.B., Kundu, T. and Ehsani, M. (2003), A comparison of steel– concrete and GFRP–concrete interface inspection by guided waves, Materials Evaluation, 61(2), 155–161.
- Nader, G. and Hamidou , D. (2007), Strength and wear resistance of sand replaced silica fume concrete , ACI Material Journal, 104 (2) , 206–214.
- Nili, M. and Ehsani, A. (2015), Investigating the effect of the cement paste and transition zone on strength development of concrete containing nanosilica and silica fume,Materials and Design, 75, 174–183.
- Nochaiya, T. , Wongkeo, W. and Chaipanich, A. (2010), Utilization of fly ash with silica fume and properties of Portland cement–fly ash–silica fume concrete, Fuel ,89 (3),768–774.
- Noorsuhada, M. N. (2016), An overview on fatigue damage assessment of reinforced concrete structures with the aid of acoustic emission technique, Construction and Building Materials, 112, 424–439.
- Ohno, K., and Ohtsu, M. (2010), Crack classification in concrete based on acoustic emission, Constrution and Building Material ,24 (12), 2339–2346.
- Pavlakovic ,B.N. (1998), Leaky guided ultrasonic waves in NDT. PhD Thesis. Imperial College of Science Technology and Medicine, London, U.K.
- Pavlakovic, B.N. and Lowe M.J.S., Cawley ,P . (1999) , The inspection of tendons in posttensioned concrete using guided ultrasonic waves Insight , 41(7),446–52.
- Pavlakovic, B.N. and Cawley, P. (2000) , DISPERSE User's Manual Version 2.0.1.1, Imperial College. London (UK): University of London .
- Pavlakovic ,B.N., Lowe, M.J.S. and Cawley ,P. (2001), High frequency low loss ultrasonic modes in imbedded bars, Journal of Applied Mechanics , 68(1), 67–75.
- Philippidis, T.P., Nikolaidis, V.N. and Anastassopoulos, A.A. (1998), Damage characterization of carbon/carbon laminates using neural network techniques on AE signals, NDT&E International 31, (5), 329–340.

- Pigeon, M. and Regourd, M. (1983), Freezing and thawing durability of three cements with various granulated blast furnace contents. International Conference on Fly Ash, Silica Fume and Slag in Concrete, vol. II, ACI Special Publication SP-79, American Concrete Institute, USA, 979–998.
- Pollock, A. (1995) , Inspecting Bridges with Acoustic Emission-Inspection Details about in Service Steel Bridges and Monitoring Weld Operations: Application Guidelines, Physical Acoustic Corporation .
- Proverbio, E. (2011), Evaluation of deterioration in reinforced concrete structures by AE technique, Material Corrosion, 62 (2) , 161–169.
- Qing, Y., Zenan, Z., Deyu, K. and Rongshen, C. (2007), Influence of nano-SiO2 addition on properties of hardened cement paste as compared with silica fume, Construction and Building Materials, 21(3), 539–545
- Randhawa , J. (2011),Monitoring early age strength and hardening of concrete using ultrasonic guided waves, M.E. Thesis , Thapar University .
- Redwood, M. (1960), Mechanical Waveguides, Pergamon Press, New York.
- Reinhardt, H. W. and Grosse, C. U. (2004), Continuous monitoring of setting and hardening of mortar and concrete, Construction and Building Materials, 18(3), 145–154.
- Reis, H., Ervin, B.L., Kuchma, D.A. and Bernhard, J.T. (2005), Estimation of Corrosion Damage in Steel Reinforced Mortar Using Guided Wave, Journal of Pressure Vessel Technology, 127 , 255-261.
- Rose Joseph, L. (2004), Ultrasonic Guided Waves in Structural Health Monitoring, Department of Engineering Science and Mechanics, Penn State University, 212 Earth-Engineering Science Building, University Park, PA 16802, USA.
- Rossen, J. E., Lothenbach, B. and Scrivener, K. L.(2015), Composition of C – S – H in pastes with increasing levels of silica fume addition, Cement and Concrete Research, 75, 14–22.
- Roy, D.M. (1999), Alkali activated cements opportunities and challenges, Cement Concrete Research , 29 (2), 249–254.
- Sanjuan, M. A., Argiz, C., Galvez, J. C. and Moragues, A. (2015), Effect of silica fume fineness on the improvement of Portland cement strength performance, Construction and Building Materials, 96, 55–64.

- Scrivener, K. , Crumbie, A. and Laugesen, P.(2004), The interfacial transition zone (ITZ) between cement paste and aggregate in concrete , Interface Science 12 , 411–421.
- Sezer, G.I. (2012), Compressive strength and sulfate resistance of limestone and/or silica fume mortars, Construction Building Material , 26 (1) , 613–618.
- Shah, S. G. and Chandra Kishen, J. M. (2010) , Fracture behavior of concrete-concrete interface using acoustic emission technique, Engineering Fracture Mechanics, 77(6), 908–924.
- Shahidan, S. (2014), Damage Classification in Reinforced Concrete Beam By, 45, 78–86.
- Sharma, S. and Mukherjee, A. (2010), Longitudinal Guided Waves for Monitoring Chloride Corrosion in Reinforcing Bars in Concrete, Structural Health Monitoring. 6(9) .
- Sharma, S. and Mukherjee, A. (2011) , Monitoring Corrosion in Oxide and Chloride Environments Using Ultrasonic Guided Waves, ASCE Journal of Materials In Civil Engineering , 2(23).
- Sharma, S. and Mukherjee (2012), Non-Destructive Evaluation Of Corrosion In Varying Environments Using Guided Waves , Research in non-destructive evaluation, 1-40.
- Sharma, S. and Mukherjee, A. (2014), Ultrasonic guided waves for monitoring the setting process of concretes with varying workabilities, Construction and Building Materials ,72 ,358–366.
- Sharma, S. and Mukherjee, A. (2015), Monitoring freshly poured concrete using ultrasonic waves guided through reinforcing bars, Cement & Concrete Composites , 55 , 337–347.
- Shih, J.Y., Chang, T.P. and Hsiao, T.C. (2006), Effect of nanosilica on characterization of Portland cement composite, Material Science Engineering A ,424 (1) , 266–274.
- Shiotani, T., Aggelis, D.G. and Makishima, O. (2009), Global monitoring of large concrete structures using acoustic emission and ultrasonic techniques: case study, Journal Bridge Eng.-ASCE 14, (3), 188–192.
- Siddique, R. (2011), Utilization of silica fume in concrete: review of hardened properties, Resource Conservation and Recycling , 55 (11) ,923–932.

- Sidhu, D. S. (2001), Early age behaviour of silica fume concrete, 27–28.
- Skal's'kyi, V. R., Koval', P. M., Serhienko, O. M. and Lotots'kyi, Y. L. (2004), Investigation of the solidification of concrete according to the signals of acoustic emission, Materials Science, 40(5), 698–701.
- Sleiman, H., Perrot, A. and Amziane,S. (2010), A new look at the measurement of cementitious paste setting by Vicat Test, Cement and Concrete Research , 40, 681-686.

- Song, H.W., Pack, S.W., Nam, S.H. , Jang, J.Ch. and Saraswathy, V. (2010), Estimation of the permeability of silica fume cement concrete , Construction Building Material ,24 (3) , 315–321.
- Soulioti, D., Barkoula, N.M., Paipetis, A., Matikas, T.E., Shiotani, T. and Aggelis, D.G. (2009), Acoustic emission behavior of steel fibre reinforced concrete under bending, Construction and Building Material , 23, 3532–3536.
- Tchamba J.C., Amziane S., Ovarlez G. and Roussel N. (2008), Lateral stress exerted by fresh cement paste on formwork : laboratory experiments, Cement and Concrete Research ,38 (4), 459–466.
- Trtnik, G., Turk, G., Kavcic, F. and Bosiljkov, V.B. (2008), Possibilities of using the ultrasonic wave transmission method to estimate initial setting time of cement paste. Cement and Concrete Research , 38 (11), 1336-1342.
- Trtnik, G. and Gams,M. (2013), The use of frequency spectrum of ultrasonic P-waves to monitor the setting process of cement pastes , Cement and Concrete Research , 43(1) , 1-11.
- Trtnik, G. and Turk, G. (2013), Influence of superplasticizers on the evolution of ultrasonic P-wave velocity through cement pastes at early age, Cement and Concrete Research, 51, 22–31.
- Trtnik, G. and Gams, M. (2014), Recent advances of ultrasonic testing of cement based materials at early ages, Ultrasonics, 54(1), 66–75.
- Trtnik, G. and Gams, M. (2015), Ultrasonic assessment of initial compressive strength gain of cement based materials. Cement and Concrete Research, 67, 148–155.
- Van Den Abeele, K., Desadeleer, W., De Schutter, G. and Wevers, M. (2009), Active and passive monitoring of the early hydration process in concrete using linear and nonlinear acoustics, Cement and Concrete Research, 39(5), 426–432.

- Von Daake, H. and Stephan, D. (2016), Setting of cement with controlled superplasticizer addition monitored by ultrasonic measurements and calorimetry, Cement and Concrete Composites, 66, 24–37.
- Watson, J.R. , Cole, P.T. , Holford, K.M. and Davies, A.W. (2001), Damage assessment using acoustic emission , Key Engineering Materials, 204–205 .
- Web References : http://iti.northwestern.edu , http://www.ni.com3.4 , http://www.ndt.net , http://dir.indiamart.com , http://viet-anag-jenius.blogspot.in , https://magareyphysics.wikispaces.com,https://www.nde-ed.org, http://www.geo.mtu.edu , www.ndt-ed.org .
- Wee, T.H. , Suryavanshi, A.K. , Wong, S.F. and Rahman, K.M.A. (2000), Sulfate resistance of concrete containing mineral admixture, ACI Material Jornal, 97 (5) , 536–549
- Wongkeo, W. and Chaipanich, A. (2010), Compressive strength, microstructure and thermal analysis of autoclaved and air cured structural lightweight concrete made with coal bottom ash and silica fume , Material Science and Engineering, A 527 (16) , 3676–3684.
- Xu, J. (2008), Nondestructive Evaluation of Prestressed Concrete Structures by Means of Acoustic Emissions Monitoring (Ph.D. thesis) , Auburn University .
- Xuan, D. X., Shui, Z. H. and Wu, S. P. (2009), Influence of silica fume on the interfacial bond between aggregate and matrix in near-surface layer of concrete, Construction and Building Materials, 23(7), 2631–2635.
- Yuyama, S., Li, Z., Ito, Y. and Arazoe, M. (1999), Quantitative analysis of fracture process in RC column foundation by moment tensor analysis of acoustic emission. Constrution and Building Material ,13, 87–97.
- Zaki , A. , Chai , H.K. , Aggelis , D.G. and Alver , N. (2015), Non –Destructive Evaluation for Corrosion Monitoring in Concrete : A Review and Capability of Acoustic Emission Technique .
- Zhang , J. , Fan , T., Ma , .H. and Li , Z. (2015) , Monitoring setting and hardening of concrete by active acoustic method : Effects of water –to –cement ratio and pozzolanic materials , Construction and Building Material ,88 , 118-125 .
- Zhang, Z., Zhang, B. and Yan, P. (2016), Comparative study of effect of raw and densified silica fume in the paste, mortar and concrete, Construction and Building Materials, 105, 82–93.

- Zhou, J.W., Xu, W.Y. and Yang, X.G. (2010), A microcrack damage model for brittle rocks under uniaxial compression, Mechanics Research Communications ,37, 399–405.
- Zhu, J., Kee, S.-H., Han, D. and Tsai, Y.-T. (2011), Effects of air voids on ultrasonic wave propagation in early age cement pastes, Cement and Concrete Research, 41(8), 872–881.